보건학석사 학위논문

Source Apportionment and Health Risk Assessment of $PM_{2.5}$ Using Dispersion-Normalized PMF at Three Cities (Seoul, Incheon, Gwangju) in South Korea

서울, 인천, 광주의 $PM_{2.5}$ 오염원 추정과
건강영향 평가

2023년 2월

서울대학교 보건대학원
환경보건학과 환경보건학전공
정 연 승

Source Apportionment and Health Risk Assessment of $PM_{2.5}$ Using Dispersion-Normalized PMF at Three Cities (Seoul, Incheon, Gwangju) in South Korea

서울, 인천, 광주의 $PM_{2.5}$ 오염원 추정과 건강영향 평가

지도 교수 이 승 묵

이 논문을 보건학석사 학위논문으로 제출함

2022년 11월

서울대학교 대학원

환경보건학과 환경보건학전공

정 연 승

정연승의 보건학석사 학위논문을 인준함

2023년 1월

위 원 장 _____ 김 호 _____ (인)

부위원장 _____ 허 종 배 _____ (인)

위 원 _____ 이 승 묵 _____ (인)

Abstract

Source Apportionment and Health Risk Assessment of $PM_{2.5}$ Using Dispersion-Normalized PMF at Three Cities (Seoul, Incheon, Gwangju) in South Korea

Yeonseung Cheong

Department of Environmental Health Sciences

Graduate School of Public Health

Seoul National University

$PM_{2.5}$, which is emitted from various sources and causes severe adverse health effects, requires systematic reduction measures based on its source identification and health impacts. Seoul, Incheon, and Gwangju are metropolitan cities with heavy $PM_{2.5}$ pollution in South Korea. These cities are situated in the western coastal areas of Korea where they are affected by long-range transported pollutants from China. PMF (Positive Matrix Factorization) is widely used for source apportionment of $PM_{2.5}$. However, the conventional PMF (C-PMF) loses information on $PM_{2.5}$ by the dispersion effects on concentration such as variations in emission strength, atmospheric chemistry, and meteorological dilution. The dispersion-normalized PMF (DN-PMF) reduces the meteorological effects and enhances the actual source strengths. The present study aimed to identify the sources of $PM_{2.5}$ in the three megacities and conduct source-specific health risk assessments of $PM_{2.5}$-bound trace elements.

In this study, both models were applied to 222, 221, and 224 $PM_{2.5}$ samples measured from September 2020 to March 2022 in Seoul, Incheon, and Gwangju, respectively. Both models identified ten sources of $PM_{2.5}$ in Seoul and Incheon, and nine sources in Gwangju. The nine common sources in the three sites were secondary nitrate, secondary sulfate, biomass burning, mobile, soil, waste incinerator, coal combustion, industry/oil combustion, and aged sea salt. Additional industry-related sources were resolved in Seoul and Incheon: industry (Seoul) and metal plating (Incheon). The DN-PMF resolved the same number of factors and mostly identical source profiles, while the source contributions were noticeably different. The differences originated from normalizing the source contributions for its degree of local dispersion. For instance, secondary nitrate and biomass burning source contributions were upscaled for periods with relatively high VCs. Also, the DN-PMF resolved more uniform mobile source contributions. The conditional bivariate probability function (CBPF) analysis was performed in each site to identify the local source locations. In general, the three cities were affected by the mobile, waste incinerator, and industry-related sources in the vicinity. Joint potential source contribution function (J-PSCF) analysis identified northeast China and some parts of Inner Mongolia as the potential source locations of the secondary nitrate, secondary sulfate, and biomass burning sources.

The DN-PMF results were then combined with the health risk assessment method to estimate the source-specific carcinogenic and non-carcinogenic risks of $PM_{2.5}$-bound trace elements. The carcinogenic risks exceeded the safety limit at all sites. As and Cr^{6+} posed a great concern to the carcinogenic risk, in which coal combustion and metal plating were its major sources. Mitigation of

carcinogenic trace elements from coal combustion and metal plating industries is necessary. Meanwhile, the non-carcinogenic risks were below the safety limit. Mn, As, and Pb were the major contributors to non-carcinogenic risks. Despite no immediate health risks, emissions from mobile, coal combustion, and industry sources should be continuously monitored to further protect the residences in the three megacities in South Korea from adverse health effects.

Keywords : $PM_{2.5}$, Source apportionment, DN-PMF (Dispersion-Normalized Positive Matrix Factorization), CBPF (Conditional Bivariate Probability Function), PSCF (Potential Source Contribution Function), Source-specific health risk assessment

Student Number : 2021-22679

Table of Contents

Chapter 1. Introduction

1.1. Study Background

$PM_{2.5}$ is emitted from various sources and causes severe adverse health effects. $PM_{2.5}$ refers to particulate matter with an aerodynamic diameter equal to or less than 2.5 μm. $PM_{2.5}$ can come from both natural sources and anthropogenic sources. Natural sources include sea salts, forest fires, and crustal dust while anthropogenic sources include combustion activities, industrial and traffic-related emissions as well as secondary formation through atmospheric chemical reactions. These various sources contribute to the complex chemical content of $PM_{2.5}$ such as the carbonaceous, ionic, and trace elements species. Its physical and chemical properties facilitate deep penetration into the lungs, some of which ultimately enter the cardiovascular system. Exposure to $PM_{2.5}$ can cause oxidative stress in the respiratory system, and the immune system may be affected (Feng et al., 2016; Yang et al., 2020). Associations of respiratory and cardiovascular admissions with $PM_{2.5}$-bound Al, Ni, and V were reported (Bell et al., 2014). Well-known carcinogenic or potentially carcinogenic elements such as Cr, As, and Pb are also present in $PM_{2.5}$. Water-soluble transition metals such as V and Cr showed associations with increased oxidative stress (Sørensen et al., 2005). Epidemiological studies reported the possible DNA damage from oxidative injuries from certain trace elements such as Mn, Ni, and Pb (Kim et al., 2004; Prahalad et al., 2000). Trace elements are mostly associated with primary source emissions, which are continuously polluting the atmosphere. It is important to study the baseline health risks from chronic exposure to $PM_{2.5}$-bound trace

elements.

South Korea is among the most polluted countries in East Asia, exceeding 3.8 times the WHO annual air quality guideline value in 2021 (https://www.iqair.com/south-korea). To improve the air quality and protect public health in South Korea, the Korean government implemented the Comprehensive Plan on Fine Dust in 2017 to tackle fine dust pollution. This plan includes early disposal of aged diesel vehicles, limited activities of coal-fired power plants, and stringent regulations on emissions from illegal incinerations and factories. In the Comprehensive Plan on Fine Dust for 2020 to 2024, Seoul, Incheon, and Gwangju were pointed out as cities with severe $PM_{2.5}$ pollution. Seoul, Incheon, and Gwangju are large metropolitan cities situated in the western coastal areas of South Korea. Seoul metropolitan city is the capital of South Korea and the largest metropolis with a dense population of 9.5 million as of 2021. As the business and financial hub of South Korea, heavy traffic, and various industrial activities both in and from the surrounding areas contribute greatly to the overall air quality in Seoul. Incheon metropolitan city is adjacent to Seoul and is comprised of industrial complexes and busy ports with a population of 2.9 million. Incheon has the second largest port in South Korea, which handled 3.3 million TEU in 2021. Also, a large coal-fired power plant (5080 MW) is located south of Incheon. The busy ports and industrial activities constantly deteriorate the air quality in Incheon. Along with Seoul and Incheon, Gwangju metropolitan city is one of the largest cities in the southwestern part of South Korea with a population of 1.4 million. Multiple large-scale national industrial complexes are dispersed in Gwangju, although not as densely populated as the other two metropolitan cities. So, pollution from mobile sources is relatively dominant in Gwangju and the city has focused its air quality control

measures on vehicles. The western coastal areas of the Korean peninsula are located downwind of China, which makes these cities easily affected by transboundary air pollutants that are introduced to Korea by the westerly winds (Han et al., 2008; Koo et al., 2008). Both domestic and long-range transport sources threaten the air quality in Seoul, Incheon, and Gwangju, thus their sources of $PM_{2.5}$ must be thoroughly investigated.

Positive matrix factorization (PMF) is widely used for source apportionment of $PM_{2.5}$ to this date (Kim et al., 2018; Manousakas et al., 2017; Park et al., 2022). With the measured concentration and its uncertainty data, PMF can provide both qualitative and quantitative information on sources of $PM_{2.5}$. However, one challenge the conventional PMF (C-PMF) faces is the loss of information from the measured concentrations due to atmospheric variations. Such atmospheric variations include changes in emission strength, atmospheric chemistry, and meteorological dilution. To reduce the effects of meteorology, the dispersion normalized PMF (hereinafter DN-PMF) has been introduced recently and extensively used (Chen et al., 2022; Dai et al., 2020; Y. Kim et al., 2022; Park et al., 2022; Song et al., 2021). Dai et al. (2020) applied the DN-PMF to hourly data in China and were able to distinguish the diel patterns of local sources. Chen et al. (2022) explored the effect of dispersion normalization on 24-hr speciated samples in New York and discovered that DN-PMF was able to reveal seasonal patterns of $PM_{2.5}$ sources.

The present study conducted simultaneous ground-based monitoring of $PM_{2.5}$ in Seoul, Incheon, and Gwangju from September 2020 to March 2022. The mass concentrations and the chemical constituents of $PM_{2.5}$ in each city were characterized. The DN-PMF and C-PMF were applied to characterize the sources of $PM_{2.5}$ in the

three metropolitans, and the effects of dispersion normalization were evaluated. Additionally, the source contributions were coupled with a health risk assessment to estimate source-specific carcinogenic risk and non-carcinogenic risk posed by trace elements. This study aimed to characterize the sources of $PM_{2.5}$ in three metropolitan cities in South Korea by using DN-PMF and perform a health risk assessment on $PM_{2.5}$-bound trace elements and their associated sources using the PMF results. This is the first study in Korea to perform spatial analysis of $PM_{2.5}$ sources of three cities in the western coastal areas using DN-PMF.

1.2. Purpose of Research

The purpose of this study is to identify and quantify the sources of $PM_{2.5}$ in Seoul, Incheon, and Gwangju by using the DN-PMF and diagnose the health risks of $PM_{2.5}$-bound trace elements in each city. The effects of dispersion normalization were evaluated by comparing the results of DN-PMF and C-PMF.

Chapter 2. Body

2.1. Materials and Methods

2.1.1.Materials and Methods

Ambient $PM_{2.5}$ samples were collected every second day during the heating season (November-March) and every sixth day during the non-heating season (April-October) from September 2020 to March 2022. The heating season in this study refers to the heating season in China to account for its transboundary influences. The total number of samples collected from Seoul, Incheon, and Gwangju was 222, 221, and 224, respectively. Daily sampling was conducted for 23 hours starting from 11:00 a.m. until 10:00 a.m. the next day.

Three-channel low-volume air samplers were operated for the collection of $PM_{2.5}$ and analyses of carbonaceous species, ionic species, and trace elements. Each channel consisted of a filter pack (URG-2000-30FG, URG, USA) and a cyclone (URG-2000-30EH, URG, USA). Two types of Teflon filters and a quartz filter were used. The flow rates of the low-volume air samplers were 16.7 L/min.

The sampling in Seoul was conducted at the rooftop of the Graduate School of Public Health building (37.46°N, 126.95°E) at Seoul National University, which is in the southern part of Seoul. Heavy traffic, mountains, and residential areas coexist in the surrounding area. The sampling site in Incheon was at the rooftop (2.7 m above ground) of the National Institute of Environmental Research (37.57°N, 126.64°E). Ports and national industrial complexes are located 4 km west of the sampling site. Thus, Incheon represents a coastal

metropolitan with industrial complexes. Sampling in Gwangju was conducted at the roof (10 m above ground) of the 3rd building of the College of Engineering (37.18°N, 126.91°E) at Chonnam National University in Gwangju. Residential areas and expressways surround the Gwangju sampling site, and national industrial complexes are located 3.3 km northwest of the sampling site. The three study sites are situated on the downwind western coastal areas of the Korean peninsula, where they receive direct influences from China.

2.1.2. Mass concentration and chemical characterization of $PM_{2.5}$

The mass concentration of $PM_{2.5}$ was gravimetrically measured using a microbalance (Quintix125D, Sartorius, Germany). The Teflon filters were preserved in a desiccator and equilibrated in a controlled environment (temperature: 21 ± 1.4℃, relative humidity: 35 ± 5%) for at least 24 hours before sampling and gravimetric measurement. The blank filters and sample filter weights before and after sampling were measured at least three times on a microbalance and the average values were recorded as their weights.

The ionic species, consisting of three anions (Cl^-, NO_3^-, SO_4^{2-}) and three cations (Na^+, NH_4^+, K^+), collected on Teflon filters were analyzed by an ion chromatograph (ICS-1100, Thermo Fisher, USA). Samples were extracted in distilled water (resistivity of 18.2 MΩ·cm), then filtered by a 0.2 μm syringe filter. The total extraction volume was 32 mL for each sample.

For the carbonaceous species, organic carbon (OC) and elemental carbon (EC) were analyzed by a carbon aerosol analyzer (Model 5L, Sunset Laboratory Inc., USA). The analysis used the thermal optical transmittance (TOT) method following the National Institute for

Occupational Safety and Health (NIOSH) 870 protocol.

The trace elements collected on Teflon filters were measured by using an energy-dispersive X-ray fluorescence (EDXRF) spectrometer (EDXRF Spectrometer, Thermo Fisher, USA). A total of 20 trace element species (Mg, Al, Si, S, Cl, K, Ca, Ti, V, Cr, Mn, Ba, Fe, Ni, Cu, Zn, As, Se, Br, Pb) were quantified.

2.1.3. Mixing layer height

The mixing layer heights for Seoul, Incheon, and Gwangju were obtained from the ERA5, which is the fifth generation of ECMWF (European Centre for Medium-Range Weather Forecasts) atmospheric re-analyses of the global climate. ERA5 hourly data on single levels from 1959 to the present are available on the website (https://cds.climate.copernicus.eu), and the modeled boundary layer heights during the sampling period for a target grid size of 1°×1° were used for each site in this study.

2.1.4. Conventional PMF (C-PMF)

Positive Matrix Factorization (PMF) model is a factor analysis model based on the least squares method that decomposes a matrix of sample data into a factor contribution matrix (g) and factor profile matrix (f). PMF is widely used in $PM_{2.5}$ source apportionment studies for its effective quantification and qualification of source contributions with concentration and uncertainty data. The basic equation of PMF is as follows:

$$x_{ij} = \sum_{k=1}^{p} g_{ik} f_{kj} + e_{ij}$$

where for a p number of independent sources, x_{ij} is the j-th species concentration of the i-th sample, g_{ik} is the particulate mass concentration from the k-th source contributing to the i-th sample, f_{kj} is the mass fraction of the j-th species from the k-th source, and e_{ij} is the residuals associated with the j-th species concentration measured in the i-th sample. The goal of PMF is to find the best solution that minimizes the residuals.

The input data for PMF was created after quality assurance and quality control (QA/QC) procedures, such as evaluating the ion balance and mass closure of each sample. The concentrations and uncertainties below the method detection limits (MDLs) were replaced with 1/2 MDL and 5/6 MDL, respectively. The uncertainties of $PM_{2.5}$, carbonaceous species, ionic species, and trace element species were calculated separately. Table 1 summarizes the uncertainty calculation of each chemical specie. E is the error fraction of the total flow for each sample.

Table 1. Uncertainty calculation for each species

	Uncertainty calculation
$PM_{2.5}$	$4 \times conc$
Carbonaceous species	$\sqrt{((0.05+E) \times conc + IDLs)^2 + (S.D.of\ Blank)^2}$
Ionic species	$\sqrt{(global\ unc \times conc)^2 + (S.D.of\ Blank)^2 + (E \times conc)^2}$
Trace elements	$\sqrt{((0.1+E) \times conc)^2 + (0.5 \times MDL)^2}$
Flow error (E)	$\frac{\lvert(total\ flow) - 16.7\rvert}{16.7}$

2.1.5. Dispersion-normalized PMF (DN-PMF)

The dispersion-normalized PMF (DN-PMF) is an enhanced version of the C-PMF. It aims to reduce the meteorological effects on concentrations by incorporating the ventilation coefficient (VC). The ventilation coefficient is defined by the product of mixing layer height (m) for period i (MLH_i) and mean wind speed (m/s) for period i ($\overline{u_i}$).

$$VC_i = MLH_i \times \overline{u_i}$$

VC is then used to normalize the concentrations ($C_{VC,i}$) by multiplying the measured concentrations (C_i) for period i by VC_i/VC_{mean}, where VC_{mean} is the average of period-specific VC values over the whole study period.

$$C_{VC,i} = C_i \times \frac{VC_i}{VC_{mean}}$$

The scaled concentrations and uncertainties are used as input data for the PMF analyses. The resolved source contributions are unnormalized so that they are scaled back to values they would have had in their original meteorological states. Further details of DN-PMF are available in recent literature (Dai et al., 2020). Averaging daily meteorological data cannot resolve the diel patterns, but the DN-PMF can provide improved seasonal patterns at the study sites (Chen et al., 2022).

2.1.6. Conditional Bivariate Probability Function (CBPF)

The conditional bivariate probability function (CBPF) model is a hybrid receptor model which combines PMF source contributions with meteorological data such as wind direction and wind speed (Uria-Tellaetxe & Carslaw, 2014). The combined data produces a polar plot that can identify the probable source locations and inflow direction to

the sampling site. The equation of CBPF is as follows.

$$CBPF_{\Delta\theta,\Delta u} = \frac{m_{\Delta\theta,\Delta u}\big|_{C\geq x}}{n_{\Delta\theta,\Delta u}}$$

Here, $m_{\Delta\theta,\Delta u}$ is the number of samples in the wind sector $\Delta\theta$ with wind speed interval Δu having concentration C greater than a threshold value x, $n_{\Delta\theta,\Delta u}$ is the total number of samples in the same wind direction-speed interval. Conventionally, the threshold values represent a high percentile of concentration such as 75th or 90th, which the 75th percentile was selected for this study. The generated polar plot not only can display the directionality of a source, but also the wind speed in which this source was mainly affected in color variation. The meteorological data (wind speed and wind direction) for the study period were obtained from the Korea Meteorological Administration's website (Seoul: Kimpo International Airport, Incheon: Incheon International Airport, Gwangju: Muan International Airport).

2.1.7.Joint Potential Source Contribution Function (J-PSCF)

The potential source contribution function (PSCF) model is used to estimate the possible source areas and long-range transport (Kim et al., 2018; Pekney et al., 2006; Zíková et al., 2016). The present study performed the PSCF model using the 96-hr backward trajectories from the HYSPLIT 4 model. The PSCF value can be computed by the following equation.

$$PSCF = \frac{m_{ij}}{n_{ij}}$$

In the equation, n_{ij} is the number of endpoints that pass the ij-th grid cell, and m_{ij} is the number of endpoints that pass the ij-th grid cell when the source contributions were greater than the threshold value. The threshold value was set to the upper 25th percentile value. PSCF

of a grid cell with small n_{ij} could be biased, so a weighting function (W) was applied as follows:

$$W = \begin{Bmatrix} 1.0, (n > 3n_{avg}) \\ 0.7, (1.5n_{avg} < n \leq 3n_{avg}) \\ 0.4, (n_{avg} < n \leq 1.5n_{avg}) \\ 0.2, (n \leq n_{avg}) \end{Bmatrix}$$

In this study, the Joint-PSCF (J-PSCF) was used to compute the potential source locations that affect multiple sites. J-PSCF combines the PSCF values for each receptor site using the equation below.

$$J - PSCF_{ij} = \frac{\sum_{n=1}^{k} ({}^{m_{ij}}/_{n})_n}{\sum_{n=1}^{k} ({}^{n_{ij}}/_{n})_n}$$

Here, k is the number of receptor sites. J-PSCF can minimize the trailing effects and the overestimation of PSCF values near the receptor site.

2.1.8.Source-specific health risk assessment

Both carcinogenic risk and non-carcinogenic risk posed by trace elements including heavy metals in $PM_{2.5}$ was estimated following the US EPA risk assessment guidelines (EPA, 2009). Since inhalation is the dominant route of $PM_{2.5}$ exposure to the human body, inhalation exposure concentration was used to calculate the carcinogenic risk and non-carcinogenic risk. Inhalation exposure concentration (EC_{inh}) can be calculated using the following equation.

$$EC_{inh} = C \times \frac{ET \times EF \times ED}{AT}$$

The exposure parameters chosen for this study are as follows. C is the concentration of the trace element in the sampling site (μg/m^3). The exposure time (ET) was chosen as 6 hours. An exposure frequency (EF) of 365 days was chosen in the present study to

represent continuous exposure to ambient $PM_{2.5}$. An exposure duration (ED) of 63.7 was chosen to represent the expected life expectancy after adulthood (19 years old) for South Koreans (NIER, 2019). Averaging time (AT) was calculated as ED×365×24.

The carcinogenic effect is estimated as the incremental probability of developing cancer over a lifetime as the result of exposure to a potential carcinogen. The risk value can be expressed as the formula below:

$$ILCR = (EC_{inh} \times IUR)$$

where ILCR is the incremental lifetime cancer risk and IUR is the inhalation unit risk. The calculated ILCR value less than the threshold value of 10^{-6} indicates negligible carcinogenic risk, while the ILCR value greater than the threshold indicates possible risk. The four target species, Cr, Ni, As, and Pb, were chosen for this study. In the case of Cr, the health effects are different for its valence states. The ratio of Cr(VI) and Cr(III) was reported to be 1:6, so 1/7 and 6/7 of Cr concentrations were used as the hexavalent and trivalent Cr concentrations, respectively (EPA, 2004; Park et al., 2008). The inhalation unit risk values for the target species were obtained from the Integrated Risk Information System (IRIS) and the Office of Environmental Health Hazard Assessment (OEHHA). The IUR values and critical health effects of each element are summarized in Table 2.

The non-carcinogenic effects of the trace elements can be estimated by the hazard quotient (HQ). The HQ for the i-th trace element is defined as follows:

$$HQ_i = EC_{inh}/RfC_i$$

$$HI = \sum_i HQ_i$$

where HQ_i is a unitless hazard quotient for the i-th trace element, and RfC_i is the chronic inhalation reference concentration for the i-

th trace element (μg/m^3). The sum of HQ of each species can be represented as the hazard index (HI). The calculated HQ and HI values less than the threshold value of 1 indicates negligible non-carcinogenic risk. The eight target species chosen for the non-carcinogenic risk assessment are Al, V, Cr, Mn, Ni, Cu, As, and Pb. The reference concentrations (RfC) were obtained from credible sources such as IRIS and OEHHA. The RfC values and the critical health effects of each element are summarized in Table 3.

The source-specific health risk assessment was then conducted by coupling the source profiles resolved from the PMF with the health risk assessment method. The trace element concentrations contributing to a specific source were calculated using the equation below.

$$C_{ij}^{k} = g_{ik} \cdot f_{kj}$$

Here, C_{ij}^{k} is the concentration of trace element j contributing to the k-th source, g_{ik} is the concentration of the k-th source in the i-th sample, and f_{kj} is the elemental fraction of trace element j contributing to the k-th source. C_{ij}^{k} is the trace element concentration used to estimate the source-specific inhalation exposure concentration. This source-specific health risk assessment method combining PMF results is not a new practice (Khan et al., 2016; Yan et al., 2022), however, most of the source apportionment studies were limited to using trace elements. This study uses the carbonaceous, ionic, and trace element species for source apportionment, which can provide detailed source profiles.

Table 2. IUR values and critical health effects of four trace elements (Cr^{6+}, Ni, As, and Pb)

Species	IUR (risk/μg/m^3)	Critical effects	Source
Cr^{6+}	1.2E-02	Liver and kidney disease, lung cancer	IRIS
Ni	2.4E-04	Lung embolisms, lung/nasal cancer	IRIS
As	4.3E-03	Lung irritation, DNA damage	IRIS
Pb	1.2E-05	Renal impairment, encephalopathic signs	OEHHA

Table 3. RfC values and critical health effects of eight trace elements (Al, V, Cr^{3+}, Cr^{6+}, Mn, Ni, Cu, As, and Pb)

Species	RfC_i (mg/m^3)	Critical effects	Source
Al	5.0E+00	Psychomotor and cognitive impairment	RAIS
V	1.0E-04	Throat pain, headaches, impairment to the nervous system	ATSDR
Cr^{3+}	1.0E-04	DNA lesions (rarely toxic compared to hexavalent form)	ATSDR, 2012
Cr^{6+}	5.0E-06	Allergic contact dermatitis and eczema, gingivitis	IRIS
Mn	5.0E-05	Hypotension, pneumonia, sperm damage	IRIS
Ni	1.4E-05	Asthma, allergic reactions, heart disorders	CalEPA
Cu	2.0E-03	Insomnia, anxiety, restlessness	MDEQ, 2009
As	1.5E-05	Heart problems, brain damage	OEHHA
Pb	1.5E-04	Hypertension, miscarriages, stillbirth	IRIS

2.1.9. Statistical analysis

Environmental data such as concentration and meteorological variables were assumed to have equal variances and the Student's t-test at $\alpha = 0.05$ were used for statistical analysis. The non-parametric Mann-Whitney U-test and Kruskal-Wallis tests at $\alpha = 0.05$ were used to test the significant differences between the two groups and multiple groups that did not pass the normality tests, respectively. The statistical analysis was performed using SigmaPlot (version 14.0).

2.2. Results and Discussion

2.2.1.Meteorology in the study sites

The daily average meteorological variables in each site were compared for the heating and non-heating seasons. Student's t-tests were performed to check statistical differences. For all sites, only the wind speeds were significantly higher during the heating season ($p \leq 0.05$), while the mixing layer heights and VCs were not significantly different between the heating and non-heating seasons. The same comparisons for the hourly meteorological parameters in each site are also available in Tables S1 through S3.

The wind speeds, mixing layer heights, and VCs were compared for each site by one-way ANOVA followed by Tukey's post hoc test. From the inter-site comparisons, only the wind speeds were significantly different across the three sites. The wind speeds were highest in the order of Incheon followed by Gwangju and Seoul. The mixing layer heights and VCs were not significantly different for each site. Still, the VCs were generally higher during the heating season. The temporal variations of daily average meteorological parameters in Seoul, Incheon, and Gwangju are shown in Figure 1. The daily average meteorology in Seoul, Incheon, and Gwangju for the three periods (whole study period, heating season, and non-heating season) is summarized in Tables 4 through 6.

Table 4. Daily average meteorological parameters in Seoul (yellow shades indicate statistically higher value at $p \leq 0.05$)

Season	Wind speed (m/s)	MLH (m)	VC (m^2/s)
All period	2.05	450.30	1708.27
Heating season	2.28	454.74	1814.70
Non-heating season	1.58	440.90	1482.76

Table 5. Daily average meteorological parameters in Incheon (yellow shades indicate statistically higher value at $p \leq 0.05$)

Season	Wind speed (m/s)	MLH (m)	VC (m^2/s)
All period	3.51	464.98	2338.65
Heating season	3.79	471.73	2521.50
Non-heating season	2.85	448.85	1901.87

Table 6. Daily average meteorological parameters in Gwangju (yellow shades indicate statistically higher value at $p \leq 0.05$)

Season	Wind speed (m/s)	MLH (m)	VC (m^2/s)
All period	2.64	460.94	2005.97
Heating season	2.86	469.42	2181.12
Non-heating season	2.18	443.15	1638.14

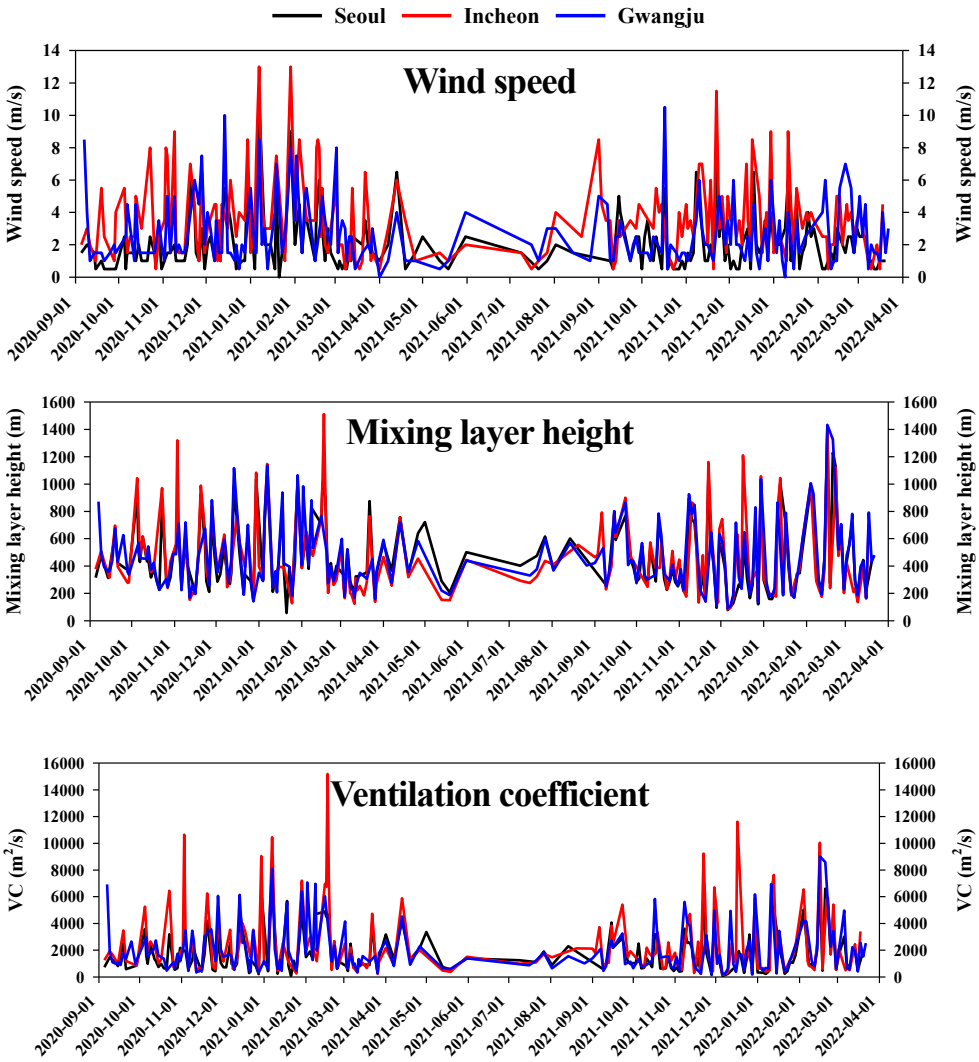

Figure 1. Temporal variations of the daily average meteorological parameters in Seoul, Incheon, and Gwangju.

2.2.2. Concentrations of $PM_{2.5}$ and its chemical constituents

2.2.2.1. Seoul

The mass concentrations ranged from 2.69 to 222.1 μg/m^3 and the average mass concentration of $PM_{2.5}$ was 24.2 (± 21.4) μg/m^3 in Seoul. The highest mass concentration was recorded on May 7, 2021, which was one of the days when Asian Dust occurred. Excluding this date, the maximum $PM_{2.5}$ mass concentration was 100 μg/m^3. High concentration events (HCEs) that exceed the 24-h ambient air quality standard for $PM_{2.5}$ in South Korea (35 μg/m^3) occurred on 48 days. The HCEs mostly occurred during the heating season (44 days, 92%). The average mass concentrations were highest in spring (34.1 μg/m^3) followed by winter (27.9 μg/m^3), autumn (17.5 μg/m^3), and summer (8.73 μg/m^3). Seoul showed the highest wintertime average mass concentration compared to those of Incheon and Gwangju. Table 7 summarizes the concentrations of $PM_{2.5}$ and its chemical constituents in Seoul, Incheon, and Gwangju. The fractions of chemical constituents in $PM_{2.5}$ by season for each site are presented in Figure 2. The different chemical fractions during the heating and non-heating seasons for each site are presented in Figure 3.

For the carbonaceous species, the average mass concentrations of OC and EC were 4.8 (± 2.2) μg/m^3 and 0.4 (± 0.2) μg/m^3, respectively. The carbonaceous species (total sum of OC and EC) accounted for 23% of the total $PM_{2.5}$ mass concentration during the whole study period. Seasonally, they accounted for in the order of summer, autumn, spring, and winter (47%, 25%, 23%, 19%), respectively. Both OC and EC concentrations were highest in winter (OC: 5.60 μg/m^3, EC: 0.41 μg/m^3), followed by spring, autumn, and summer. The carbonaceous species accounted for 22% and 28% of the

total $PM_{2.5}$ mass during the heating and non-heating season, respectively. Its concentrations were significantly higher during the heating season than during the non-heating season ($p \leq 0.001$).

For the ionic species, the average mass concentrations of NO_3^-, SO_4^{2-}, and NH_4^+ were 6.5 (± 7.0) μg/m^3, 3.0 (± 2.0) μg/m^3, and 3.1 (± 2.9) μg/m^3, respectively. The average mass concentrations of Na^+, Cl^-, and K^+ were 0.2 (± 0.3) μg/m^3, 0.4 (± 0.4) μg/m^3, and 0.2 (± 0.1) μg/m^3, respectively. The ionic species were the most abundant species of $PM_{2.5}$ and they accounted for 61% of the total $PM_{2.5}$ mass concentration. The abundance of the ionic species was similar in spring (60%), autumn (59%), and winter (63%), while it was the lowest in summer (40%). The ionic species accounted for 63% and 51% of the total $PM_{2.5}$ mass during the heating and non-heating season, respectively. Its concentrations were significantly higher during the heating season than during the non-heating season ($p \leq 0.001$).

The trace elements were classified as crustal elements (Al, Si, K, Ca, Ti, Fe) and non-crustal elements (Mg, S, Cl, V, Cr, Mn, Ba, Ni, Cu, Zn, As, Se, Br, Pb). The average mass concentrations of the crustal elements and non-crustal elements were 1.4 (± 4.3) μg/m^3 and 2.0 (± 1.2) μg/m^3, respectively. The total trace elements accounted for 16% (crustal elements: 7%, non-crustal elements: 9%) of the total $PM_{2.5}$ mass concentration. The average concentration of the crustal elements was highest in spring (3.30 μg/m^3), while the average concentration of the non-crustal elements was highest in winter (2.42 μg/m^3). Frequent dust events occur during the spring season, which may support the seasonal characteristics of crustal elements concentration. The trace elements accounted for 14% and 22% of the total $PM_{2.5}$ mass during the heating and non-heating season, respectively. There were no significant differences in its

concentrations during the heating and non-heating seasons.

2.2.2.2.Incheon

The mass concentrations ranged from 2.99 to 193.9 μg/m^3 and the average mass concentration of $PM_{2.5}$ was 24.6 (± 20.0) μg/m^3 in Incheon, which ranked the highest among the study sites. Excluding the same date (May 7, 2021), the highest mass concentration over the study period was 107.1 μg/m^3. HCEs in Incheon occurred for 40 days. The HCEs mostly occurred during the heating season (36 days, 90%). The average mass concentrations were highest in spring (34.7 μg/m^3) followed by winter (26.8 μg/m^3), autumn (19.5 μg/m^3), and summer (11.8 μg/m^3). In general, Incheon showed the highest average $PM_{2.5}$ mass concentrations except for winter, in which Seoul had the highest average concentration of 27.9 μg/m^3.

For the carbonaceous species, the average mass concentrations of OC and EC were 5.8 (± 2.7) μg/m^3 and 0.6 (± 0.3) μg/m^3, respectively. Both OC and EC mass concentrations in Incheon were the highest compared to other sites. The carbonaceous species accounted for 26% of the total $PM_{2.5}$ mass concentration over the whole study period, while its seasonal abundances were highest in summer, followed by autumn, winter, and spring (37%, 30%, 27%, and 19%). Both OC and EC concentrations were highest in winter (OC: 6.70 μg/m^3, EC: 0.63 μg/m^3) and lowest in summer (OC: 4.21 μg/m^3, EC: 0.28 μg/m^3). The carbonaceous species accounted for 25% and 30% of the total $PM_{2.5}$ mass during the heating and non-heating season, respectively. Its concentrations were significantly higher during the heating season than during the non-heating season ($p \leq 0.001$).

For the ionic species, the average mass concentrations of NO_3^-,

SO_4^{2-}, and NH_4^+ were 6.3 (± 6.8) μg/m^3, 2.9 (± 2.0) μg/m^3, and 3.1 (± 2.8) μg/m^3, respectively. The average mass concentrations of Na^+, Cl^-, and K^+ were 0.4 (± 0.6) μg/m^3, 0.8 (± 0.6) μg/m^3, and 0.2 (± 0.1) μg/m^3, respectively. The ionic species were the most abundant species of $PM_{2.5}$ and they accounted for 56% of the total $PM_{2.5}$ mass concentration. The abundance of the ionic species was about 60% for each season except for summer (49%). The ionic species accounted for 58% and 49% of the total $PM_{2.5}$ mass during the heating and non-heating season, respectively. Its concentrations were significantly higher during the heating season than during the non-heating season ($p \leq 0.001$).

The average mass concentrations of the crustal elements and non-crustal elements were 1.8 (± 4.2) μg/m^3 and 2.5 (± 1.4) μg/m^3, respectively. The total trace elements accounted for 17% (crustal elements: 7%, non-crustal elements: 10%) of the total $PM_{2.5}$ mass concentration. The average concentration of the crustal elements was highest in spring (3.68 μg/m^3), which might have been affected by transboundary dust events. The average concentration of the non-crustal elements was highest in winter (3.06 μg/m^3), which was the highest among all sites for that season. The trace elements accounted for 17% and 20% of the total $PM_{2.5}$ mass during the heating and non-heating season, respectively. Its concentrations were significantly higher during the heating season than during the non-heating season ($p \leq 0.05$).

2.2.2.3. Gwangju

The mass concentrations ranged from as low as 0.14 to 179.9 μg/m^3 and the average mass concentration of $PM_{2.5}$ was 18.9 (± 16.5) μg/m^3 in Gwangju. The maximum mass concentration was 95.9 μg/m^3

after excluding the Asian Dust events. HCEs in Gwangju occurred for 18 days, which was comparably smaller than the occurrences in Seoul and Incheon. The HCEs mostly occurred during the heating season (16 days, 89%). The average mass concentrations were highest in spring (25.7 μg/m^3) followed by winter (20.7 μg/m^3), autumn (14.4 μg/m^3), and summer (9.02 μg/m^3).

For the carbonaceous species, the average mass concentrations of OC and EC were 4.5 (± 2.1) μg/m^3 and 0.4 (± 0.2) μg/m^3, respectively. The carbonaceous species accounted for 26% of the total $PM_{2.5}$ mass concentration over the study period. The seasonal characteristics for Gwangju were the same as those of Seoul and Incheon, showing the highest abundance in summer (40%), followed by autumn (32%), winter (23%), and spring (20%). The concentrations of OC and EC were the highest in winter (OC: 4.76 μg/m^3, EC: 0.41 μg/m^3) and the lowest in summer (OC: 3.63 μg/m^3, EC: 0.17 μg/m^3). The carbonaceous species accounted for 24% and 32% of the total $PM_{2.5}$ mass during the heating and non-heating season, respectively. Its concentrations were significantly higher during the heating season than during the non-heating season ($p \leq 0.01$).

For the ionic species, the average mass concentrations of NO_3^-, SO_4^{2-}, and NH_4^+ were 4.8 (± 4.8) μg/m^3, 2.7 (± 1.6) μg/m^3, and 2.3 (± 2.0) μg/m^3, respectively. The average mass concentrations of Na^+, Cl^-, and K^+ were 0.3 (± 0.3) μg/m^3, 0.4 (± 0.3) μg/m^3, and 0.1 (± 0.1) μg/m^3, respectively. The ionic species were the most abundant species of $PM_{2.5}$, accounting for 57% of the total $PM_{2.5}$ mass concentration. Seasonally, the highest fractions were in winter (62%), and the lowest was in summer (44%). The ionic species accounted for 60% and 48% of the total $PM_{2.5}$ mass during the heating and non-heating season, respectively. Its concentrations were significantly higher during the

heating season than during the non-heating season ($p \leq 0.001$).

The average mass concentrations of the crustal elements and the non-crustal elements were 1.3 (± 4.2) μg/m^3 and 1.9 (± 1.0) μg/m^3, respectively. The total trace elements accounted for 17% (crustal elements: 7%, non-crustal elements: 10%) of the total $PM_{2.5}$ mass concentration. The average concentration of the crustal elements was the highest in spring (3.37 μg/m^3), while the average concentration of the non-crustal elements was the highest in winter (2.35 μg/m^3). The trace elements accounted for 16% and 20% of the total $PM_{2.5}$ mass during the heating and non-heating season, respectively. Its concentrations were significantly higher during the heating season than during the non-heating season ($p \leq 0.001$).

2.2.2.4. Inter-site comparisons

The average mass concentrations of $PM_{2.5}$ in Seoul, Incheon, and Gwangju all exceeded the annual ambient air quality standard in South Korea (15 μg/m^3). The time series plot of $PM_{2.5}$ mass concentration in each site is available in Figure S1. One-way ANOVA followed by Tukey's post hoc test was performed to compare the differences in the $PM_{2.5}$ levels in the three sites. The $PM_{2.5}$ concentrations in Gwangju were significantly lower than those in Seoul and Incheon. Incheon had the highest average $PM_{2.5}$ mass concentration, but it was not significantly higher than Seoul. Seoul and Incheon are adjacent cities to each other, so the variations in concentrations were similar.

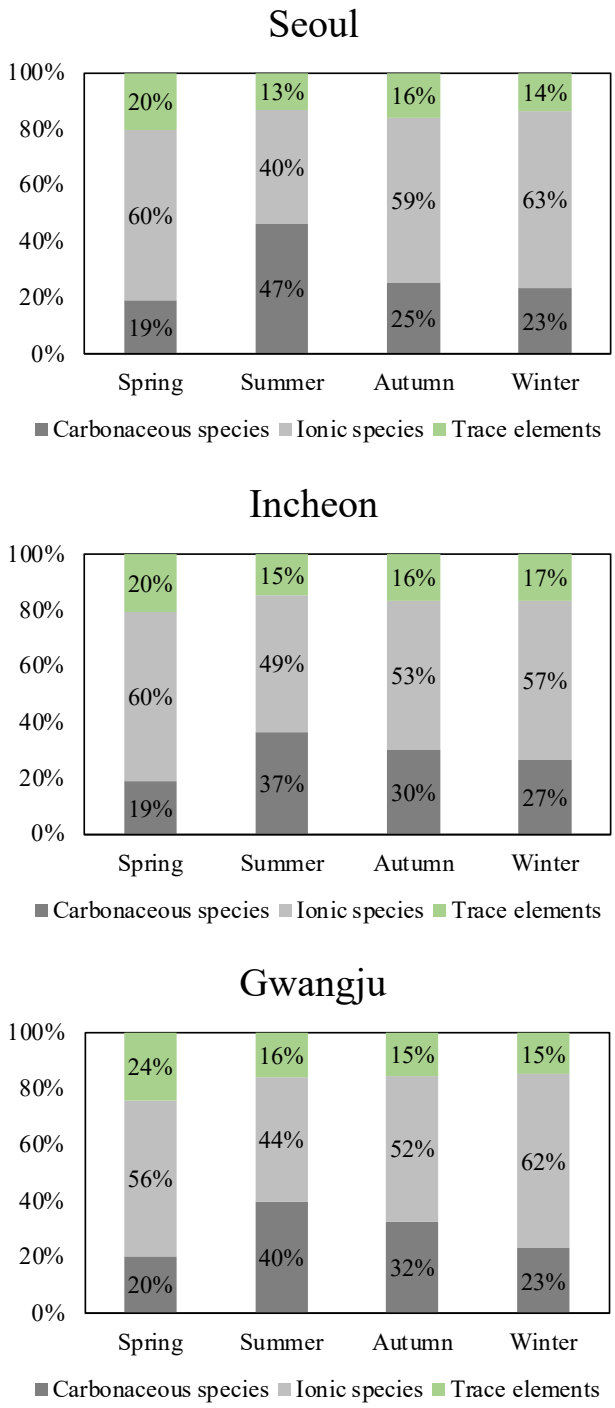

Figure 2. Fractions of chemical constituents in $PM_{2.5}$ by season in Seoul, Incheon, and Gwangju.

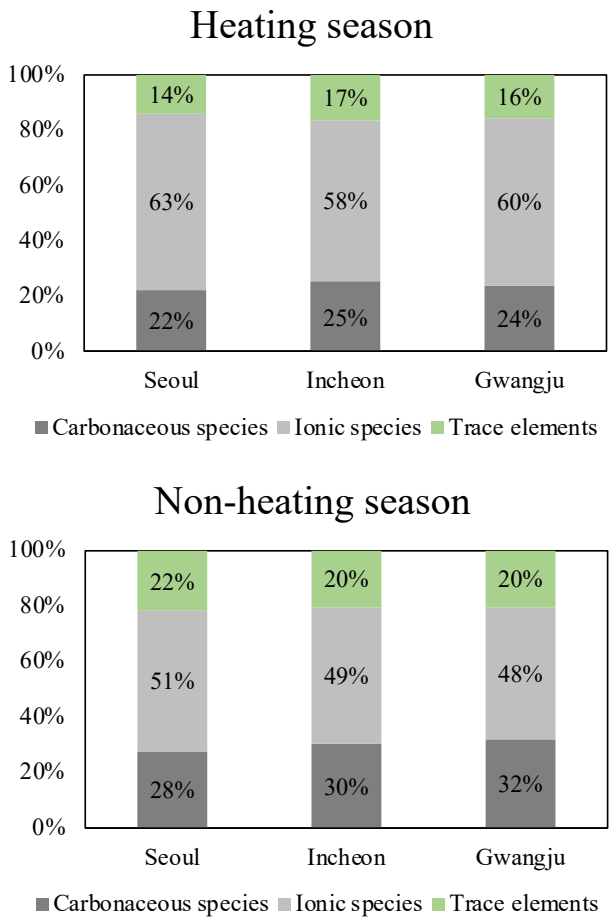

Figure 3. Fractions of chemical constituents in $PM_{2.5}$ by heating and non-heating seasons in Seoul, Incheon, and Gwangju.

Table 7. $PM_{2.5}$ mass concentration and its chemical constituents in Seoul, Incheon, and Gwangju

Site		Seoul		Incheon		Gwangju	
Species	Unit	Average	SD	Average	SD	Average	SD
$PM_{2.5}$	μg/m^3	24.2	21.4	24.6	20.0	18.8	16.5
OC	μg/m^3	4.79	2.22	5.82	2.71	4.45	2.14
EC	μg/m^3	0.36	0.17	0.59	0.30	0.36	0.22
NO_3^-	μg/m^3	6.54	7.03	6.27	6.83	4.82	4.84
SO_4^{2-}	μg/m^3	2.97	1.97	2.94	1.97	2.73	1.58
NH_4^+	μg/m^3	3.11	2.94	3.06	2.81	2.33	1.98
Cl^-	μg/m^3	0.45	0.38	0.77	0.57	0.43	0.31
Na^+	μg/m^3	0.20	0.28	0.41	0.63	0.25	0.35
K^+	μg/m^3	0.17	0.11	0.18	0.10	0.13	0.11
∑Trace elements	μg/m^3	3.48	5.50	4.23	5.56	3.13	5.22
Crustal	ng/m^3	1448.9	4252.4	1763.2	4160.9	1277.3	4240.8
Non-crustal	ng/m^3	2029.9	1246.9	2465.2	1397.9	1856.0	982.4
Mg	ng/m^3	72.8	133.0	74.5	138.0	68.9	149.6
Al	ng/m^3	178.4	665.4	208.1	676.7	167.4	705.8
Si	ng/m^3	513.8	1996.2	617.6	1996.1	490.2	2067.6
S	ng/m^3	1410.6	939.5	1395.8	842.2	1265.2	690.6
Cl	ng/m^3	453.4	414.6	864.1	653.9	453.4	401.6
K	ng/m^3	302.4	476.1	326.3	456.2	246.1	452.2
Ca	ng/m^3	156.8	348.4	205.4	323.8	127.5	319.9
Ti	ng/m^3	18.4	61.4	21.1	60.5	16.1	58.4
V	ng/m^3	0.4	1.6	0.4	1.6	0.3	1.3
Cr	ng/m^3	1.6	1.0	5.2	6.3	1.3	2.8
Mn	ng/m^3	15.0	20.8	27.5	26.8	12.0	19.3
Ba	ng/m^3	5.0	4.7	5.6	5.8	4.7	4.9
Fe	ng/m^3	278.9	727.8	392.6	700.5	230.0	663.6
Ni	ng/m^3	0.9	0.8	3.1	3.9	0.7	0.9
Cu	ng/m^3	3.2	3.5	6.7	11.8	3.3	4.0
Zn	ng/m^3	40.0	35.4	58.4	36.2	28.5	28.7
As	ng/m^3	4.6	6.4	5.4	8.4	1.9	2.4
Se	ng/m^3	0.9	0.9	0.8	0.8	0.9	0.8
Br	ng/m^3	6.1	4.1	8.9	7.4	5.5	6.9
Pb	ng/m^3	15.5	10.6	20.2	15.2	9.4	7.3

2.2.3.Source apportionment using DN-PMF and C-PMF

In this study, 222, 221, and 224 samples were simultaneously collected from September 2020 to March 2022 in Seoul, Incheon, and Gwangju, respectively. The ion balance and the mass closure of each measurement were examined to screen the outliers before creating the input data for the PMF analyses. Both the DN-PMF and C-PMF identified ten sources in Seoul and Incheon, and nine sources in Gwangju. The source profiles with DISP intervals of DN-PMF and C-PMF are shown together, and the time series plots of the source contributions are presented in Figures 4 through 6. The time series plots of the source contributions in each site are shown in Figures 7 through 9. The comparisons of source contributions resolved from the DN-PMF and C-PMF in Seoul, Incheon, and Gwangju are listed in Table 8, Table 10, and Table 12, respectively. The same comparisons by heating seasons in Seoul, Incheon, and Gwangju are listed in Table 9, Table, 11, and Table 13, respectively. Both models resolved the same number of factors, and the source profiles were mostly identical. Slight differences were found in the concentrations and DISP intervals of some species in the DN-PMF. These might be due to the modeling uncertainties or different constrained values; however, the key marker species remained the same in the DN-PMF. The noticeable differences were observed in the source contributions.

The first factor showed high loadings and narrow DISP intervals of NO_3^- and NH_4^+, thus this factor was named secondary nitrate. The secondary nitrate factor explained about 73% of NO_3^- and 54% of NH_4^+ in the C-PMF and DN-PMF results at Seoul, Incheon, and Gwangju, respectively. Low temperatures and high relative humidity accelerate the formation of secondary nitrate (Steinfeld, 1998). In Seoul, the

secondary nitrate source accounted for 46% (10.8 μg/m^3) in the DN-PMF and 40% (9.42 μg/m^3) in the C-PMF. In Incheon, secondary nitrate accounted for 37% (9.06 μg/m^3) in the DN-PMF and 32% (7.71 μg/m^3) in the C-PMF. In Gwangju, the secondary nitrate accounted for 36% (6.54 μg/m^3) in the DN-PMF and 33% (6.01 μg/m^3) in the C-PMF. The secondary nitrate contributions were enhanced in the DN-PMF at all sites. Given the nature of secondary nitrate, its source contributions were significantly higher during the heating season for both the DN-PMF and C-PMF. Relatively higher VCs during the heating season might have scaled up the source contributions in the DN-PMF. The secondary nitrate contributions in Seoul, Incheon, and Gwangju were not statistically different. Local NO_X emissions as well as regional transport both influence secondary nitrate formation, hence the possible source locations were explored using CBPF and PSCF (Ma et al., 2017). The CBPF plot in Seoul showed increased source contributions at low wind speeds of 2 m/s near the sampling site (Figure S4.a). The hotspots highlighted in the CBPF plots were mostly identical to those of the mobile and industry sources, implying substantial influences from local NO_X emissions. In Incheon, the source contribution increased when the southerly wind prevailed, but also during calm atmospheric conditions (Figure S5.a). In Gwangju, there was a high probability that the secondary nitrate was formed locally (Figure S6.a). The CBPF plots of secondary nitrate and biomass burning sources illustrated similar patterns. Several studies concluded that ammonia reduction may significantly reduce secondary inorganic aerosols (Xia et al., 2016; Ye et al., 2019). It can be inferred that ammonia released from agricultural lands in Gwangju might have contributed to the formation of the secondary nitrate aerosols. The J-PSCF map during the heating season highlighted high PSCF values in

Chinese provinces such as Hebei, Shandong, and Jiangsu Provinces (Figure 13.a). The BTH (Beijing-Tianjin-Hebei) region is densely populated by iron and steel industries, which is reported to contribute a significant amount of NO_X and SO_2 emissions (Yang et al., 2019). Shandong and Jiangsu Provinces are reported to emit a significant amount of NO_X from vehicular fleets (Song et al., 2019; Sun et al., 2016).

The secondary sulfate source was characterized by high loadings and narrow DISP intervals of SO_4^{2-} and NH_4^+. This factor explained about 58% of SO_4^{2-} and 22% of NH_4^+ at Seoul, Incheon, and Gwangju, respectively. Secondary sulfate is generally high in summer when strong photochemical reactions promote its formation. Interestingly, its source contributions in the three sites were generally higher during the heating season. This might have resulted from the lack of summertime samples or increased primary sulfate sources during the heating season. In Seoul, the secondary sulfate source accounted for 12% (2.72 μg/m^3) in the DN-PMF and 11% (2.49 μg/m^3) in the C-PMF. Its source contribution in Seoul was significantly higher during the non-heating season in the DN-PMF ($p \leq 0.05$). In Incheon, secondary sulfate accounted for 13% (3.22 μg/m^3) in the DN-PMF in contrast to 19% (4.58 μg/m^3) in the C-PMF. The DN-PMF results were significantly lower than that of C-PMF ($p \leq 0.001$). Its source contributions during the heating season were significantly higher for both models (DN-PMF: $p \leq 0.01$, C-PMF: $p \leq 0.001$). Higher VCs allowed for active dispersion of secondary sulfate, so it was scaled up after normalization. In Gwangju, the secondary sulfate contributions were 15% (2.68 μg/m^3) in the DN-PMF and 16% (2.92 μg/m^3) in the C-PMF. The difference in the source contributions was eliminated in the DN-PMF between the heating and non-heating season. There were no

significant differences in secondary sulfate source contributions among Seoul, Incheon, and Gwangju. On a local scale, the CBPF plots created in Seoul and Incheon indicated that there was a high probability that the secondary source was located SW, where the Incheon port and Sihwa and Banwol industrial complexes are situated (Figure S4.b and Figure S5.b). The SO_2 emissions from these facilities may be considered an important source of local secondary sulfate formation. The CBPF plot in Gwangju implied that the source of secondary sulfate was local rather than regional transport, possibly from industrial activities and coal combustion (Figure S6.c). The CBPF plots of the secondary sulfate and coal combustion in Gwangju during the non-heating season displayed similar inflow directions. The long-range transport of this secondary pollutant was also investigated by the J-PSCF. High PSCF values were found in Shanxi Province, BTH (Beijing-Tianjin-Hebei) region, Shandong, and Jiangsu Provinces, which were mostly identical to the possible source areas of secondary nitrate. Shanxi Province has abundant coal resources, and active coal-related activities pose health risks from heavy metals as well as a significant amount of sulfur emissions can be inferred (Li et al., 2022; Su et al., 2021). The potential source areas of secondary sulfate also included the YRD region and some parts of the East China Sea, areas well known for busy vessel traffic (Bie et al., 2021; Kang et al., 2019). Intensive industrial production and traffic activities well characterize the YRD region, where several coal-fired power plants and industrial boilers emit SO_2 gases that facilitate its secondary formation (Jia et al., 2020). The PSCF map generated during the heating season included Jiaxiang city in Shandong Province, where thermal power plants are operated by coal combustion to provide electricity for urban and industrial uses (Figure 13.b). Sulfate emissions from coal combustion

might have contributed to the formation and transboundary transport of secondary sulfate to the coastal areas of South Korea (Kuang et al., 2022). The PSCF map during the non-heating season indicated the Yellow Sea, Zhejiang and Fujian Provinces, and the coastal areas near Minamata in Japan as the possible source locations (Figure 14.a). The Shanghai port, one of the world's busiest ports on the coastal areas of the Yellow Sea, may be held responsible for intensive sulfur emissions from shipping activities (Wang et al., 2019).

High loadings and tight DISP intervals of OC and K^+ were used to characterize the biomass burning emissions. OC and K^+ explained 22% and 59% of biomass burning factor, respectively. Water-soluble potassium, which is present in biomass burning plumes, is a well-known tracer for biomass burning identification (Cheng et al., 2013; Echalar et al., 1995). The biomass burning source contributions in Seoul accounted for 10% (2.44 μg/m^3) in the DN-PMF and 17% (3.95 μg/m^3) in the C-PMF. Its source contribution in the DN-PMF was significantly lower than that in the C-PMF ($p \leq 0.001$). Since there are no farmlands in the urban areas of Seoul, the biomass burning emissions can be considered as meat-cooking origins. To investigate which meteorological parameter resulted in the differences in the source contribution, the hourly wind speeds, mixing layer heights, and VCs were categorized into two different time groups and compared. One group represented the dining hours (17:00 to 23:00) when people gather after working hours and dine, and the other hours (00:00 to 16:00) when intensive meat-cooking activities were not expected. The mixing layer heights and VCs were significantly lower during the dining hours, while the wind speeds were significantly higher during the other hours (Tables S1 through S3). Stable atmospheric conditions can be inferred from the diurnal patterns as shown in Figure S3. One

possible explanation was that the meat-cooking emissions concentrated during the dining hours when the VCs were low, which is not a favorable condition for local dispersion, and the DN-PMF took this into account and scaled down the source contribution. Its source contribution increased from the northerly winds at low wind speeds of 2-4 m/s (Figure 10). Its CBPF hot spots implied the possible source areas near Hongik University, Jongno-gu, and Yongsan-gu, which are among the busiest places in Seoul where many people gather for meetings on the weekends. Especially, numerous large-scale meat-cooking restaurants are in Samgakji, Yongsan-gu. The source contribution in Seoul increased from Friday throughout the weekend in the weekday plot. Also, it showed a slight increase during the winter of 2021 compared to that of 2020. Strict social distancing measures were alleviated in November 2021, and the source contribution increment reflected the increased social gatherings in Seoul. These results imply that the cooking emissions affected the Seoul sampling site. In Incheon, the biomass burning source accounted for 12% (2.85 μg/m^3) in the DN-PMF and 10% (2.36 μg/m^3) in the C-PMF. Interestingly, the source contributions were significantly higher during the non-heating season, showing peaks in April and May for both DN-PMF and C-PMF ($p \leq 0.001$). However, significant differences in its source contribution in the DN-PMF and C-PMF were found during the heating season. Significantly higher wind speeds and relatively higher VCs during the heating season provided favorable conditions for local dispersion, thus the source contribution was scaled up in the DN-PMF. The CBPF plot in Incheon showed a high probability that the source areas were present in the NE and the vicinity of the sampling site (Figure 11). A separate CBPF plot created during the non-heating season indicated the NE direction, and its source strength was most

likely the strongest during that season. There was a cluster of meat-cooking restaurants in Gimpo-si, which is situated NE of Incheon. Several camping sites were dispersed near the Incheon site and alongside the Han River. The unprecedented pandemic has caused dramatic changes in people's lives in Korea, one of which is increased recreational activities. Camping activities soared in 2021 compared to 2020, and outdoor barbecuing activities might have contributed to the peak in its source contribution. The biomass burning contributions were different among the three sites (Kruskal-Wallis, $p \leq 0.05$). The post hoc analysis using Dunn's method revealed that only Incheon had a significantly higher source contribution than Gwangju. In Gwangju, the source contributions were 13% (2.47 μg/m^3) in the DN-PMF and 14% (2.62 μg/m^3) in the C-PMF. There were no significant differences in its DN-PMF and C-PMF resolved source contributions. The biomass burning source was introduced to Gwangju from the SSW at wind speeds of 6 m/s where the local farmlands are located 10 km south of the sampling site (Figure 12). As a less urban area compared to Seoul and Incheon, field crops residue burning and illegal incineration of plastic wastes after harvesting were the likely sources of biomass burning in Gwangju. The source contribution was dominant during the heating season, which can be explained by the field burning of crops in harvesting seasons including November. The monthly source contribution plots displayed the highest peak in February 2022. Also, combustion activities were frequent on the weekends when the public officers are off duty. Although the Korean government implemented stringent measures to prevent uncontrolled agricultural burning, it appears that there are still many rural residents that burn agricultural wastes. In short, the biomass burning source contributions increased on weekends at all sites for different reasons (Figure S7).

Possible influences of biomass burning activities from distant areas were investigated by the J-PSCF analysis. The J-PSCF map created during the heating season suspected the Inner Mongolia, BTH (Beijing-Tianjin-Hebei) region, and Jiangsu Provinces as the potential source locations of biomass burning emissions (Figure 13.c). Many studies have reported that agriculture-related open burning and biomass fuel consumption in rural areas as the main contributor to biomass burning emissions in the BTH region (Dong et al., 2022; Li et al., 2020; Zhao et al., 2022). A study conducted in Ordos city, located in the southeastern part of Inner Mongolia, found regional biomass burning and biogenic sources accounted for about 40% (Khuzestani et al., 2018). Despite the recent stringent air quality policies in China, open burning of crop residues is still in practice (Wang et al., 2022).

Mobile sources featured high loadings and narrow DISP intervals of OC, EC, Fe, and Ti at all sites. OC and EC are well-known molecular markers associated with traffic (Chow et al., 2003; El Haddad et al., 2009; Schauer et al., 2002). The mobile factor explained about 33% of OC and 44% of EC from the model results at all sites. Some fractions of Mg, Al, Si, and Ca were observed in the profiles. These crustal elements are non-exhaust species mostly originating from roadside dust and can also be used as tracers for vehicular source (Viana et al., 2008). Zn, Cu, and Fe, which are indicators of additive in motor oil (Zn) and abrasion of brake linings (Cu, Fe), were recognized in the source profiles with small uncertainty bounds at Incheon and Gwangju (Thorpe & Harrison, 2008). In Seoul, the mobile source accounted for 9% (2.18 μg/m^3) and 10% (2.37 μg/m^3) in the DN-PMF and C-PMF, respectively. Generally, vehicle activities show no seasonal patterns, which was consistent with the model results in Seoul. There were no significant differences in the mobile source contributions between the

heating and non-heating seasons in Seoul for both DN-PMF and C-PMF results. The CBPF plot suggests that Seoul was influenced by traffic emissions at NW winds at low windspeeds under 5 m/s (Figure 10). Olympic-daero and Gangbyeon expressway and local roads, which suffer from frequent traffic congestion, were identified from the CBPF plot. In Incheon, the mobile source contribution was significantly reduced to 12% (2.84 μg/m^3) in the DN-PMF compared to 15% (3.70 μg/m^3) in the C-PMF ($p \leq 0.001$). The statistical results were different for DN-PMF and C-PMF in Incheon. The DN-PMF source contribution was significantly lower during the heating season ($p \leq 0.05$). The lower contributions in the DN-PMF implied that traffic emissions peaking at commute hours were scaled down. Thus, more reasonable temporal patterns were obtained in the DN-PMF through dispersion normalization. There was a high probability that the source location was located north of the sampling site (Figure 11). The busy traffic in the 2nd Capital Region Ring Expressway, which connects Incheon and Gimpo-si, was the likely source area of traffic emissions. In Gwangju, the mobile source accounted for 15% (2.77 μg/m^3) in the DN-PMF and 14% (2.52 μg/m^3) in the C-PMF. Its mobile source contributions resolved in the DN-PMF and C-PMF were not statistically different ($p = 0.214$). However, the effects of dispersion normalization were also recognized in the DN-PMF results in Gwangju. While the C-PMF result showed that there were significant differences ($p = 0.001$) between the heating and non-heating seasons, the DN-PMF showed no significant differences ($p = 0.12$). The CBPF plot of Gwangju implied the local influences at very low wind speeds (approximately 2 m/s) in the east. An expressway (Honam expressway) and local roads are close to the sampling site, where frequent traffic congestion occur (Figure 12). The mobile source contributions in the three sites were not

significantly different from each other.

The soil factor included representative crustal elements such as Mg, Al, Si, Ca, Ti, and Mn illustrating high concentrations and tight DISP intervals. OC, EC, and NO_3^- also appeared in the source profiles of the three sites. The soil source in Seoul accounted for 6% (1.48 μg/m^3) in the DN-PMF and 6% (1.32 μg/m^3) in the C-PMF. In Incheon, the soil contribution accounted for 7% (1.60 μg/m^3) in the DN-PMF, while it accounted for 4% (1.00 μg/m^3) in the C-PMF. The soil contribution in the DN-PMF was significantly higher. In Gwangju, the soil source accounted for 3% (0.622 μg/m^3) in the DN-PMF and 5% (0.903 μg/m^3) in the C-PMF. The soil source contribution in Incheon was significantly higher in the DN-PMF in Incheon ($p \leq 0.01$), while it was higher in the C-PMF in Gwangju ($p \leq 0.01$). The differences in the source contributions might come from the fact that soil sources are less likely influenced by local dispersion, but further evidence needs to be established. The CBPF plots of Seoul illustrated dominant flow from the west at all wind speed ranges (Figure S4.e). Incheon appeared to be affected by the soil particles from NW winds with high wind speeds of over 10 m/s (Figure S5.f). Its CBPF plots in Gwangju showed increased soil contribution at SW winds with wind speeds of 5 m/s (Figure S6.g). In general, the soil source in the three sites was most likely to originate from nearby mountains and road dust resuspension. The soil contribution in Gwangju was significantly lower than the other sites (Kruskal-Wallis, $p \leq 0.05$). Located far south of Seoul and Incheon, Gwangju may have received less influence from transboundary soil particles. Also, the relatively smaller traffic volume in Gwangju might have caused less amount of resuspended road dust.

The waste incinerator source was identified by high loadings and a narrow DISP interval of Cl^-. Cl^- emission is largely from the

combustion of polyvinylchloride plastics (Li et al., 2019; Yang et al., 2016). Additionally, small portions of Pb and Zn were also found at Incheon and Gwangju. Pb and Zn can be emitted from municipal waste incinerators and were reported to be found in cyclone ashes (Gao et al., 2002; Morishita et al., 2006; Yoo et al., 2002). Cl^- explained 71% of the incinerator factor on average for all sites. In Incheon, species such as NH_4^+, K^+, Pb, and Zn explained 16% of the source characteristics, while the same species explained less than 10% in Seoul and Gwangju sites. In Seoul, the waste incinerator source accounted for 5% (1.17 μg/m^3) and 6% (1.32 μg/m^3) in the DN-PMF and C-PMF. In Incheon, the source contributions accounted for 10% (2.46 μg/m^3) in the DN-PMF and 10% (2.40 μg/m^3) in the C-PMF. In Gwangju, the source contributions were 7% (1.29 μg/m^3) in the DN-PMF and 5% (0.910 μg/m^3) in the C-PMF. The waste incinerator contributions in all sites were significantly higher during the heating season for both DN-PMF and C-PMF results ($p \leq 0.001$). The waste incinerator source in Seoul showed dependence on NW and SSE winds at wind speeds of 5 m/s (Figure 10). Yangcheon and Mapo resource recovery centers are located 10 km NW of the sampling site in Seoul. Other resource recovery centers such as Anyang and Seongnam city municipal waste incinerators were found in the SSE of the sampling site. Incheon was affected by waste incineration emissions from the SE at high wind speeds of 6 m/s, where three major waste management facilities are situated (Figure 11). Bucheon-si waste management facility, Gwangmyeong resource recovery center, and Ansan resource recovery centers are located SE of Incheon. Since the sampling sites in Seoul and Incheon are relatively nearby, the waste incinerator sources affected both sites depending on the dominant wind directions. The CBPF plot created for Gwangju showed increased source

contributions when the SW wind with high wind speeds of over 10 m/s prevailed (Figure 12). The CBPF plot overlayed on Google Maps identified a municipal waste incinerator in the SW direction of the sampling site. The waste incinerator source contribution was significantly higher in Incheon compared to the other two cities (Kruskal-Wallis, $p \leq 0.05$), while the differences were not significant for Seoul and Gwangju.

Coal combustion can be distinguished by distinctive tracers such as As and Pb (Gieré et al., 2006; Wang et al., 2006). As and Pb are emitted from coal combustion processes such as coal-fired power plants. The two species explained 80% and 32% of the coal combustion activity at all sites, respectively. The coal combustion source contributions in Seoul and Gwangju were significantly higher during the non-heating season in both the DN-PMF ($p \leq 0.001$) and C-PMF ($p \leq 0.01$). In contrast, the DN-PMF and C-PMF results in Incheon were not statistically different between the heating and non-heating seasons. In Seoul, the coal combustion source accounted for 4% (0.986 μg/m^3) in the DN-PMF and 4% (0.852 μg/m^3) in the C-PMF. In Incheon, it accounted for 4% (0.924 μg/m^3) in the DN-PMF and 4% (0.896 μg/m^3) in the C-PMF. In Gwangju, the source contribution accounted for 5% (0.953 μg/m^3) in the DN-PMF and 8% (1.40 μg/m^3) in the C-PMF. The CBPF plots in Seoul showed the source inflow direction from the NW at low wind speeds of less than 3 m/s and SW with high wind speeds of over 6 m/s (Figure 10). Multiple small-scale industries located in Gimpo-si are NW of Seoul (Park et al., 2019). Siwha and Banwol industrial complexes are situated at the SW of Seoul. The CBPF plots at the upper 25% and 5% criteria displayed different source locations in Incheon. The upper 25% CBPF plot illustrated high source contribution in the close NW (Figure 11). The Hankun industrial

complex was located very close to Incheon. The CBPF at the upper 5% implied significant influences from the SW at relatively high wind speeds of 6 m/s. Yeongheung power plant and the Incheon Coal Pier were situated in SW and their emissions were likely to contribute 3.5 μg/m^3 to Incheon. The coal combustion source was introduced in Gwangju by the northerly winds at wind speeds of 4 m/s (Figure 12). There were no coal-fired power plants near the vicinity of Gwangju, instead, a crematory and a few steel manufacturers were situated in the north direction. Hazardous air pollutants such as Pb, Cd, and Hg, along with As are reported to be emitted from crematories (Xue et al., 2016). As is also associated with the metallurgical industries (Thomaidis et al., 2003). A source apportionment study in Gwangju in 2014 identified this source as the smelting process (Yu & Park, 2021). The coal combustion source profile in Gwangju also featured Mg and Zn, tracers for non-ferrous metallurgy, and together with As and Pb supported the possible influence of the metallurgical industries found by the CBPF. The source contributions in the three sites were compared, and no significant differences were found. There was a noticeable decrease in coal combustion contribution at all sites. The dramatic dip in source contributions occurred at the beginning of 2021. To tackle $PM_{2.5}$ pollution during the winter season, the Korean government conducted the first seasonal PM management plan, which started from December 2019 to March 2020. The study period includes two seasonal management periods (SMP) (second SMP: December 2020-March 2021, third SMP: December 2021-March 2022). The coal combustion source contributions of periods before the second SMP (September 2020-November 2020) and during the SMP (December 2020-March 2021) were compared. There was an average of 78% (73%-85%) reduction between the two periods. The average source

contributions during the two periods for each site are summarized in Table 14. During the SMP, intensive reduction efforts are required in various sectors. In the case of coal-fired power plants, the power generation is limited to 80%, and on extreme pollution days, they are required to shut down. These results suggest that the $PM_{2.5}$ mitigation policies were effective.

The next source displayed characteristics of oil combustion sources mixed with industrial sources at all sites. Ni and V are distinctive tracers for crude oil combustion from vessels (Jeong et al., 2017; Schembari et al., 2014). The oil combustion source profiles at all sites featured some industrial fingerprints such as Fe, Cu, and Zn, thus it was named industry/oil combustion source. Cr, Mn, Fe, Cu, Zn, and Pb are tracer species of various types of industrial activities, in which Fe and Mn represent ferrous metallurgy and Cu, Zn, and Pb represent non-ferrous metallurgy sources (Querol et al., 2007; Swietlicki et al., 1996). Seoul featured another industrial source with narrow DISP intervals of Cr, Mn, Zn, and Pb, most likely indicating emissions from non-ferrous metallurgy industries. Incheon was affected by a unique metal plating source featuring large fractions and short DISP intervals of Cr and Ni (Sun et al., 2017). In Seoul, the industry/oil combustion source accounted for 2% (0.492 μg/m^3) and 2% (0.508 μg/m^3) in the DN-PMF and C-PMF, respectively. In Incheon, its contributions were 2% (0.536 μg/m^3) and 1% (0.295 μg/m^3) in the DN-PMF and C-PMF, respectively. The source contribution in Incheon was significantly higher in the DN-PMF ($p \leq 0.001$). Higher wind speeds and VCs normalized the source contribution during the heating season. Constant sea breeze during the non-heating season might have affected the atmospheric dispersion, in which the DN-PMF scaled the source contribution up. In Gwangju, the industry/oil

combustion source accounted for 3% (0.483 μg/m^3) and 2% (0.416 μg/m^3) in the DN-PMF and C-PMF, respectively. The CBPF plots of the industry/oil combustion source during the non-heating season in Seoul indicated a high probability that the source locations were in the SW and SE (Figure 10). It was likely that the emissions from shipping activities at ports in Incheon flowed into Seoul at relatively high wind speeds of 6 m/s. Its CBPF plots for the whole study period also pointed out the industrial complex Seongnam-si, located 20 km SE of Seoul. Also, the CBPF plot of the industry source in Seoul showed increased source contribution from the NW at low wind speeds of 3 m/s or less. Several industrial complexes were found in the west of the sampling site. Seoul Digital Industrial Complex and Onsu Industrial Complex are within 10 km of the Seoul site. These industrial complexes consist of petrochemical, machinery, and metallurgical industries. The CBPF plot of Incheon highlighted the increment of the metal plating source contribution when the NW winds with wind speeds higher than 10 m/s prevailed (Figure 11). A cluster of metallurgy industries was situated 5 km NW of Incheon. In Incheon, the CBPF plots using the upper 25% and 5% highlighted quite different possible source locations. Using the conventional upper 25% criteria, the industrial complex in Paju-si appeared to be the possible source. The industrial complex in Paju-si is located 20 km NE of Incheon, and its source contribution increased at relatively high wind speeds of 8 m/s or more. The CBPF plot at the upper 5% revealed dominant source contributions of up to 1.9 μg/m^3 from the south wind sector. The Namdong Industrial Complex and the port of Incheon are all situated south of Incheon. The probable source locations pointed out in the CBPF plots in Gwangju were mainly in the west at wind speeds of less than 6 m/s, where a cluster of national industrial complexes was present (Figure 12). Three major industrial

complexes in the west of the sampling site are the Pyeongdong industrial complex, Hanam industrial complex, and Bonchon industrial complex. The J-PSCF map of the industry/oil combustion source during the non-heating season highlighted the East Sea, Yellow Sea, and some East China Sea areas as the source locations, coinciding with the shipping lanes (Figure 14.b). It appears that the three Korean cities are influenced by domestic port activities as well as vessel traffics in the distant seas. The industry/oil combustion source contributions were not statistically different among the three sites.

The high presence of Na^+ with tight DISP interval with some Cl^- implied the influence of marine aerosols. Fresh sea salt is reported to be found exclusively in coarse particle fraction (Zhao & Gao, 2008), and the lack of Cl^- indicated that this source was aged sea salt. The long retention time of sea salt particles in the atmosphere provide open opportunities for chloride chemistry, such as reaction with HNO_3 and H_2SO_4, which depletes Cl^- (Knipping & Dabdub, 2003; Yao & Zhang, 2012). Some presence of Cl^- was observed in the source profile in Incheon, which implied that this source was mixed with fresh sea salts. This well agreed with the proximity of the Incheon site to the West Sea. The aged sea salt factor explained 84% of Na^+ at all sites. In Seoul, the aged sea salt source accounted for 3% (0.521 μg/m^3) in the DN-PMF and 3% (0.559 μg/m^3) in the C-PMF. Significantly higher source contribution was found during the heating season in the C-PMF ($p \leq 0.01$), which was reduced in the DN-PMF for the same period ($p = 0.257$). Aged sea salt particles are long-range transported particles that are easily affected by wind speeds and directions. DN-PMF enhances the regional nature of aged sea salt by lowering its local effect (Dai et al., 2020). The differences in the source contribution indicate that the DN-PMF reduced the influence of local dispersion in

Seoul. Under the reduced local dispersion effects, the dominant NW winds during the heating season might have introduced the aged sea salt particles into Seoul. In Incheon, the aged sea salt accounted for 2% (0.586 μg/m^3) and 3% (0.616 μg/m^3) in the DN-PMF and C-PMF, respectively. The effects of dispersion normalization were not found in Incheon as well as the differences between the heating and non-heating seasons. Incheon is relatively close to the West Sea, so the influences of aged sea salt particles were mostly driven by its regional effects. The dispersion normalization of the local effects on the aged sea salt source might not have played an important role in Incheon. Gwangju showed similar source contributions in both DN-PMF and C-PMF, which were 3% (0.521 μg/m^3) and 3% (0.559 μg/m^3), respectively. The DN-PMF and C-PMF results were not statistically different. Gwangju showed significantly higher source contribution during the non-heating season for both DN-PMF ($p \leq 0.01$) and C-PMF ($p \leq 0.05$). Overall, there were no inter-site differences in the aged sea salt contributions among the three. The aged sea salt source contribution increased in Seoul at winds from the SW and the SE at wind speeds of 5 m/s. The CBPF plot drawn for the non-heating season indicated influences from the SW and the east, which well agreed with the dominant westerly wind in summer in Seoul (Figure 10). The aged sea salt particles were introduced to Incheon with fast NW winds and slow SW winds (Figure 11). The West Sea is located west of Incheon, and the proximity of the ocean is well reflected in its CBPF plot. The CBPF plot of Gwangju implied influences of the aged sea salt particles from the south and SW at moderate wind speeds where the western coastal areas are situated (Figure S6.h).

Table 8. Comparison of source contribution resolved in DN-PMF and

C-PMF in Seoul (yellow shades indicate $p \leq 0.05$)

Source	p value	Higher
Secondary nitrate	0.081	-
Secondary sulfate	0.942	-
Biomass burning	$p \leq 0.001$	C-PMF
Mobile	0.26	-
Soil	0.12	-
Waste incinerator	0.179	-
Coal combustion	0.81	-
Industry	0.932	-
Industry/Oil combustion	0.96	-
Aged sea salt	0.048	C-PMF

Table 9. Comparison of source contributions in the DN-PMF and C-PMF by heating seasons in Seoul (yellow shades indicate $p \leq 0.05$)

Source	DN-PMF		C-PMF	
	p value	Higher	p value	Higher
Secondary nitrate	$p \leq 0.001$	Heating	$p \leq 0.001$	Heating
Secondary sulfate	0.049	Non-heating	0.424	-
Biomass burning	$p \leq 0.001$	Heating	$p \leq 0.001$	Heating
Mobile	0.927	-	0.942	-
Soil	0.005	Heating	0.024	Heating
Waste incinerator	$p \leq 0.001$	Heating	$p \leq 0.001$	Heating
Coal combustion	0.007	Non-heating	0.009	Non-heating
Industry	0.023	Non-heating	0.419	-
Industry/Oil combustion	$p \leq 0.001$	Non-heating	$p \leq 0.001$	Non-heating
Aged sea salt	0.257	-	0.002	Heating

Table 10. Comparison of the source contributions resolved in DN-PMF and C-PMF in Incheon (yellow shades indicate $p \leq 0.05$)

Source	p value	Higher
Secondary nitrate	0.121	-
Secondary sulfate	$p \leq 0.001$	C-PMF
Biomass burning	0.011	DN-PMF
Mobile	0.021	C-PMF
Waste incinerator	0.91	-
Soil	0.009	DN-PMF
Coal combustion	0.622	-
Aged sea salt	0.108	-
Industry/Oil combustion	$p \leq 0.001$	DN-PMF
Metal plating	0.445	-

Table 11. Comparison of the source contributions in the DN-PMF and C-PMF by heating seasons in Incheon (yellow shades indicate $p \leq 0.05$)

Source	DN-PMF		C-PMF	
	p value	Higher	p value	Higher
Secondary nitrate	$p \leq 0.001$	Heating	$p \leq 0.001$	Heating
Secondary sulfate	0.008	Heating	$p \leq 0.001$	Heating
Biomass burning	$p \leq 0.001$	Non-heating	$p \leq 0.001$	Non-heating
Mobile	0.153	-	0.022	Heating
Waste incinerator	$p \leq 0.001$	Heating	$p \leq 0.001$	Heating
Soil	0.062	-	0.225	-
Coal combustion	0.923	-	0.843	-
Aged sea salt	0.223	-	0.642	-
Industry/Oil combustion	$p \leq 0.001$	Non-heating	$p \leq 0.001$	Non-heating
Metal plating	0.021	Heating	0.048	Heating

Table 12. Comparison of the source contributions resolved in DN-PMF and C-PMF in Gwangju (yellow shades indicate $p \leq 0.05$)

Source	p value	Higher
Secondary nitrate	0.336	-
Mobile	0.214	-
Secondary sulfate	0.303	-
Biomass burning	0.415	-
Waste incinerator	0.08	-
Coal combustion	0.01	C-PMF
Soil	0.006	C-PMF
Aged sea salt	0.267	-
Industry/Oil combustion	0.439	-

Table 13. Comparison of the source contributions in the DN-PMF and C-PMF by heating seasons in Gwangju (yellow shades indicate $p \leq 0.05$)

Source	DN-PMF		C-PMF	
	p value	Higher	p value	Higher
Secondary nitrate	$p \leq 0.001$	Heating	$p \leq 0.001$	Heating
Mobile	0.12	-	0.001	Heating
Secondary sulfate	0.467	-	0.021	Heating
Biomass burning	0.103	-	0.087	-
Waste incinerator	$p \leq 0.001$	Heating	$p \leq 0.001$	Heating
Coal combustion	$p \leq 0.001$	Non-heating	0.002	Non-heating
Soil	0.073	-	0.097	-
Aged sea salt	0.011	Non-heating	0.029	Non-heating
Industry/Oil combustion	$p \leq 0.001$	Non-heating	$p \leq 0.001$	Non-heating

Table 14. Average source contributions of coal combustion source for periods before and during the second SMP (unit: μg/m^3)

Site	Before second SMP	Second SMP	Difference
Seoul	2.60	0.400	-85%
Incheon	2.15	0.482	-78%
Gwangju	2.06	0.556	-73%

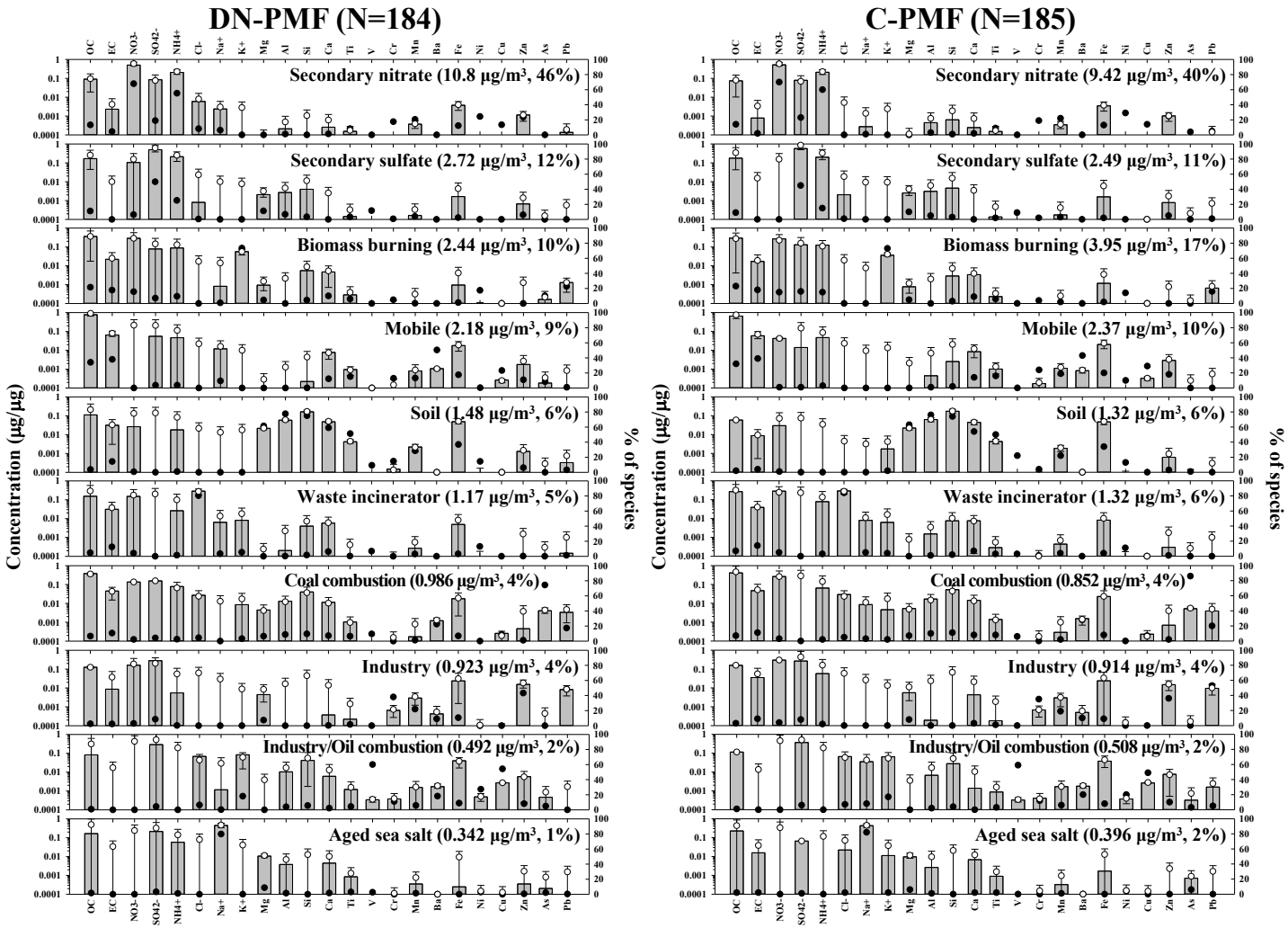

Figure 4. Source profiles in Seoul (left: DN-PMF, right: C-PMF).

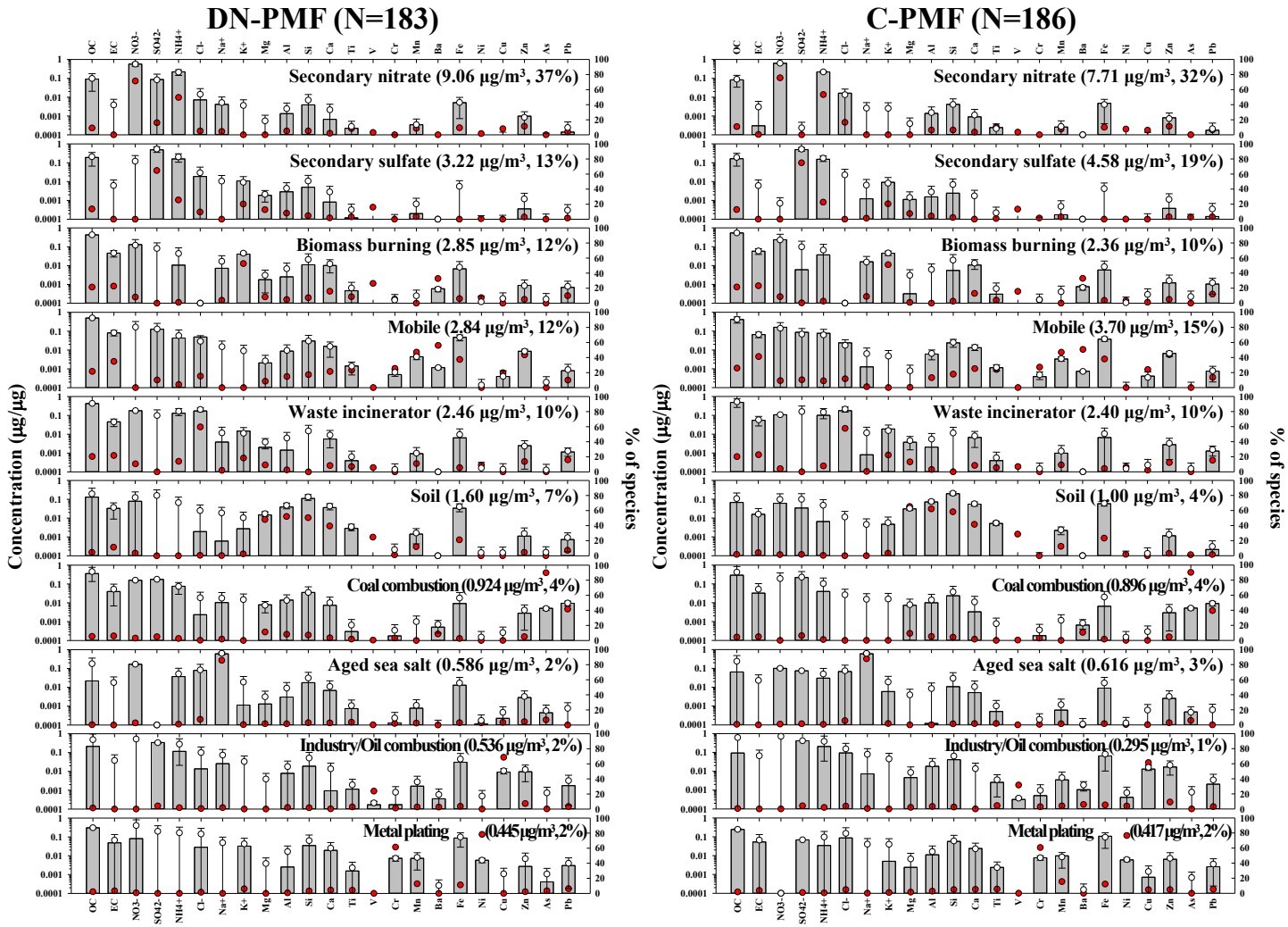

Figure 5. Source profiles in Incheon (left: DN-PMF, right: C-PMF).

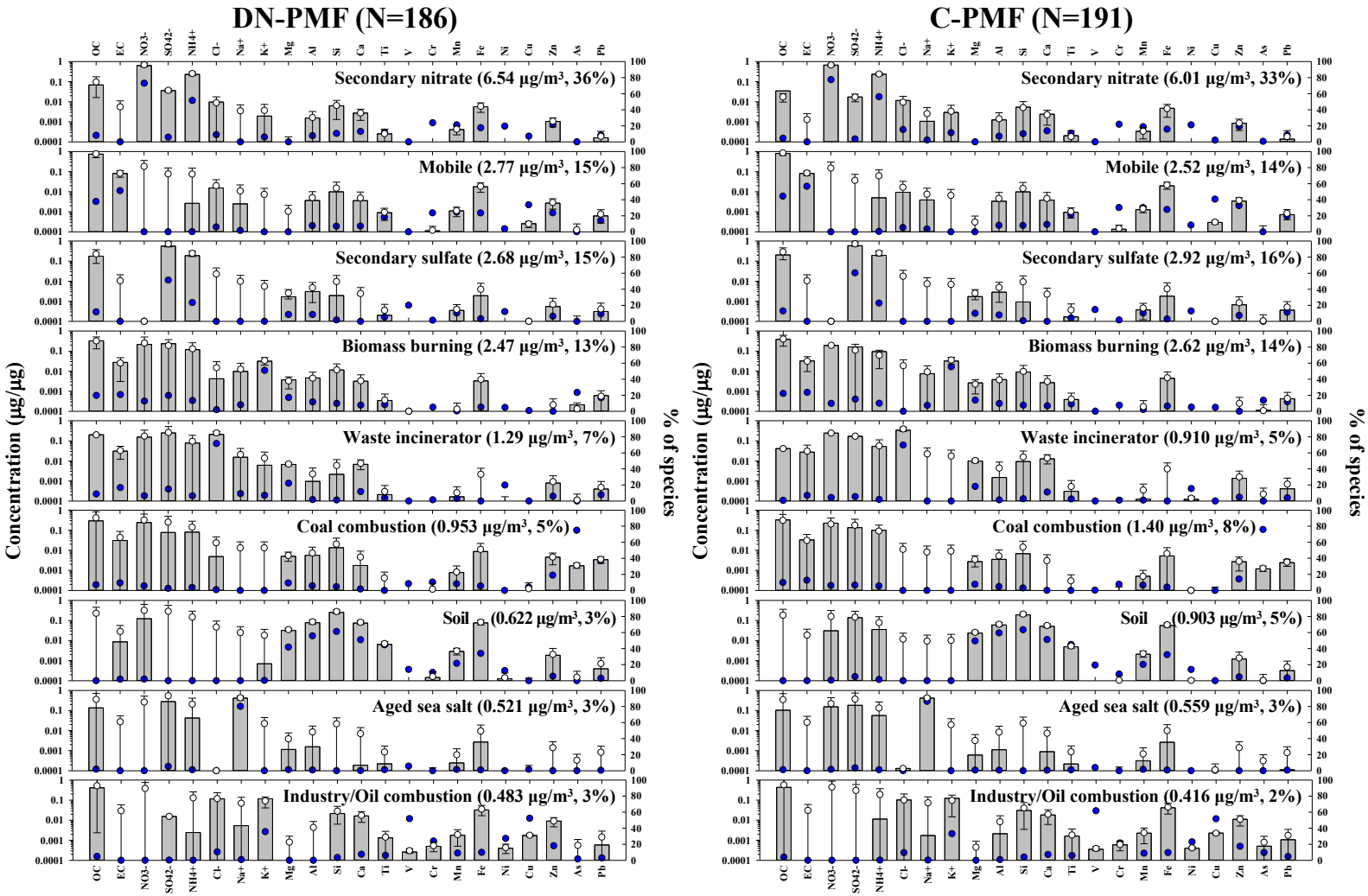

Figure 6. Source profiles in Gwangju (left: DN-PMF, right: C-PMF).

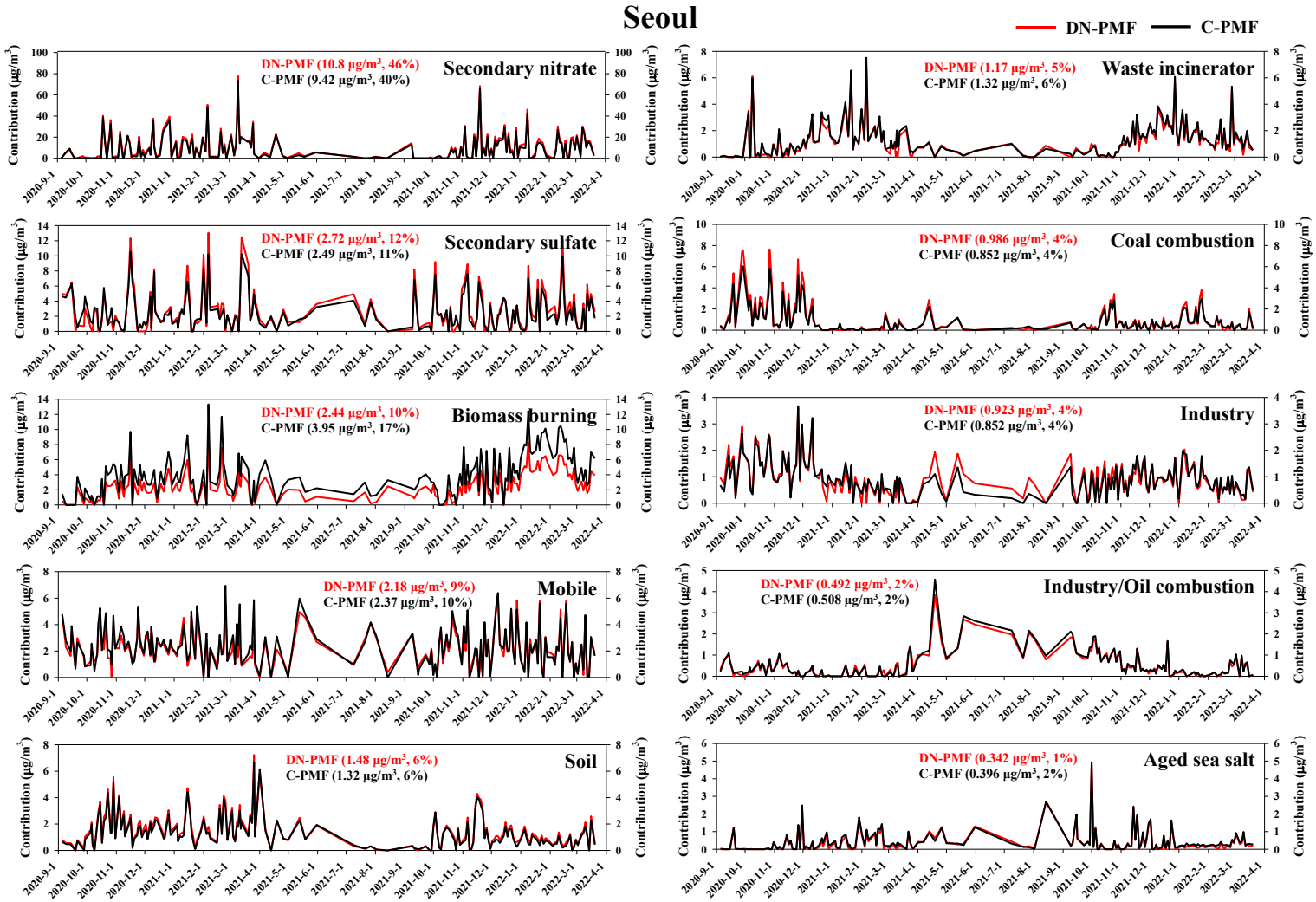

Figure 7. Source contributions from DN-PMF and C-PMF in Seoul.

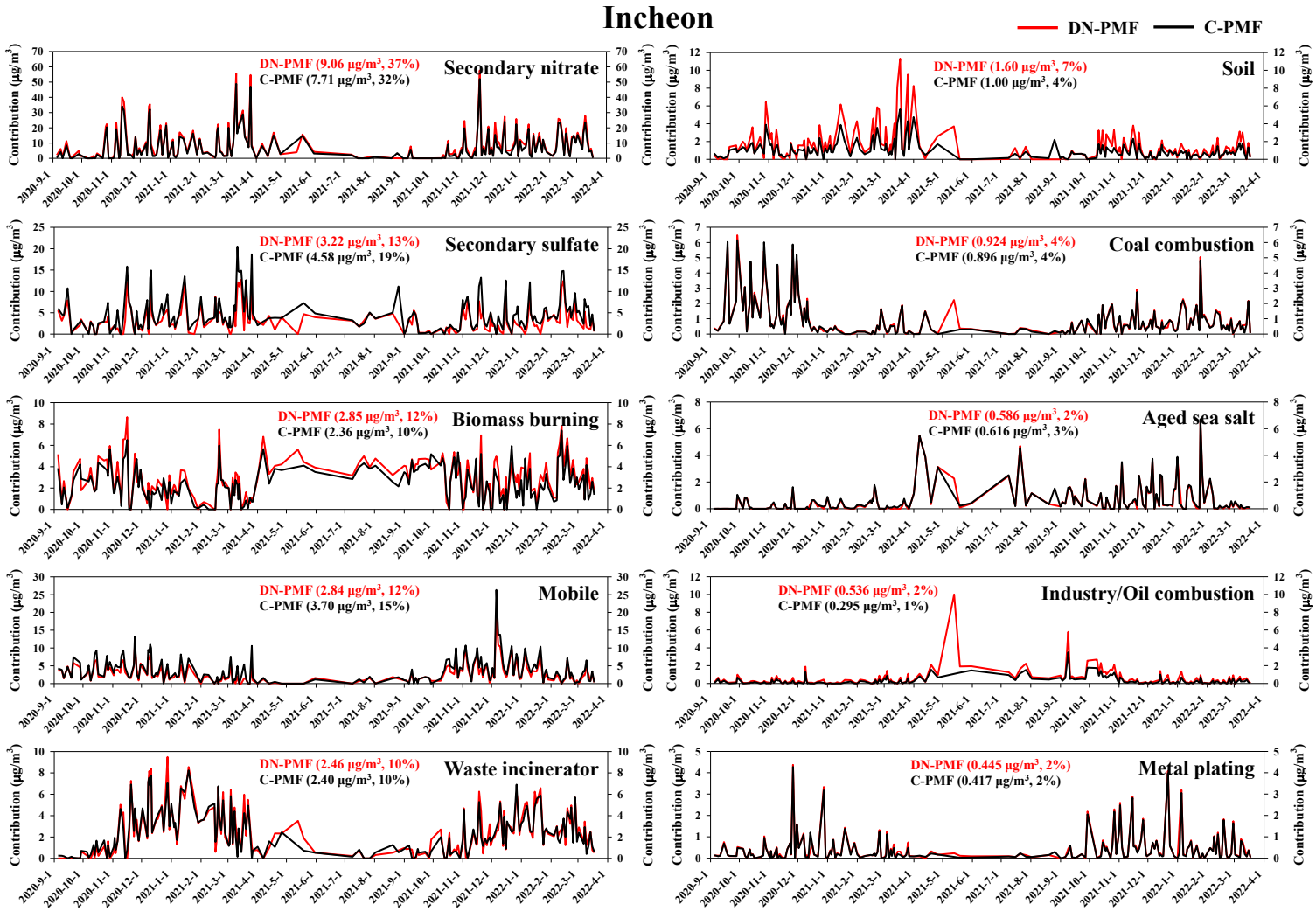

Figure 8. Source contributions from DN-PMF and C-PMF in Incheon.

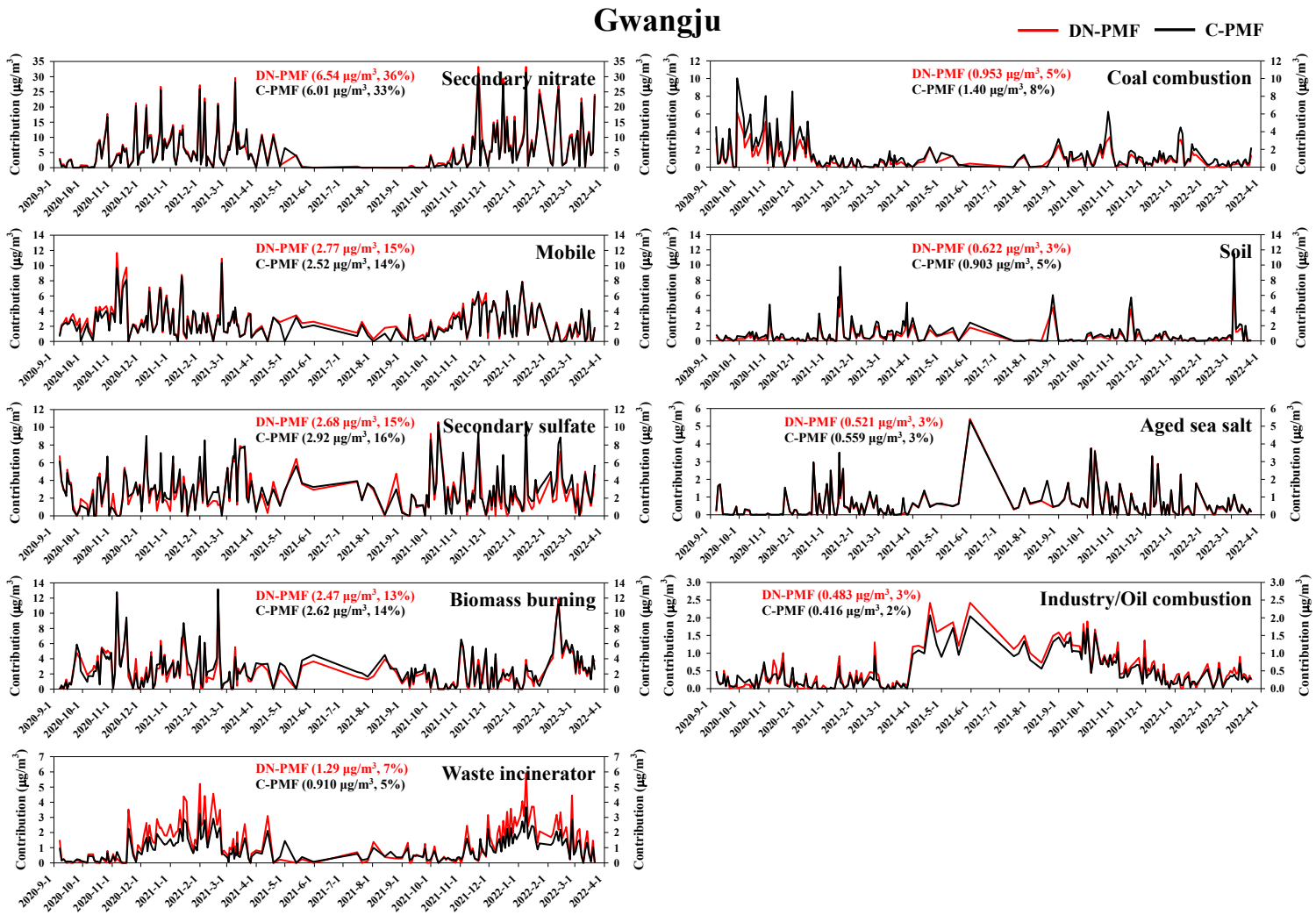

Figure 9. Source contributions from DN-PMF and C-PMF in Gwangju.

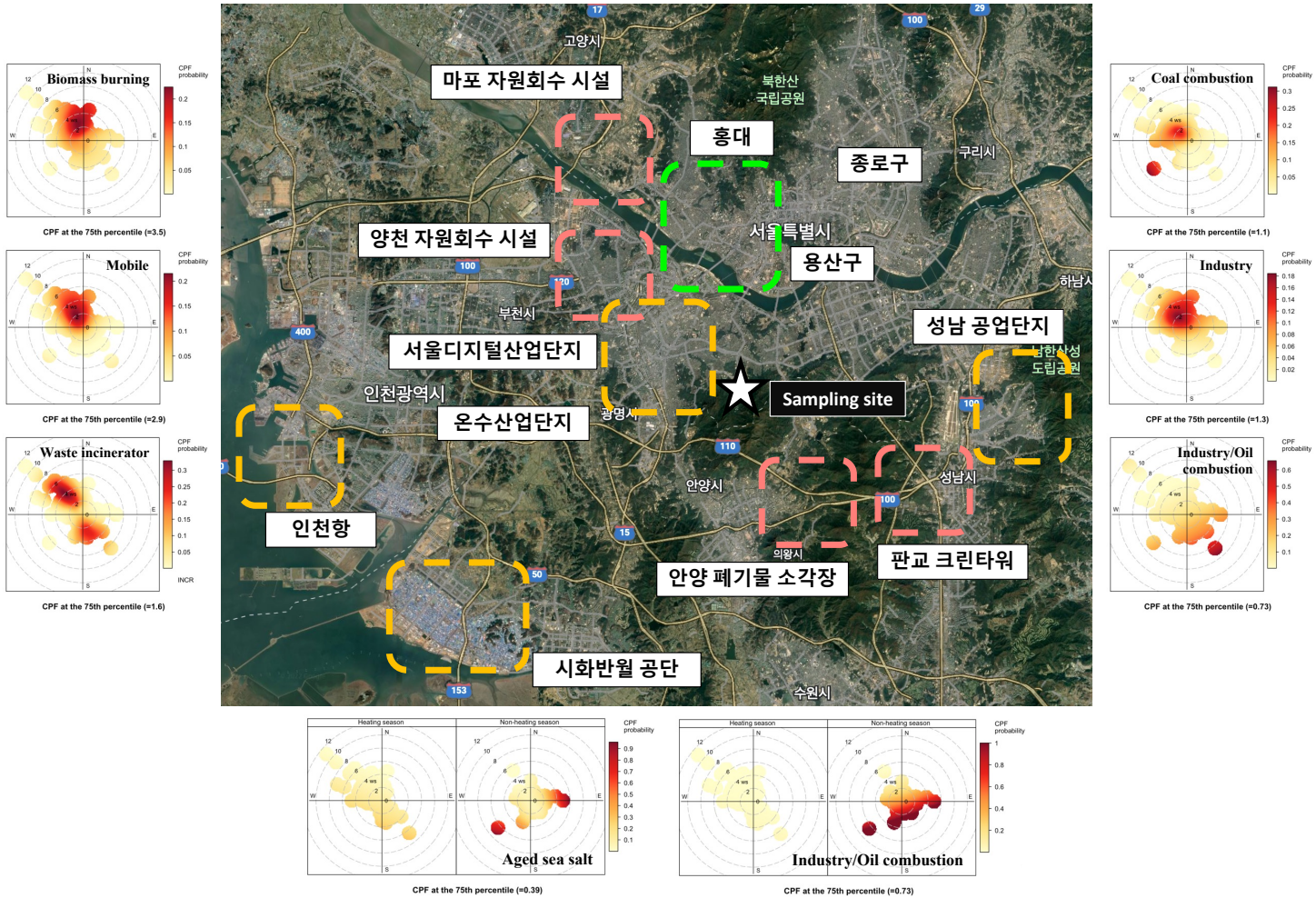

Figure 10. CBPF plots and source location map of Seoul.

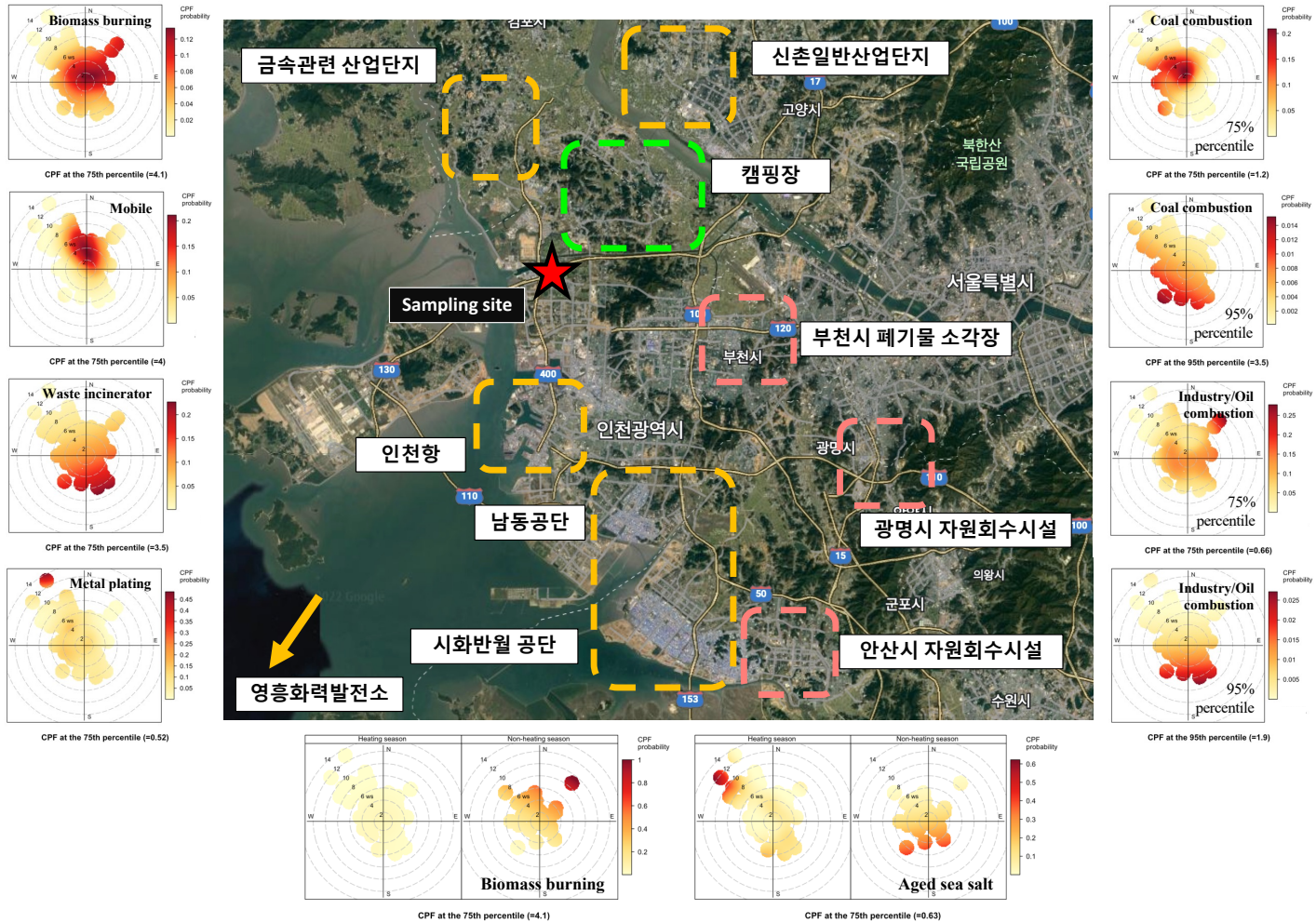

Figure 11. CBPF plots and source location map of Incheon.

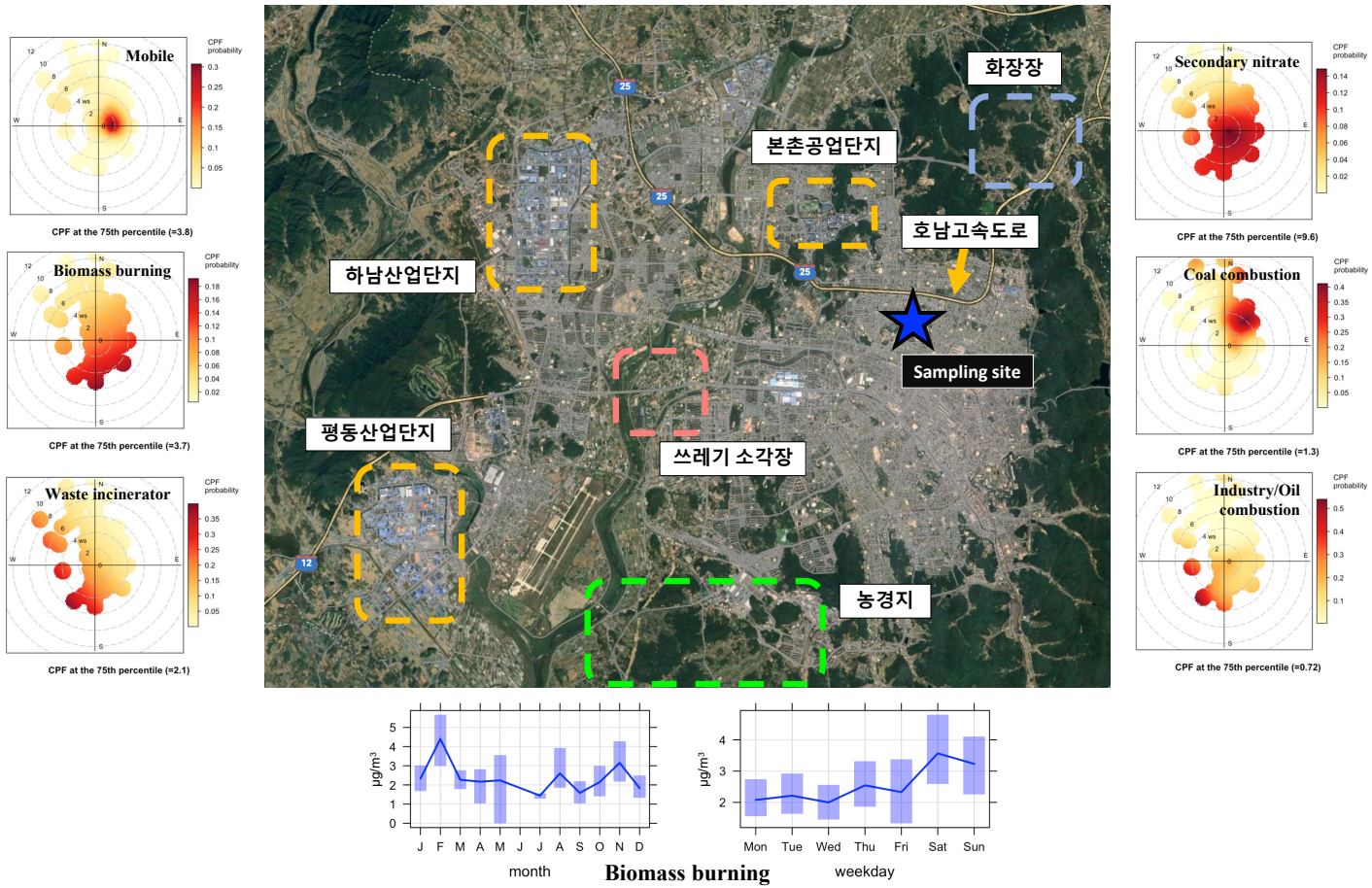

Figure 12. CBPF plots and source location map of Gwangju.

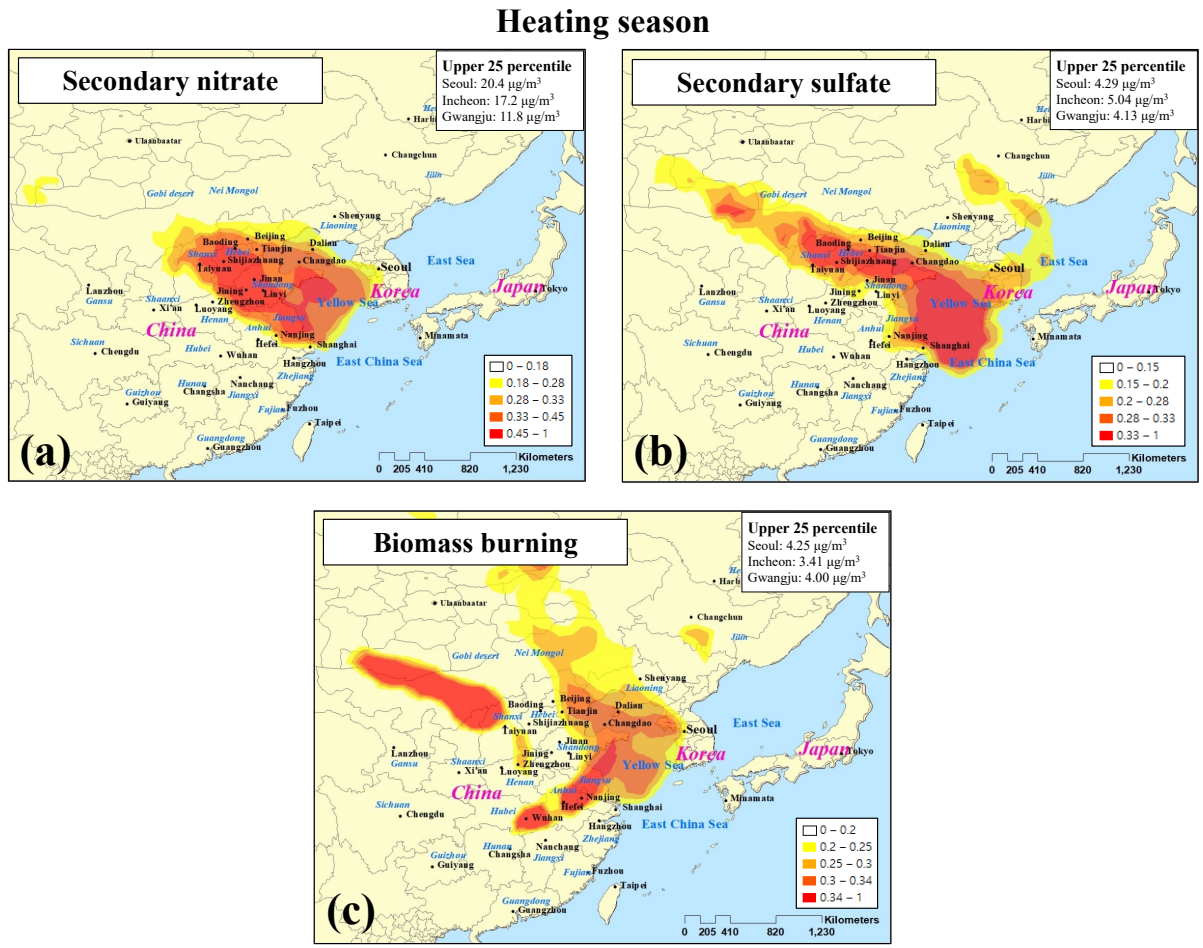

Figure 13. J-PSCF plots of (a) secondary nitrate; (b) secondary sulfate; (c) biomass burning during the heating season.

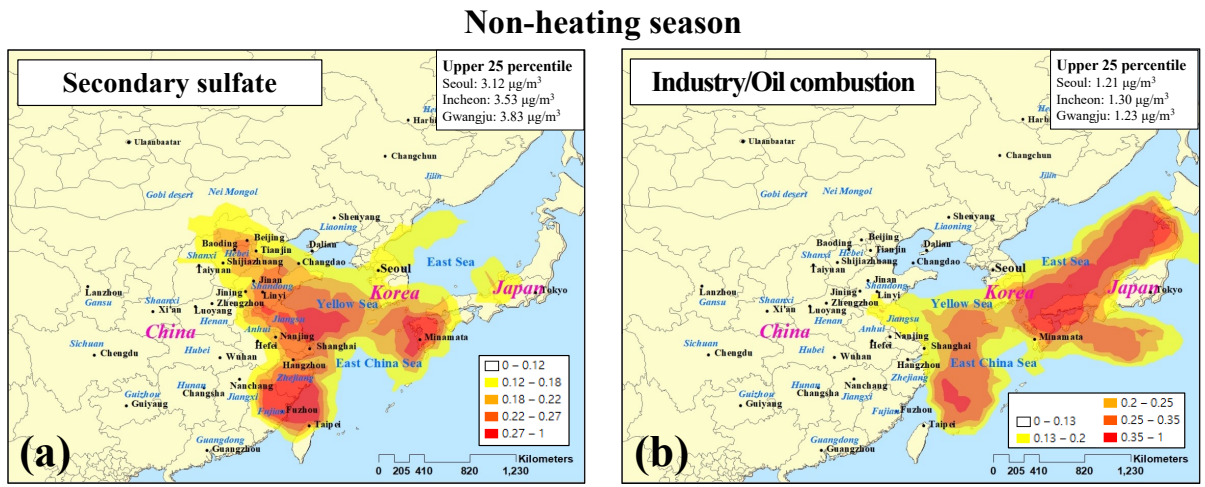

Figure 14. J-PSCF plots of (a) secondary sulfate; (b) industry/oil combustion during the non-heating season.

2.2.4. Carcinogenic risk using DN-PMF results

The carcinogenic risks of the four trace elements, Cr^{6+}, Ni, As, and Pb, and their related sources were estimated using the daily source contributions from the DN-PMF results. The median concentrations of each trace element were used to estimate the carcinogenic risk (ILCR). The box plots of ILCR of four trace elements in the three sites are illustrated in Figures 15 through 17.

The ILCR of Cr^{6+} in the Seoul, Incheon, and Gwangju sites were 5.7E-07, 1.1E-06, and 3.5E-07, respectively. Only $ILCR_{(VI)}$ of Incheon exceeded the safety limit of 1.0E-06. The other sources contributing to the carcinogenic effects of Cr^{6+} in the three sites are listed in Table 15. In Seoul, Cr^{6+} emissions from the industry source accounted for 41% (2.4E-07) of the $ILCR_{Cr(VI)}$. In Incheon, metal plating and mobile sources contributed greatly, accounting for 84% of the total carcinogenic risk together. In Gwangju, Cr^{6+} emitted from the mobile source accounted for 34% (1.2E-07).

The ILCR of Ni in the Seoul, Incheon, and Gwangju sites were 3.5E-08, 8.7E-08, and 3.0E-08, respectively. All study sites were safe from the potential carcinogenic risks of inhaled Ni particles. The other sources contributing to the carcinogenic effects of Ni in the three sites are listed in Table 16. In Seoul, Ni from secondary nitrate source accounted for 27% (9.7E-09), followed closely by industry/oil combustion, which accounted for 24% (8.4E-09) of the $ILCR_{Ni}$. In Incheon, the metal plating source accounted for 67% (5.8E-08) of the $ILCR_{Ni}$. In Gwangju, the industry/oil combustion accounted for 28% (8.4E-09), followed by secondary nitrate source, which accounted for 25% (7.4E-09) of the $ILCR_{Ni}$. Since secondary nitrates are influenced by local NO_X precursors from industrial activities, the presence of

industry-related Ni in the secondary nitrate profile was reasonable. The industrial emissions in Seoul and Gwangju need to be managed carefully.

The ILCR of As in the Seoul, Incheon, and Gwangju sites were 2.6E-06, 2.8E-06, and 1.5E-06, respectively. The $ILCR_{As}$ at all sites exceeded the safety limit, implying the carcinogenic risk potentials. In detail, the coal combustion source posed the greatest concern to the health risk, which accounted for 64% (1.7E-06), 94% (2.6E-06), and 70% (1.0E-06) in Seoul, Incheon, and Gwangju, respectively. The other sources contributing to the carcinogenic effects of As in the three sites are listed in Table 17.

The ILCR of Pb in the Seoul, Incheon, and Gwangju sites were 3.7E-08, 3.9E-08, and 2.0E-08, respectively. The other sources contributing to the $ILCR_{Pb}$ in the three sites are listed in Table 18. The carcinogenic risks of Pb at all sites were considered negligible. In Seoul, Pb emissions from the industry source accounted for 56% (2.1E-08) of the $ILCR_{Pb}$. On the contrary, the coal combustion source was the common major emitter of Pb in Incheon and Gwangju, which accounted for 35% (1.4E-08) and 29% (5.9E-09), respectively.

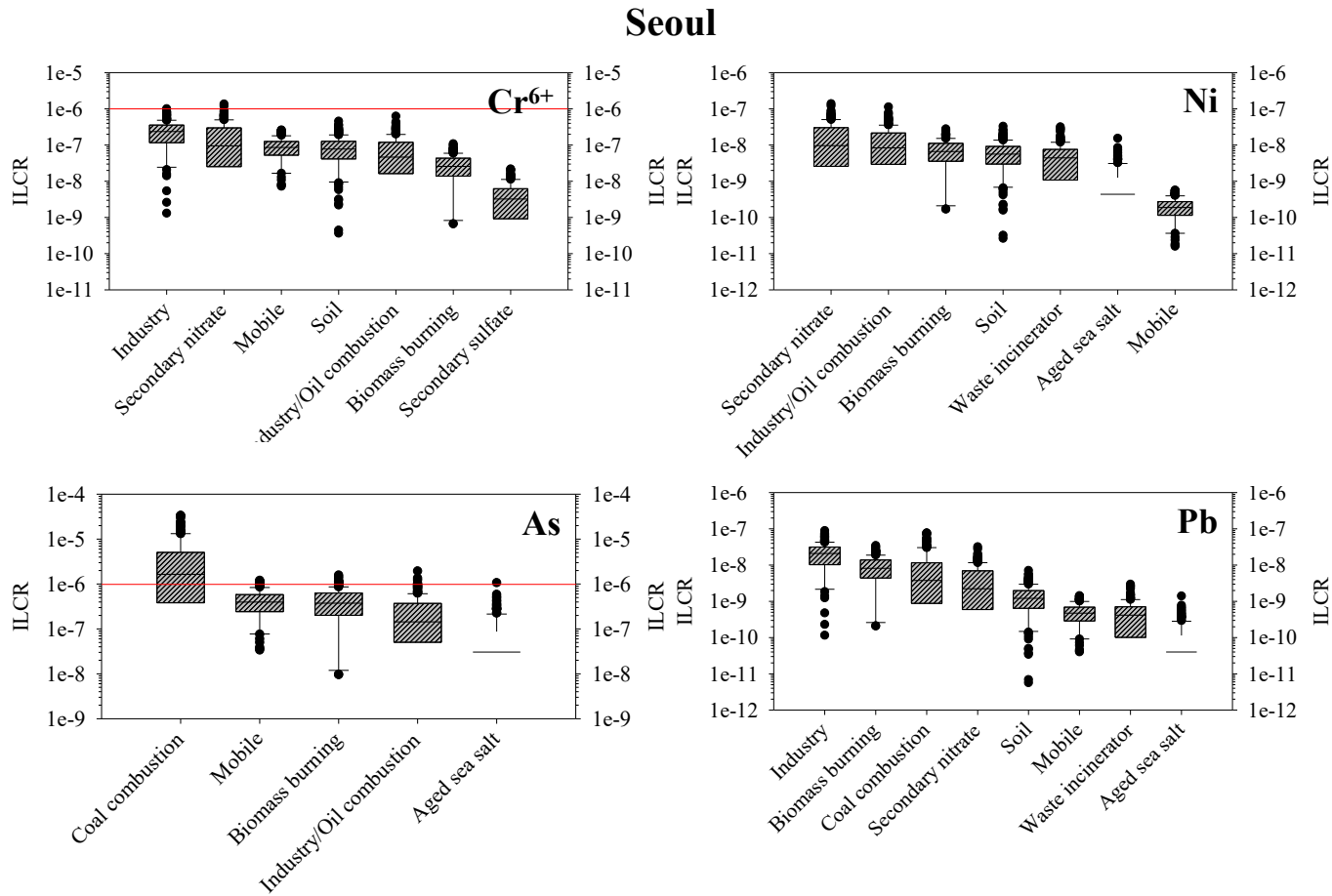

Figure 15. Box plots of ILCR of four trace elements in Seoul (Cr^{6+}, Ni, As, Pb).

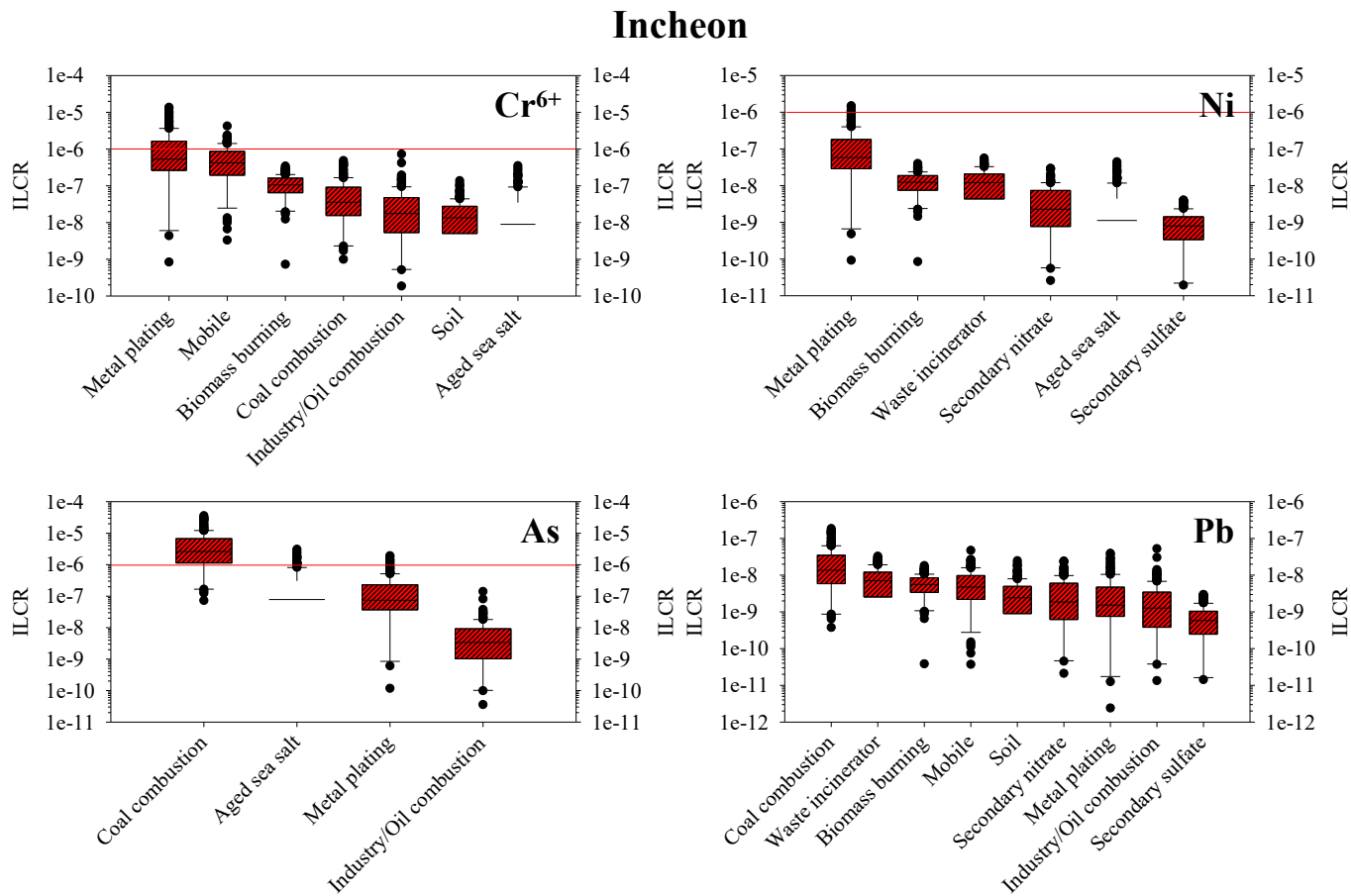

Figure 16. Box plots of ILCR of four trace elements in Incheon (Cr^{6+}, Ni, As, Pb).

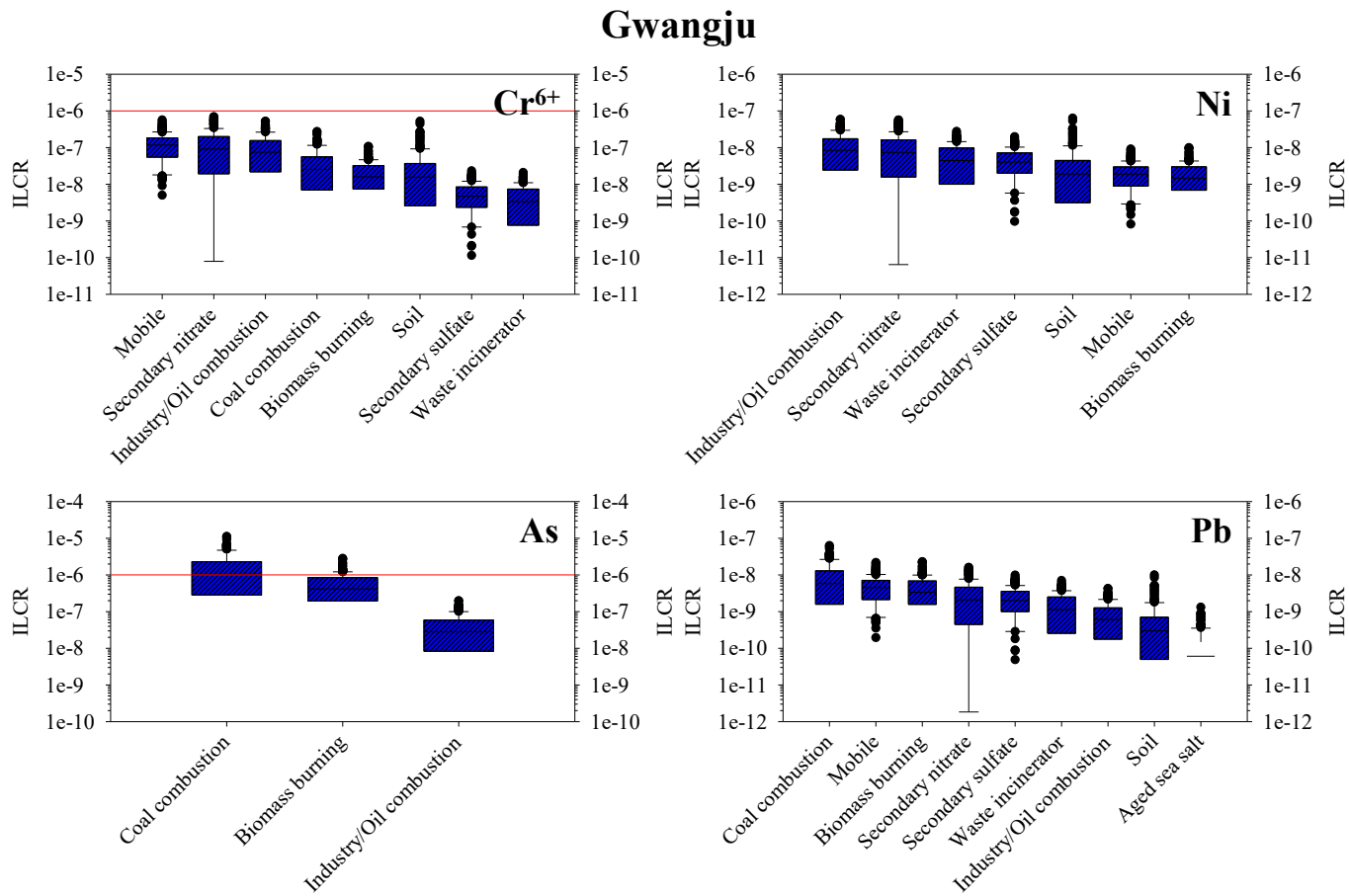

Figure 17. Box plots of ILCR of four trace elements in Gwangju (Cr^{6+}, Ni, As, Pb).

Table 15. ILCR of Cr^{6+} in Seoul, Incheon, and Gwangju

Seoul		Incheon		Gwangju	
Source	ILCR (%)	Source	ILCR (%)	Source	ILCR (%)
Industry	2.4E-07 (41%)	Metal plating	5.3.E-07 (47%)	Mobile	1.2E-07 (34%)
Secondary nitrate	9.6E-08 (17%)	Mobile	4.2.E-07 (37%)	Secondary nitrate	9.1E-08 (26%)
Mobile	8.6E-08 (15%)	Biomass burning	1.1.E-07 (9%)	Industry/Oil combustion	7.5E-08 (22%)
Soil	7.8E-08 (14%)	Coal combustion	3.6.E-08 (3%)	Coal combustion	2.5E-08 (7%)
Industry/Oil combustion	4.7E-08 (8%)	Industry/Oil combustion	1.8.E-08 (2%)	Biomass burning	1.6E-08 (5%)
Biomass burning	2.6E-08 (5%)	Soil	1.4.E-08 (1%)	Soil	1.6E-08 (4%)
Secondary sulfate	3.3E-09 (1%)	Aged sea salt	9.0.E-09 (1%)	Secondary sulfate	4.8E-09 (1%)
Coal combustion	-	Secondary nitrate	-	Waste incinerator	3.4E-09 (1%)
Waste incinerator	-	Waste incinerator	-	Aged sea salt	-
Aged sea salt	-	Secondary sulfate	-	-	-
$ILCR_{Cr(VI)}$	5.7E-07	$ILCR_{Cr(VI)}$	1.1E-06	$ILCR_{Cr(VI)}$	3.5E-07

Table 16. ILCR of Ni in Seoul, Incheon, and Gwangju

Seoul		Incheon		Gwangju	
Source	ILCR (%)	Source	ILCR (%)	Source	ILCR (%)
Secondary nitrate	9.7E-09 (27%)	Metal plating	5.8.E-08 (67%)	Industry/Oil combustion	8.4E-09 (28%)
Industry/Oil combustion	8.4E-09 (24%)	Biomass burning	1.2.E-08 (14%)	Secondary nitrate	7.4E-09 (25%)
Biomass burning	6.7E-09 (19%)	Waste incinerator	1.2.E-08 (14%)	Waste incinerator	4.5E-09 (15%)
Soil	5.6E-09 (16%)	Secondary nitrate	2.3.E-09 (3%)	Secondary sulfate	4.0E-09 (14%)
Waste incinerator	4.4E-09 (13%)	Aged sea salt	1.1.E-09 (1%)	Soil	1.9E-09 (6%)
Aged sea salt	4.4E-10 (1%)	Secondary sulfate	7.9.E-10 (1%)	Mobile	1.9E-09 (6%)
Mobile	1.9E-10 (1%)	Mobile	-	Biomass burning	1.5E-09 (5%)
Secondary sulfate	-	Soil	-	Aged sea salt	-
Coal combustion	-	Industry/Oil combustion	-	Coal combustion	-
Industry	-	Coal combustion	-	-	-
$ILCR_{Ni}$	3.5E-08	$ILCR_{Ni}$	8.7E-08	$ILCR_{Ni}$	3.0E-08

Table 17. ILCR of As in Seoul, Incheon, and Gwangju

Seoul		Incheon		Gwangju	
Source	ILCR (%)	Source	ILCR (%)	Source	ILCR (%)
Coal combustion	1.7E-06 (64%)	Coal combustion	2.6.E-06 (94%)	Coal combustion	1.0E-06 (70%)
Mobile	4.0E-07 (15%)	Aged sea salt	7.8.E-08 (3%)	Biomass burning	4.2E-07 (28%)
Biomass burning	3.7E-07 (14%)	Metal plating	7.5.E-08 (3%)	Industry/Oil combustion	2.9E-08 (2%)
Industry/Oil combustion	1.4E-07 (6%)	Industry/Oil combustion	3.4.E-09 (0%)	Aged sea salt	-
Aged sea salt	3.0E-08 (1%)	Mobile	-	Mobile	-
Secondary sulfate	-	Secondary nitrate	-	Soil	-
Soil	-	Soil	-	Secondary sulfate	-
Waste incinerator	-	Waste incinerator	-	Secondary nitrate	-
Secondary nitrate	-	Secondary sulfate	-	Waste incinerator	-
Industry	-	Biomass burning	-	-	-
$ILCR_{As}$	2.6E-06	$ILCR_{As}$	2.8E-06	$ILCR_{As}$	1.5E-06

Table 18. ILCR of Pb in Seoul, Incheon, and Gwangju

Seoul		Incheon		Gwangju	
Source	ILCR (%)	Source	ILCR (%)	Source	ILCR (%)
Industry	2.1E-08 (56%)	Coal combustion	1.4.E-08 (35%)	Coal combustion	5.9E-09 (29%)
Biomass burning	8.2E-09 (22%)	Waste incinerator	7.1.E-09 (18%)	Mobile	4.6E-09 (23%)
Coal combustion	3.8E-09 (10%)	Biomass burning	5.6.E-09 (14%)	Biomass burning	3.4E-09 (17%)
Secondary nitrate	2.2E-09 (6%)	Mobile	4.8.E-09 (12%)	Secondary nitrate	2.1E-09 (11%)
Soil	1.2E-09 (3%)	Soil	2.4.E-09 (6%)	Secondary sulfate	2.0E-09 (10%)
Mobile	4.7E-10 (1%)	Secondary nitrate	1.9.E-09 (5%)	Waste incinerator	1.1E-09 (6%)
Waste incinerator	4.2E-10 (1%)	Metal plating	1.5.E-09 (4%)	Industry/Oil combustion	6.1E-10 (3%)
Aged sea salt	4.0E-11 (0%)	Industry/Oil combustion	1.3.E-09 (3%)	Soil	3.0E-10 (1%)
Secondary sulfate	-	Secondary sulfate	5.8.E-10 (2%)	Aged sea salt	6.1E-11 (0%)
Industry/Oil combustion	-	Aged sea salt	-	-	-
$ILCR_{Pb}$	3.7E-08	$ILCR_{Pb}$	3.9E-08	$ILCR_{Pb}$	2.0E-08

2.2.5.Non-carcinogenic risk DN-PMF results

The non-carcinogenic risks of the eight trace elements, Al, Cr, Mn, Ni, Cu, As, and Pb, and their associated sources were estimated using the daily source contributions obtained from the DN-PMF. For Cr, separate HQ values were calculated for each oxidation state (trivalent and hexavalent forms). The median concentrations of each trace element were used to estimate the non-carcinogenic risk (HQ). The box plots of HQ of eight trace elements in the three sites are illustrated in Figures 18 through 20.

The HQ of Al in Seoul, Incheon, and Gwangju were 4.4E-06, 1.9E-05, and 2.8E-06, respectively. The other sources contributing to the non-carcinogenic effects of Al in the three sites are listed in Table 19. Incheon showed the greatest HQ_{Al}, although its non-carcinogenic risk was below the threshold limit of 1. Al mainly originated from soil particles at all sites. In Incheon and Gwangju, the mobile source was the second largest contributor to HQ_{Al}.

The HQ of V in Seoul, Incheon, and Gwangju were 4.1E-04, 4.7E-04, and 3.9E-04, respectively. The other sources contributing to the non-carcinogenic effects of V in the three sites are listed in Table 20. The industry/oil combustion sources were the dominant contributor to the HQ_V in the Seoul and Gwangju sites, while the biomass burning source was the dominant source in Incheon. The industry/oil combustion source accounted for 60% (2.5E-04) and 57% (2.3E-04) in Seoul and Gwangju, respectively.

The HQ of Cr^{3+} in Seoul, Incheon, and Gwangju were 4.8E-04, 5.7E-03, and 1.7E-03, respectively. The other sources that contributed to the non-carcinogenic effects of Cr^{3+} in the three sites are listed in Table 21. The industry source in Seoul accounted for 41%

(2.0E-04) of the estimated $HQ_{Cr(III)}$. The metal plating source accounted for 47% (2.7E-03) in Incheon, while the mobile source accounted for 34% (5.9E-04) in Gwangju. The HQ of Cr^{6+} in Seoul, Incheon, and Gwangju were 9.5E-03, 1.9E-02, and 5.8E-03, respectively. The other sources that contributed to the non-carcinogenic effects of Cr^{6+} in the three sites are listed in Table 22. The industry source in Seoul accounted for 41% (4.0E-03). Cr^{6+} from metal plating accounted for 47% (8.9E-03) of the estimated $HQ_{Cr(VI)}$ in Incheon. The mobile source accounted for 34% (2.0E-03) of the risk in Gwangju.

The HQ of Mn in Seoul, Incheon, and Gwangju were 5.0E-02, 8.0E-02, and 3.6E-02, respectively. The other sources contributing to the non-carcinogenic effects of Mn in the three sites are listed in Table 23. The HQ_{Mn} did not exceed the recommended safety limit at all sites. Mn from the soil and industry sources together accounted for 52% (2.6E-02) of the estimated HQ_{Mn} in Seoul. In Incheon and Gwangju, Mn was largely emitted from mobile sources, which accounted for 55% (4.4E-02) and 37% (1.4E-02), respectively.

The HQ of Ni in Seoul, Incheon, and Gwangju were 1.1E-02, 2.6E-02, and 8.7E-03, respectively. The other sources contributing to the non-carcinogenic effects of Ni in the three sites are listed in Table 24. In Seoul and Gwangju, the secondary nitrate and industry/oil combustion sources together accounted for 51% (3.4E-03) and 53% (4.6E-03) of the estimated risks. Ni particles from the metal plating industries contributed greatly up to 67% (1.7E-02) of the total HQ_{Ni} in Incheon.

The HQ of Cu in Seoul, Incheon, and Gwangju were 2.1E-04, 4.2E-04, and 1.7E-04, respectively. The other sources contributing to the non-carcinogenic effects of Cu in the three sites are listed in Table

25. In Seoul and Incheon, Cu emissions from the industry/oil combustion source accounted for 47% (9.7E-05) and 66% (2.8E-04), respectively. The same source also contributed 44% of the calculated HQ in Gwangju, albeit not being the greatest contributor.

The HQ of As in Seoul, Incheon, and Gwangju were 4.0E-02, 4.3E-02, and 5.2E-06, respectively. The other sources contributing to the non-carcinogenic effects of As in the three sites are listed in Table 26. All sites were affected by the coal combustion generated As in common, which accounted for 64% (2.6E-02), 94% (4.1E-02), and 70% (3.6E-06) in Seoul, Incheon, and Gwangju, respectively. In contrast to the $ILCR_{As}$ in the study sites, the HQ_{As} values were within safe boundaries.

The HQ of Pb in Seoul, Incheon, and Gwangju were 2.1E-02, 8.6E-02, and 1.1E-02, respectively. The other sources contributing to the HQ_{Pb} values in the three sites are listed in table 27. Pb from the industry source accounted for 56% (1.2E-02) of the estimated HQ_{Pb} in Seoul. In contrast, Pb emitted from coal combustion activities accounted for 35% (3.0E-02) and 29% (3.3E-03) in Incheon and Gwangju, respectively.

The HQs of each trace element at all sites did not exceed the safety limit, and so did the HIs. The ILCR and HI values of each site are available in Table S4.

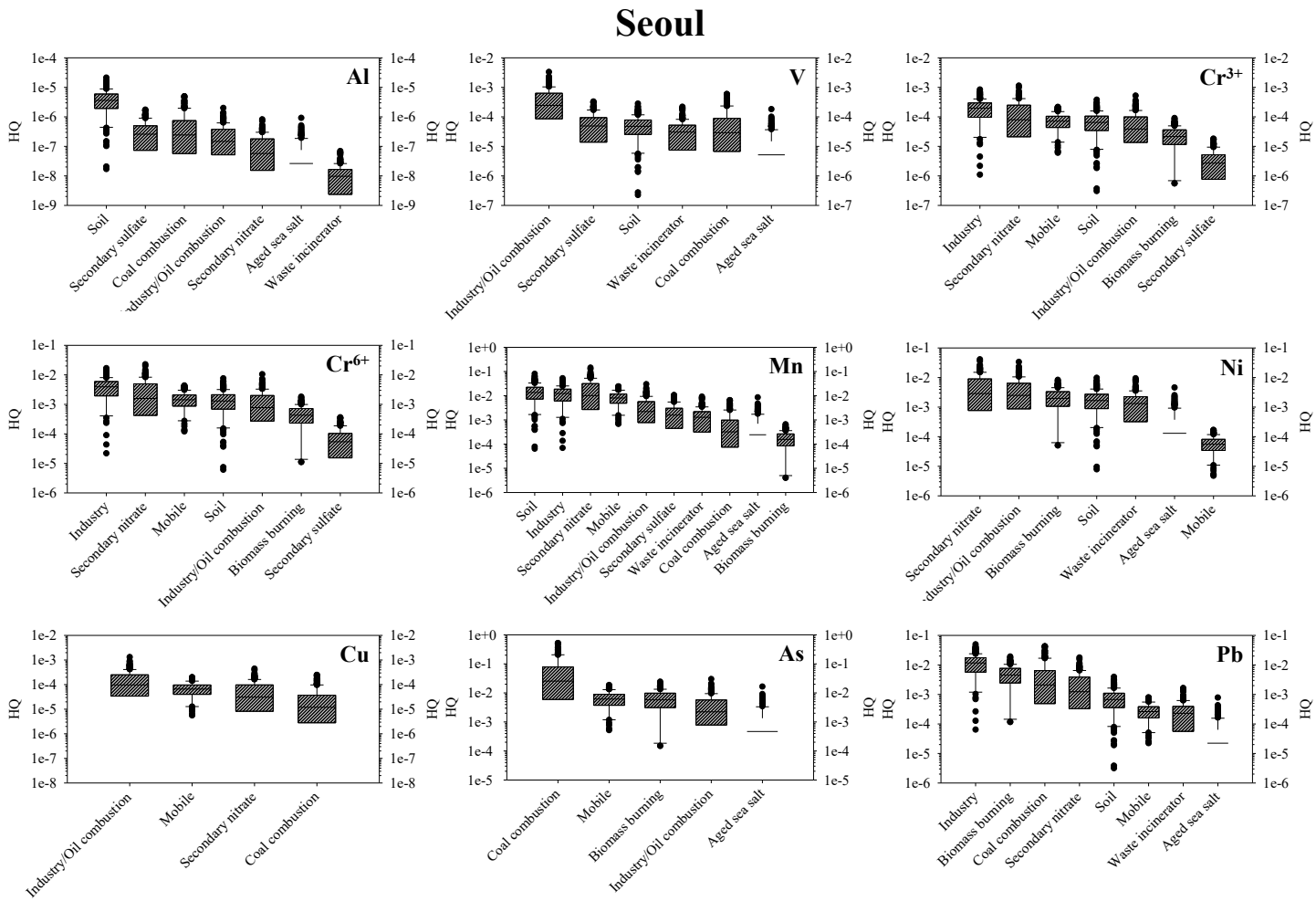

Figure 18. Box plots of HQ of eight trace elements in Seoul (Al, V, Cr^{3+}, Cr^{6+}, Mn, Ni, Cu, As, Pb).

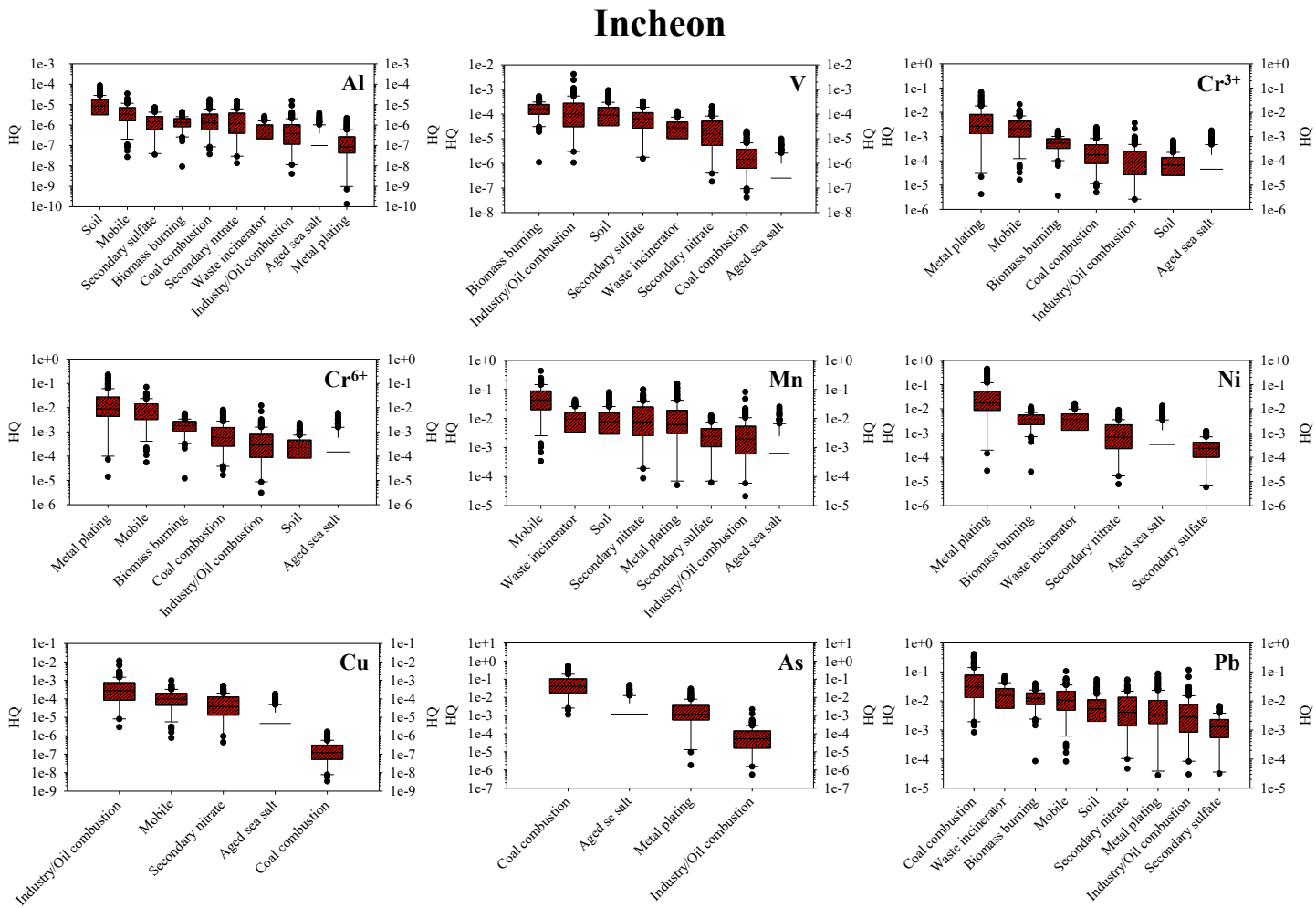

Figure 19. Box plots of HQ of eight trace elements in Incheon (Al, V, Cr^{3+}, Cr^{6+}, Mn, Ni, Cu, As, Pb).

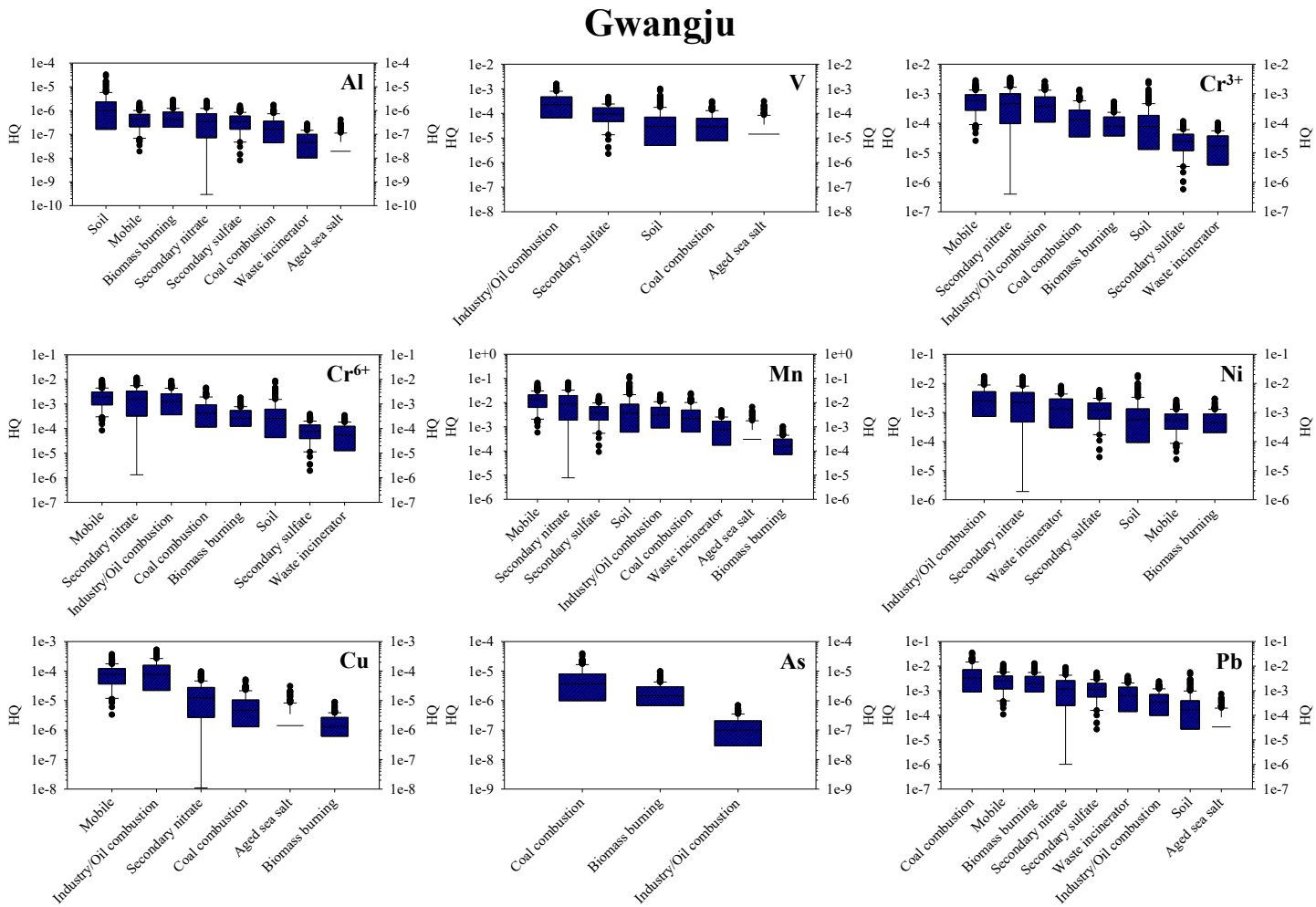

Figure 20. Box plots of HQ of eight trace elements in Gwangju (Al, V, Cr^{3+}, Cr^{6+}, Mn, Ni, Cu, As, Pb).

Table 19. HQ of Al in Seoul, Incheon, and Gwangju

Seoul		Incheon		Gwangju	
Source	HQ (%)	Source	HQ (%)	Source	HQ (%)
Soil	3.6E-06 (83%)	Soil	8.6.E-06 (46%)	Soil	9.9E-07 (36%)
Secondary sulfate	2.6E-07 (6%)	Mobile	3.5.E-06 (19%)	Mobile	4.5E-07 (16%)
Coal combustion	2.4E-07 (6%)	Secondary sulfate	1.5.E-06 (8%)	Biomass burning	4.3E-07 (15%)
Industry/Oil combustion	1.5E-07 (3%)	Biomass burning	1.3.E-06 (7%)	Secondary nitrate	3.4E-07 (12%)
Secondary nitrate	5.8E-08 (1%)	Coal combustion	1.3.E-06 (7%)	Secondary sulfate	3.3E-07 (12%)
Aged sea salt	2.6E-08 (1%)	Secondary nitrate	1.2.E-06 (6%)	Coal combustion	1.6E-07 (6%)
Waste incinerator	9.7E-09 (0%)	Waste incinerator	5.9.E-07 (3%)	Waste incinerator	4.6E-08 (2%)
Biomass burning	-	Industry/Oil combustion	3.8.E-07 (2%)	Aged sea salt	1.9E-08 (1%)
Industry	-	Aged sea salt	1.0.E-07 (1%)	Industry/Oil combustion	-
Mobile	-	Metal plating	8.6.E-08 (0%)		
HQ_{Al}	4.4E-06	HQ_{Al}	1.9E-05	HQ_{Al}	2.8E-06

Table 20. HQ of V in Seoul, Incheon, and Gwangju

Seoul		Incheon		Gwangju	
Source	HQ (%)	Source	HQ (%)	Source	HQ (%)
Industry/Oil combustion	2.5E-04 (60%)	Biomass burning	1.6.E-04 (35%)	Industry/Oil combustion	2.3E-04 (58%)
Secondary sulfate	4.9E-05 (12%)	Industry/Oil combustion	1.0.E-04 (22%)	Secondary sulfate	9.5E-05 (24%)
Soil	4.8E-05 (12%)	Soil	9.1.E-05 (20%)	Soil	3.0E-05 (8%)
Waste incinerator	3.1E-05 (8%)	Secondary sulfate	6.5.E-05 (14%)	Coal combustion	2.9E-05 (7%)
Coal combustion	2.9E-05 (7%)	Waste incinerator	2.8.E-05 (6%)	Aged sea salt	1.4E-05 (4%)
Aged sea salt	5.2E-06 (1%)	Secondary nitrate	1.6.E-05 (3%)	Biomass burning	-
Biomass burning	-	Coal combustion	1.5.E-06 (0%)	Mobile	-
Secondary nitrate	-	Aged sea salt	2.5.E-07 (0%)	Secondary nitrate	-
Industry	-	Mobile	-	Waste incinerator	-
Mobile	-	Metal plating	-	-	-
HQ_V	4.1E-04	HQ_V	4.7E-04	HQ_V	4.0E-04

Table 21. HQ of Cr^{3+} in Seoul, Incheon, and Gwangju

Seoul		Incheon		Gwangju	
Source	HQ (%)	Source	HQ (%)	Source	HQ (%)
Industry	2.0E-04 (41%)	Metal plating	2.7.E-03 (47%)	Mobile	5.9E-04 (34%)
Secondary nitrate	8.0E-05 (17%)	Mobile	2.1.E-03 (37%)	Secondary nitrate	4.6E-04 (26%)
Mobile	7.2E-05 (15%)	Biomass burning	5.3.E-04 (9%)	Industry/Oil combustion	3.8E-04 (22%)
Soil	6.5E-05 (14%)	Coal combustion	1.8.E-04 (3%)	Coal combustion	1.3E-04 (7%)
Industry/Oil combustion	3.9E-05 (8%)	Industry/Oil combustion	8.8.E-05 (2%)	Biomass burning	8.0E-05 (5%)
Biomass burning	2.2E-05 (5%)	Soil	6.8.E-05 (1%)	Soil	7.9E-05 (4%)
Secondary sulfate	2.7E-06 (1%)	Aged sea salt	4.5.E-05 (1%)	Secondary sulfate	2.4E-05 (1%)
Coal combustion	-	Secondary nitrate	-	Waste incinerator	1.7E-05 (1%)
Waste incinerator	-	Waste incinerator	-	Aged sea salt	-
Aged sea salt	-	Secondary sulfate	-	-	-
$HQ_{Cr(III)}$	4.8E-04	$HQ_{Cr(III)}$	5.7E-03	$HQ_{Cr(III)}$	1.7E-03

Table 22. HQ of Cr^{6+} in Seoul, Incheon, and Gwangju

Seoul		Incheon		Gwangju	
Source	HQ (%)	Source	HQ (%)	Source	HQ (%)
Industry	4.0E-03 (41%)	Metal plating	8.9.E-03 (47%)	Mobile	2.0E-03 (34%)
Secondary nitrate	1.6E-03 (17%)	Mobile	7.1.E-03 (37%)	Secondary nitrate	1.5E-03 (26%)
Mobile	1.4E-03 (15%)	Biomass burning	1.8.E-03 (9%)	Industry/Oil combustion	1.3E-03 (22%)
Soil	1.3E-03 (14%)	Coal combustion	6.0.E-04 (3%)	Coal combustion	4.2E-04 (7%)
Industry/Oil combustion	7.8E-04 (8%)	Industry/Oil combustion	2.9.E-04 (2%)	Biomass burning	2.7E-04 (5%)
Biomass burning	4.3E-04 (5%)	Soil	2.3.E-04 (1%)	Soil	2.6E-04 (4%)
Secondary sulfate	5.4E-05 (1%)	Aged sea salt	1.5.E-04 (1%)	Secondary sulfate	7.9E-05 (1%)
Coal combustion	-	Secondary nitrate	-	Waste incinerator	5.6E-05 (1%)
Waste incinerator	-	Waste incinerator	-	Aged sea salt	-
Aged sea salt	-	Secondary sulfate	-	-	-
$HQ_{Cr(VI)}$	9.5E-03	$HQ_{Cr(VI)}$	1.9E-02	$HQ_{Cr(VI)}$	5.8E-03

Table 23. HQ of Mn in Seoul, Incheon, and Gwangju

Seoul		Incheon		Gwangju	
Source	HQ (%)	Source	HQ (%)	Source	HQ (%)
Soil	1.4E-02 (27%)	Mobile	4.4.E-02 (55%)	Mobile	1.3E-02 (37%)
Industry	1.2E-02 (25%)	Waste incinerator	9.6.E-03 (12%)	Secondary nitrate	9.0E-03 (25%)
Secondary nitrate	1.0E-02 (20%)	Soil	7.8.E-03 (10%)	Secondary sulfate	3.8E-03 (10%)
Mobile	8.1E-03 (16%)	Secondary nitrate	7.6.E-03 (10%)	Soil	3.7E-03 (10%)
Industry/Oil combustion	2.2E-03 (4%)	Metal plating	6.2.E-03 (8%)	Industry/Oil combustion	3.1E-03 (9%)
Secondary sulfate	1.6E-03 (3%)	Secondary sulfate	2.5.E-03 (3%)	Coal combustion	2.2E-03 (6%)
Waste incinerator	1.3E-03 (3%)	Industry/Oil combustion	2.0.E-03 (2%)	Waste incinerator	7.8E-04 (2%)
Coal combustion	3.2E-04 (1%)	Aged sea salt	6.4.E-04 (1%)	Aged sea salt	3.0E-04 (1%)
Aged sea salt	2.4E-04 (0%)	Coal combustion	-	Biomass burning	1.5E-04 (0%)
Biomass burning	1.6E-04 (0%)	Biomass burning	-	-	-
HQ_{Mn}	5.0E-02	HQ_{Mn}	8.0E-02	HQ_{Mn}	3.7E-02

Table 24. HQ of Ni in Seoul, Incheon, and Gwangju

Seoul		Incheon		Gwangju	
Source	HQ (%)	Source	HQ (%)	Source	HQ (%)
Secondary nitrate	2.9E-03 (27%)	Metal plating	1.7.E-02 (67%)	Industry/Oil combustion	2.5E-03 (28%)
Industry/Oil combustion	2.5E-03 (24%)	Biomass burning	3.7.E-03 (14%)	Secondary nitrate	2.2E-03 (25%)
Biomass burning	2.0E-03 (19%)	Waste incinerator	3.6.E-03 (14%)	Waste incinerator	1.3E-03 (15%)
Soil	1.7E-03 (16%)	Secondary nitrate	6.8.E-04 (3%)	Secondary sulfate	1.2E-03 (14%)
Waste incinerator	1.3E-03 (13%)	Aged sea salt	3.4.E-04 (1%)	Soil	5.7E-04 (6%)
Aged sea salt	1.3E-04 (1%)	Secondary sulfate	2.4.E-04 (1%)	Mobile	5.7E-04 (6%)
Mobile	5.6E-05 (1%)	Mobile	-	Biomass burning	4.4E-04 (5%)
Secondary sulfate	-	Soil	-	Aged sea salt	-
Coal combustion	-	Industry/Oil combustion	-	Coal combustion	-
Industry	-	Coal combustion	-	-	-
HQ_{Ni}	1.1E-02	HQ_{Ni}	2.6E-02	HQ_{Ni}	8.8E-03

Table 25. HQ of Cu in Seoul, Incheon, and Gwangju

Seoul		Incheon		Gwangju	
Source	HQ (%)	Source	HQ (%)	Source	HQ (%)
Industry/Oil combustion	9.7E-05 (47%)	Industry/Oil combustion	2.8.E-04 (66%)	Mobile	7.8E-05 (45%)
Mobile	6.6E-05 (32%)	Mobile	9.7.E-05 (23%)	Industry/Oil combustion	7.6E-05 (44%)
Secondary nitrate	3.1E-05 (15%)	Secondary nitrate	3.8.E-05 (9%)	Secondary nitrate	1.3E-05 (7%)
Coal combustion	1.2E-05 (6%)	Aged sea salt	4.8.E-06 (1%)	Coal combustion	4.7E-06 (3%)
Secondary sulfate	-	Coal combustion	1.2.E-07 (0%)	Aged sea salt	1.4E-06 (1%)
Soil	-	Soil	-	Biomass burning	1.3E-06 (1%)
Waste incinerator	-	Waste incinerator	-	Soil	-
Biomass burning	-	Secondary sulfate	-	Secondary sulfate	-
Aged sea salt	-	Metal plating	-	Waste incinerator	-
Industry	-	Biomass burning	-	-	-
HQ_{Cu}	2.1E-04	HQ_{Cu}	4.2E-04	HQ_{Cu}	1.7E-04

Table 26. HQ of As in Seoul, Incheon, and Gwangju

Seoul		Incheon		Gwangju	
Source	HQ (%)	Source	HQ (%)	Source	HQ (%)
Coal combustion	2.6E-02 (64%)	Coal combustion	4.1.E-02 (94%)	Coal combustion	3.6E-06 (70%)
Mobile	6.2E-03 (15%)	Aged sea salt	1.2.E-03 (3%)	Biomass burning	1.5E-06 (28%)
Biomass burning	5.8E-03 (14%)	Metal plating	1.2.E-03 (3%)	Industry/Oil combustion	1.0E-07 (2%)
Industry/Oil combustion	2.2E-03 (6%)	Industry/Oil combustion	5.3.E-05 (0%)	Aged sea salt	-
Aged sea salt	4.7E-04 (1%)	Mobile	-	Mobile	-
Secondary sulfate	-	Secondary nitrate	-	Soil	-
Soil	-	Soil	-	Secondary sulfate	-
Waste incinerator	-	Waste incinerator	-	Secondary nitrate	-
Secondary nitrate	-	Secondary sulfate	-	Waste incinerator	-
Industry	-	Biomass burning	-	-	-
HQ_{As}	4.0E-02	HQ_{As}	4.3E-02	HQ_{As}	5.2E-06

Table 27. HQ of Pb in Seoul, Incheon, and Gwangju

Seoul		Incheon		Gwangju	
Source	HQ (%)	Source	HQ (%)	Source	HQ (%)
Industry	1.2E-02 (56%)	Coal combustion	3.0.E-02 (35%)	Coal combustion	3.3E-03 (29%)
Biomass burning	4.6E-03 (22%)	Waste incinerator	1.6.E-02 (18%)	Mobile	2.5E-03 (23%)
Coal combustion	2.1E-03 (10%)	Biomass burning	1.2.E-02 (14%)	Biomass burning	1.9E-03 (17%)
Secondary nitrate	1.2E-03 (6%)	Mobile	1.1.E-02 (12%)	Secondary nitrate	1.2E-03 (11%)
Soil	6.7E-04 (3%)	Soil	5.4.E-03 (6%)	Secondary sulfate	1.1E-03 (10%)
Mobile	2.6E-04 (1%)	Secondary nitrate	4.1.E-03 (5%)	Waste incinerator	6.4E-04 (6%)
Waste incinerator	2.3E-04 (1%)	Metal plating	3.4.E-03 (4%)	Industry/Oil combustion	3.4E-04 (3%)
Aged sea salt	2.2E-05 (0%)	Industry/Oil combustion	2.8.E-03 (3%)	Soil	1.7E-04 (1%)
Secondary sulfate	-	Secondary sulfate	1.3.E-03 (2%)	Aged sea salt	3.4E-05 (0%)
Industry/Oil combustion	-	Aged sea salt	-	-	-
HQ_{Pb}	2.1E-02	HQ_{Pb}	8.6E-02	HQ_{Pb}	1.1E-02

Chapter 3. Conclusion

3.1. Comparison of DN-PMF and C-PMF

The concentrations used for conventional PMF analysis are affected by various atmospheric conditions, such as meteorology-induced atmospheric dispersion. DN-PMF helps to reduce the meteorological effects and enhance the actual source strengths. Both DN-PMF and C-PMF were applied to $PM_{2.5}$ speciated data collected in Seoul, Incheon, and Gwangju to better obtain the undisturbed source information and the effects of dispersion normalization effects were evaluated.

Both models resolved the same number of factors and similar source profiles while the source contributions varied for each city. The source profiles were slightly different, but the DISP intervals of marker species were mostly unchanged. The slight differences in concentration and DISP interval lengths were probably due to modeling uncertainties and different constrained values. The nine common sources resolved from the PMF analyses were secondary nitrate, secondary sulfate, mobile, biomass burning, soil, waste incinerator, coal combustion, industry/oil combustion, and aged sea salt. Seoul and Incheon featured additional industrial sources: an industry source in Seoul and a metal plating source in Incheon. The contributions of secondary nitrate were dominant at all sites, meaning that there were significant influences from local NO_X emissions. Control strategies should focus on local NO_X sources such as vehicles and industrial complexes during the heating season. The source contributions of nine common sources in each site were statistically

compared. Only the biomass burning, waste incinerator, and soil sources showed statistically different source contributions among the three sites. The biomass burning and waste incinerator sources were significantly higher in Incheon compared to Seoul and Gwangju. The soil contribution was significantly low in Gwangju. Being located south of Seoul and Incheon, Gwangju was less likely to be affected by transboundary soil components. Also, local factors such as resuspended road dust might have had fewer effects due to the smaller traffic volume than the other two megacities.

The source contributions resolved in the DN-PMF and C-PMF were compared, and the reduction of meteorological influences was evaluated. In Seoul, the biomass burning and aged sea salt source contributions in the DN-PMF were significantly lower than that in the C-PMF ($p \leq 0.05$). Meat-cooking was the possible biomass burning activity in Seoul, and significantly lower mixing layer heights and VCs during the active dining hours might have caused the overestimation of biomass burning emissions, thus it was scaled down in the DN-PMF. The biomass burning contribution in Incheon displayed a unique seasonal pattern. Its source contribution was significantly higher during the non-heating season in both the DN-PMF and C-PMF, which was different from Seoul and Gwangju. The possible source location was found to be NE of the Incheon site, where several camping sites existed. The unprecedented pandemic has dramatically changed people's lifestyles, such as increased recreational activities. Among those activities, outdoor camping has increased in Korea as well. The increased camping activities and their related grilling emissions during the non-heating season in 2021 were suggested as a possible explanation. The source contribution during the heating season in the DN-PMF was significantly higher than that in the C-PMF. Significantly

higher VCs during the heating season in Incheon might have caused the underestimation of biomass burning source contribution in the C-PMF during the heating season, which was scaled up in the DN-PMF. Vehicle emissions do not show seasonal patterns, which was consistent in both the DN-PMF and C-PMF in Seoul. In Incheon and Gwangju, the seasonal differences in the mobile source contributions were eliminated in the DN-PMF, which were more reasonable results. The aged sea salt source contribution was significantly reduced in the DN-PMF in Seoul. Reducing the local effects allowed for enhancing the regional nature of the aged sea salt source. The daily average meteorological data can provide improved seasonal patterns, and in this study, more reasonable source contributions were obtained in the DN-PMF. Since meteorology is different for each site, DN-PMF seems to be more suitable for obtaining the actual source strengths.

The CBPF plots created for each site were useful in verifying the local source locations. For instance, the CBPF plots of the mobile, waste incinerator, coal combustion, and industry sources were easily found by overlaying the plots on the maps of each sampling site. For sources that show seasonality, such as industry/oil combustion sources, drawing separate CBPF plots for the heating and non-heating season was required to clarify source inflow directions. The potential source areas of secondary nitrate and secondary sulfate were identified from the J-PSCF maps. These secondary pollutants shared common potential source areas in northeastern China, such as Shanxi Province, BTH region, Shandong, and Jiangsu Provinces. For secondary sulfate, areas near the Yangtze River Delta (YRD) and the coastal areas were also highlighted in the PSCF map during the non-heating season. The biomass burning emissions can be long-range transported to the western coastal cities in Korea from China or Inner

Mongolia during the harvesting seasons. The possible source areas pointed out in the J-PSCF map during the heating season implied that agricultural burning activities in northeast China and Inner Mongolia still exist and contribute to the enhanced source contributions in the three Korean cities. High J-PSCF values during the non-heating season of the industry/oil combustion source were found in the oceans surrounding China and Korea, explaining the heavy oil combustion of vessels in the marine territories. The CBPF and J-PSCF analysis in Seoul, Incheon, and Gwangju revealed that these cities were influenced by both local primary sources and long-range transport pollutants from China. We found that the seasonal management plan on fine dust was effective in reducing $PM_{2.5}$ from local sources, so we express positive expectations toward future mitigation policies by the Korean government. Meanwhile, it is physically challenging to counteract foreign influences such as long-range transport sources. Therefore, collaborative efforts to reduce transboundary $PM_{2.5}$ between the Korean and the Chinese government must be followed to substantially improve the air quality in both countries.

3.2. Source-specific health risk assessment

The present study explored the carcinogenic and non-carcinogenic risks posed by the trace elements and their related sources resolved in the DN-PMF. The mass concentrations were used to calculate the health risks. The health risks may be driven by the toxic component of $PM_{2.5}$, such as organic compounds, rather than the abundance of specific components. However, the collected filters were unsuitable for organic compound analysis, so the health risks were estimated using the mass fractions of each trace element. This method is still useful in that the estimated risk values provide insights into the

minimum health risks from primary emission sources.

There were potential carcinogenic risks at all sites. Incheon showed the greatest ILCR (4.0E-06) while Gwangju showed the lowest ILCR (1.9E-06). There was a two folds difference between the maximum and the minimum ILCR. The estimated ILCR of As alone exceeded the safety limit at all sites. Especially, the coal combustion source contributed greatly, ranging from 64% up to 94% to the carcinogenic risk of As. Many studies including a recent study conducted in metropolitan cities in Korea have commonly expressed health concerns such as cancer, cardiovascular and respiratory diseases from coal combustion source (Chen et al., 2021; Huang et al., 2018; S. Kim et al., 2022; Lee et al., 2022). As mentioned in the previous section, the second seasonal management plan in Korea during the winter seasons proved its effectiveness, showing a great decrease in coal combustion contribution by up to 76%. The future seasonal management plan will bring more strict measures on various sectors, and among them, coal combustion sources should be managed carefully. Reducing coal consumption along with implementing green energy systems could help prevent possible health concerns from As. Other trace elements such as Cr^{6+}, Ni, and Pb did not show concerning risks in Seoul and Gwangju, except for Cr^{6+} in Incheon. The ILCR of Cr^{6+} in Incheon (1.1E-06) marginally exceeded the safety limit. Together, the metal plating and mobile sources accounted for 84% of the health risk of Cr^{6+}. For Incheon, emissions from its site-specific metal plating source should be consistently monitored and controlled.

In the case of non-carcinogenic risks, the HQs did not exceed the safety limit at all sites. In detail, there was a 4 folds difference between the maximum and the minimum HQ. Although there were no potential health risks, the major contributor elements were Mn, As,

and Pb. Mn and As accounted for 68% of the HI in Seoul, Mn and Pb accounted for 64% of the HI in Incheon, and Mn accounted for 56% of the HI in Gwangju. These trace elements were associated with industry, mobile, and coal combustion sources. Along with control measures on coal combustion, consistent mobile and industrial emissions monitoring should also be required.

3.3. Limitations of this study

The intensive $PM_{2.5}$ sampling was focused during the heating season throughout the whole study period, so this study lacked samples representing the summertime. This study identified the biomass burning source by indicators such as K^+, however, the specific types of biomass burning were not conclusive with the single ionic species tracer. Organic compounds analysis should allow for more detailed source types of biomass burning as well as separation between gasoline and diesel vehicles. Regarding the health risk assessment, we acknowledge the significant toxicities of organic compounds, however, the collected sample filters in this study were not suitable for organic compounds analysis, so the health risk assessment was limited to trace elements. Nevertheless, the health risk assessment of trace elements can provide valuable information on minimum risks from exposure to ambient PM. The whole study period was during the COVID-19 pandemic, and the unprecedented pandemic has affected human activities such as reduced industrial and vehicle emissions. Therefore, the conclusions of this study may be drawn from underestimated source contributions. Further studies after the pandemic period are necessary to properly assess the health risks of $PM_{2.5}$ in South Korea.

References

Bell, M. L., Ebisu, K., Leaderer, B. P., Gent, J. F., Lee, H. J., Koutrakis, P., Wang, Y., Dominici, F., & Peng, R. D. (2014). Associations of PM2.5 constituents and sources with hospital admissions: analysis of four counties in Connecticut and Massachusetts (USA) for persons >/= 65 years of age. *Environ Health Perspect*, *122*(2), 138-144. https://doi.org/10.1289/ehp.1306656

Bie, S., Yang, L., Zhang, Y., Huang, Q., Li, J., Zhao, T., Zhang, X., Wang, P., & Wang, W. (2021). Source appointment of PM2.5 in Qingdao Port, East of China. *Sci Total Environ*, *755*(Pt 1), 142456. https://doi.org/10.1016/j.scitotenv.2020.142456

Chen, R., Jia, B., Tian, Y., & Feng, Y. (2021). Source-specific health risk assessment of PM2.5-bound heavy metals based on high time-resolved measurement in a Chinese megacity: insights into seasonal and diurnal variations. *Ecotoxicol Environ Saf*, *216*, 112167. https://doi.org/10.1016/j.ecoenv.2021.112167

Chen, Y., Rich, D. Q., & Hopke, P. K. (2022). Long-term PM2.5 source analyses in New York City from the perspective of dispersion normalized PMF. *Atmospheric Environment*, *272*. https://doi.org/10.1016/j.atmosenv.2022.118949

Cheng, Y., Engling, G., He, K. B., Duan, F. K., Ma, Y. L., Du, Z. Y., Liu, J. M., Zheng, M., & Weber, R. J. (2013). Biomass burning contribution to Beijing aerosol. *Atmospheric Chemistry and Physics*, *13*(15), 7765-7781. https://doi.org/10.5194/acp-13-7765-2013

Chow, J. C., Watson, J. G., Ashbaugh, L. L., & Magliano, K. L. (2003). Similarities and differences in PM10 chemical source profiles for geological dust from the San Joaquin Valley, California. *Atmospheric Environment*, *37*(9-10), 1317-1340. https://doi.org/10.1016/s1352-2310(02)01021-x

Dai, Q., Liu, B., Bi, X., Wu, J., Liang, D., Zhang, Y., Feng, Y., & Hopke, P. K. (2020). Dispersion Normalized PMF Provides Insights into the Significant Changes in Source Contributions to PM2.5 after the COVID-19 Outbreak. *Environ Sci Technol*, *54*(16), 9917-9927. https://doi.org/10.1021/acs.est.0c02776

Dong, J., Wang, X., Li, J., Hao, C., & Jiao, L. (2022). The Spatial-Temporal Differentiation of Aerosol Optical Properties and Types in the Beijing–Tianjin–Hebei Region Based on the Ecological Functional Zones. *Sustainability*, *14*(19). https://doi.org/10.3390/su141912656

Echalar, F., Gaudichet, A., Cachier, H., & Artaxo, P. (1995). Aerosol emissions by tropical forest and savanna biomass burning: Characteristic trace elements and fluxes. *Geophysical Research Letters*, *22*(22), 3039-3042. https://doi.org/https://doi.org/10.1029/95GL03170

El Haddad, I., Marchand, N., Dron, J., Temime-Roussel, B., Quivet, E., Wortham, H., Jaffrezo, J. L., Baduel, C., Voisin, D., Besombes, J. L., & Gille, G. (2009). Comprehensive primary particulate organic

characterization of vehicular exhaust emissions in France. *Atmospheric Environment*, *43*(39), 6190-6198. https://doi.org/10.1016/j.atmosenv.2009.09.001

EPA. (2004). *Region 9, Preliminary remediation goals, air- water calculations.*

EPA. (2009). *Risk Assessment Guidance for Superfund Volume I: Human Health Evaluation Manual (Part F, Supplemental Guidance for Inhalation Risk Assessment).*

Feng, S., Gao, D., Liao, F., Zhou, F., & Wang, X. (2016). The health effects of ambient PM2.5 and potential mechanisms. *Ecotoxicol Environ Saf*, *128*, 67-74. https://doi.org/10.1016/j.ecoenv.2016.01.030

Gao, Y., Nelson, E. D., Field, M. P., Ding, Q., Li, H., Sherrell, R. M., Gigliotti, C. L., Van Ry, D. A., Glenn, T. R., & Eisenreich, S. J. (2002). Characterization of atmospheric trace elements on PM2.5 particulate matter over the New York-New Jersey harbor estuary. *Atmospheric environment (1994)*, *36*(6), 1077-1086. https://doi.org/10.1016/S1352-2310(01)00381-8

Gieré, R., Blackford, M., & Smith, K. (2006). TEM Study of PM2.5 Emitted from Coal and Tire Combustion in a Thermal Power Station. *Environmental Science & Technology*, *40*(20), 6235-6240. https://doi.org/10.1021/es060423m

Han, Y.-J., Kim, T.-S., & Kim, H. (2008). Ionic constituents and source analysis of PM2.5 in three Korean cities. *Atmospheric Environment*, *42*(19), 4735-4746. https://doi.org/10.1016/j.atmosenv.2008.01.047

Huang, R. J., Cheng, R., Jing, M., Yang, L., Li, Y., Chen, Q., Chen, Y., Yan, J., Lin, C., Wu, Y., Zhang, R., El Haddad, I., Prevot, A. S. H., O'Dowd, C. D., & Cao, J. (2018). Source-Specific Health Risk Analysis on Particulate Trace Elements: Coal Combustion and Traffic Emission As Major Contributors in Wintertime Beijing. *Environ Sci Technol*, *52*(19), 10967-10974. https://doi.org/10.1021/acs.est.8b02091

Jeong, J.-H., Shon, Z.-H., Kang, M., Song, S.-K., Kim, Y.-K., Park, J., & Kim, H. (2017). Comparison of source apportionment of PM 2.5 using receptor models in the main hub port city of East Asia: Busan. *Atmospheric Environment*, *148*, 115-127. https://doi.org/10.1016/j.atmosenv.2016.10.055

Jia, H., Huo, J., Fu, Q., Duan, Y., Lin, Y., Jin, X., Hu, X., & Cheng, J. (2020). Insights into chemical composition, abatement mechanisms and regional transport of atmospheric pollutants in the Yangtze River Delta region, China during the COVID-19 outbreak control period. *Environmental Pollution*, *267*. https://doi.org/10.1016/j.envpol.2020.115612

Kang, M., Guo, H., Wang, P., Fu, P., Ying, Q., Liu, H., Zhao, Y., & Zhang, H. (2019). Characterization and source apportionment of marine aerosols over the East China Sea. *Sci Total Environ*, *651*(Pt 2), 2679-2688. https://doi.org/10.1016/j.scitotenv.2018.10.174

Khan, M. F., Latif, M. T., Saw, W. H., Amil, N., Nadzir, M. S. M., Sahani, M., Tahir, N. M., & Chung, J. X. (2016). Fine particulate matter in the tropical environment: monsoonal effects, source apportionment, and health risk assessment. *Atmospheric Chemistry and Physics*, *16*(2),

597-617. https://doi.org/10.5194/acp-16-597-2016
Khuzestani, R. B., Schauer, J. J., Shang, J., Cai, T., Fang, D., Wei, Y., Zhang, L., & Zhang, Y. (2018). Source apportionments of PM2.5 organic carbon during the elevated pollution episodes in the Ordos region, Inner Mongolia, China. *Environ Sci Pollut Res Int*, *25*(13), 13159-13172. https://doi.org/10.1007/s11356-018-1514-4
Kim, J. Y., Mukherjee, S., Ngo, L. C., & Christiani, D. C. (2004). Urinary 8-hydroxy-2'-deoxyguanosine as a biomarker of oxidative DNA damage in workers exposed to fine particulates. *Environ Health Perspect*, *112*(6), 666-671. https://doi.org/10.1289/ehp.6827
Kim, S., Kim, T. Y., Yi, S. M., & Heo, J. (2018). Source apportionment of PM2.5 using positive matrix factorization (PMF) at a rural site in Korea. *J Environ Manage*, *214*, 325-334. https://doi.org/10.1016/j.jenvman.2018.03.027
Kim, S., Yang, J., Park, J., Song, I., Kim, D. G., Jeon, K., Kim, H., & Yi, S. M. (2022). Health effects of PM2.5 constituents and source contributions in major metropolitan cities, South Korea. *Environ Sci Pollut Res Int*, *29*(55), 82873-82887. https://doi.org/10.1007/s11356-022-21592-1
Kim, Y., Jeon, K., Park, J., Shim, K., Kim, S. W., Shin, H. J., Yi, S. M., & Hopke, P. K. (2022). Local and transboundary impacts of PM2.5 sources identified in Seoul during the early stage of the COVID-19 outbreak. *Atmos Pollut Res*, *13*(8), 101510. https://doi.org/10.1016/j.apr.2022.101510
Knipping, E. M., & Dabdub, D. (2003). Impact of Chlorine Emissions from Sea-Salt Aerosol on Coastal Urban Ozone. *Environmental Science & Technology*, *37*(2), 275-284. https://doi.org/10.1021/es025793z
Koo, Y.-S., Kim, S.-T., Yun, H.-Y., Han, J.-S., Lee, J.-Y., Kim, K.-H., & Jeon, E.-C. (2008). The simulation of aerosol transport over East Asia region. *Atmospheric Research*, *90*(2-4), 264-271. https://doi.org/10.1016/j.atmosres.2008.03.014
Kuang, B., Zhang, F., Shen, J., Shen, Y., Qu, F., Jin, L., Tang, Q., Tian, X., & Wang, Z. (2022). Chemical characterization, formation mechanisms and source apportionment of PM2.5 in north Zhejiang Province: The importance of secondary formation and vehicle emission. *Sci Total Environ*, *851*(Pt 2), 158206. https://doi.org/10.1016/j.scitotenv.2022.158206
Lee, Y. S., Kim, Y. K., Choi, E., Jo, H., Hyun, H., Yi, S. M., & Kim, J. Y. (2022). Health risk assessment and source apportionment of PM2.5-bound toxic elements in the industrial city of Siheung, Korea. *Environ Sci Pollut Res Int*. https://doi.org/10.1007/s11356-022-20462-0
Li, L., Qi, H., & Li, X. (2022). Composition, Source Apportionment, and Health Risk of PM2.5-Bound Metals during Winter Haze in Yuci College Town, Shanxi, China. *Toxics*, *10*(8). https://doi.org/10.3390/toxics10080467
Li, X., Yang, K., Han, J., Ying, Q., & Hopke, P. K. (2019). Sources of humic-like substances (HULIS) in PM2.5 in Beijing: Receptor modeling approach. *Sci Total Environ*, *671*, 765-775. https://doi.org/10.1016/j.scitotenv.2019.03.333
Li, Z., Wang, Y., Li, Z., Guo, S., & Hu, Y. (2020). Levels and Sources of PM2.5-

associated PAHs during and after the Wheat Harvest in a Central Rural Area of the Beijing-Tianjin-Hebei (BTH) Region. *Aerosol and Air Quality Research*, *20*(5), 1070-1082. https://doi.org/10.4209/aaqr.2020.03.0083

Ma, Q., Wu, Y., Zhang, D., Wang, X., Xia, Y., Liu, X., Tian, P., Han, Z., Xia, X., Wang, Y., & Zhang, R. (2017). Roles of regional transport and heterogeneous reactions in the PM2.5 increase during winter haze episodes in Beijing. *Sci Total Environ*, *599-600*, 246-253. https://doi.org/10.1016/j.scitotenv.2017.04.193

Manousakas, M., Papaefthymiou, H., Diapouli, E., Migliori, A., Karydas, A. G., Bogdanovic-Radovic, I., & Eleftheriadis, K. (2017). Assessment of PM2.5 sources and their corresponding level of uncertainty in a coastal urban area using EPA PMF 5.0 enhanced diagnostics. *Sci Total Environ*, *574*, 155-164. https://doi.org/10.1016/j.scitotenv.2016.09.047

Morishita, M., Keeler, G. J., Wagner, J. G., & Harkema, J. R. (2006). Source identification of ambient PM2.5 during summer inhalation exposure studies in Detroit, MI. *Atmospheric Environment*, *40*(21), 3823-3834. https://doi.org/10.1016/j.atmosenv.2006.03.005

NIER. (2019). *Korean Exposure Factors Handbook*.

Park, E. J., Kim, D. S., & Park, K. (2008). Monitoring of ambient particles and heavy metals in a residential area of Seoul, Korea. *Environ Monit Assess*, *137*(1-3), 441-449. https://doi.org/10.1007/s10661-007-9779-y

Park, J., Kim, H., Kim, Y., Heo, J., Kim, S.-W., Jeon, K., Yi, S.-M., & Hopke, P. K. (2022). Source apportionment of PM2.5 in Seoul, South Korea and Beijing, China using dispersion normalized PMF. *Science of The Total Environment*, *833*, 155056. https://doi.org/https://doi.org/10.1016/j.scitotenv.2022.155056

Park, M.-B., Lee, T.-J., Lee, E.-S., & Kim, D.-S. (2019). Enhancing source identification of hourly PM2.5 data in Seoul based on a dataset segmentation scheme by positive matrix factorization (PMF). *Atmospheric Pollution Research*, *10*(4), 1042-1059. https://doi.org/10.1016/j.apr.2019.01.013

Pekney, N. J., Davidson, C. I., Zhou, L., & Hopke, P. K. (2006). Application of PSCF and CPF to PMF-Modeled Sources of PM2.5in Pittsburgh. *Aerosol Science and Technology*, *40*(10), 952-961. https://doi.org/10.1080/02786820500543324

Prahalad, A. K., Inmon, J., Ghio, A. J., & Gallagher, J. E. (2000). Enhancement of 2‘-Deoxyguanosine Hydroxylation and DNA Damage by Coal and Oil Fly Ash in Relation to Particulate Metal Content and Availability. *Chemical Research in Toxicology*, *13*(10), 1011-1019. https://doi.org/10.1021/tx000110j

Querol, X., Viana, M., Alastuey, A., Amato, F., Moreno, T., Castillo, S., Pey, J., de la Rosa, J., Sánchez de la Campa, A., Artíñano, B., Salvador, P., García Dos Santos, S., Fernández-Patier, R., Moreno-Grau, S., Negral, L., Minguillón, M. C., Monfort, E., Gil, J. I., Inza, A., . . . Zabalza, J. (2007). Source origin of trace elements in PM from regional

background, urban and industrial sites of Spain. *Atmospheric Environment*, *41*(34), 7219–7231. https://doi.org/10.1016/j.atmosenv.2007.05.022

Schauer, J. J., Kleeman, M. J., Cass, G. R., & Simoneit, B. R. T. (2002). Measurement of Emissions from Air Pollution Sources. 5. C1–C32 Organic Compounds from Gasoline-Powered Motor Vehicles. *Environmental Science & Technology*, *36*(6), 1169–1180. https://doi.org/10.1021/es0108077

Schembari, C., Bove, M. C., Cuccia, E., Cavalli, F., Hjorth, J., Massabò, D., Nava, S., Udisti, R., & Prati, P. (2014). Source apportionment of PM10 in the Western Mediterranean based on observations from a cruise ship. *Atmospheric Environment*, *98*, 510–518. https://doi.org/10.1016/j.atmosenv.2014.09.015

Song, L., Dai, Q., Feng, Y., & Hopke, P. K. (2021). Estimating uncertainties of source contributions to PM2.5 using moving window evolving dispersion normalized PMF. *Environ Pollut*, *286*, 117576. https://doi.org/10.1016/j.envpol.2021.117576

Song, R., Yang, L., Liu, M., Li, C., & Yang, Y. (2019). Spatiotemporal Distribution of Air Pollution Characteristics in Jiangsu Province, China. *Advances in Meteorology*, *2019*, 1–14. https://doi.org/10.1155/2019/5907673

Sørensen, M., Schins, R. P. F., Hertel, O., & Loft, S. (2005). Transition Metals in Personal Samples of PM2.5 and Oxidative Stress in Human Volunteers. *Cancer Epidemiology, Biomarkers & Prevention*, *14*(5), 1340–1343. https://doi.org/10.1158/1055-9965.Epi-04-0899

Steinfeld, J. I. (1998). Atmospheric Chemistry and Physics: From Air Pollution to Climate Change. *Environment: Science and Policy for Sustainable Development*, *40*(7), 26–26. https://doi.org/10.1080/00139157.1999.10544295

Su, Y., Liu, X., Teng, Y., & Zhang, K. (2021). A Preliminary Study on Dependence of Mercury Distribution on the Degree of Coalification in Ningwu Coalfield, Shanxi, China. *Energies*, *14*(11). https://doi.org/10.3390/en14113119

Sun, J., Hu, G., Yu, R., Lin, C., Wang, X., & Huang, Y. (2017). Human health risk assessment and source analysis of metals in soils along the G324 Roadside, China, by Pb and Sr isotopic tracing. *Geoderma*, *305*, 293–304. https://doi.org/10.1016/j.geoderma.2017.06.017

Sun, S., Jiang, W., & Gao, W. (2016). Vehicle emission trends and spatial distribution in Shandong province, China, from 2000 to 2014. *Atmospheric Environment*, *147*, 190–199. https://doi.org/10.1016/j.atmosenv.2016.09.065

Swietlicki, E., Puri, S., Hansson, H.-C., & Edner, H. (1996). Urban air pollution source apportionment using a combination of aerosol and gas monitoring techniques. *Atmospheric Environment*, *30*(15), 2795–2809. https://doi.org/https://doi.org/10.1016/1352-2310(95)00322-3

Thomaidis, N. S., Bakeas, E. B., & Siskos, P. A. (2003). Characterization of lead, cadmium, arsenic and nickel in PM2.5 particles in the Athens atmosphere, Greece. *Chemosphere*, *52*(6), 959–966.

https://doi.org/10.1016/s0045-6535(03)00295-9
Thorpe, A., & Harrison, R. M. (2008). Sources and properties of non-exhaust particulate matter from road traffic: a review. *Sci Total Environ*, *400*(1-3), 270-282. https://doi.org/10.1016/j.scitotenv.2008.06.007
Uria-Tellaetxe, I., & Carslaw, D. C. (2014). Conditional bivariate probability function for source identification. *Environmental Modelling & Software*, *59*, 1-9. https://doi.org/10.1016/j.envsoft.2014.05.002
Viana, M., Kuhlbusch, T. A. J., Querol, X., Alastuey, A., Harrison, R. M., Hopke, P. K., Winiwarter, W., Vallius, M., Szidat, S., Prévôt, A. S. H., Hueglin, C., Bloemen, H., Wåhlin, P., Vecchi, R., Miranda, A. I., Kasper-Giebl, A., Maenhaut, W., & Hitzenberger, R. (2008). Source apportionment of particulate matter in Europe: A review of methods and results. *Journal of Aerosol Science*, *39*(10), 827-849. https://doi.org/10.1016/j.jaerosci.2008.05.007
Wang, S., Feng, H., Zou, B., Yang, Z., & Ding, Y. (2022). Correlation between biomass burning and air pollution in China: Spatial heterogeneity and corresponding factors. *Global and Planetary Change*, *213*. https://doi.org/10.1016/j.gloplacha.2022.103823
Wang, X., Bi, X., Sheng, G., & Fu, J. (2006). Chemical Composition and Sources of PM10 and PM2.5 Aerosols in Guangzhou, China. *Environmental Monitoring and Assessment*, *119*(1), 425-439. https://doi.org/10.1007/s10661-005-9034-3
Wang, X., Shen, Y., Lin, Y., Pan, J., Zhang, Y., Louie, P. K. K., Li, M., & Fu, Q. (2019). Atmospheric pollution from ships and its impact on local air quality at a port site in Shanghai. *Atmospheric Chemistry and Physics*, *19*(9), 6315-6330. https://doi.org/10.5194/acp-19-6315-2019
Xia, D., Jiang, B., & Xie, Y. (2016). Modeling and analysis of PM2.5 generation for key factors identification in China. *Atmospheric Environment*, *134*, 208-216. https://doi.org/10.1016/j.atmosenv.2016.03.055
Xue, Y., Tian, H., Yan, J., Xiong, C., Pan, T., Nie, L., Wu, X., Li, J., Wang, W., Gao, J., Zhu, C., & Wang, K. (2016). Present and future emissions of HAPs from crematories in China. *Atmospheric Environment*, *124*, 28-36. https://doi.org/10.1016/j.atmosenv.2015.10.079
Yan, R. H., Peng, X., Lin, W., He, L. Y., Wei, F. H., Tang, M. X., & Huang, X. F. (2022). Trends and Challenges Regarding the Source-Specific Health Risk of PM2.5-Bound Metals in a Chinese Megacity from 2014 to 2020. *Environ Sci Technol*, *56*(11), 6996-7005. https://doi.org/10.1021/acs.est.1c06948
Yang, H., Tao, W., Liu, Y., Qiu, M., Liu, J., Jiang, K., Yi, K., Xiao, Y., & Tao, S. (2019). The contribution of the Beijing, Tianjin and Hebei region's iron and steel industry to local air pollution in winter. *Environ Pollut*, *245*, 1095-1106. https://doi.org/10.1016/j.envpol.2018.11.088
Yang, H. H., Luo, S. W., Lee, K. T., Wu, J. Y., Chang, C. W., & Chu, P. F. (2016). Fine particulate speciation profile and emission factor of municipal solid waste incinerator established by dilution sampling method. *J Air Waste Manag Assoc*, *66*(8), 807-814. https://doi.org/10.1080/10962247.2016.1184195
Yang, L., Li, C., & Tang, X. (2020). The Impact of PM2.5 on the Host Defense

of Respiratory System. *Front Cell Dev Biol*, *8*, 91. https://doi.org/10.3389/fcell.2020.00091

Yao, X., & Zhang, L. (2012). Chemical processes in sea-salt chloride depletion observed at a Canadian rural coastal site. *Atmospheric Environment*, *46*, 189-194. https://doi.org/10.1016/j.atmosenv.2011.09.081

Ye, Z., Guo, X., Cheng, L., Cheng, S., Chen, D., Wang, W., & Liu, B. (2019). Reducing PM2.5 and secondary inorganic aerosols by agricultural ammonia emission mitigation within the Beijing-Tianjin-Hebei region, China. *Atmospheric Environment*, *219*. https://doi.org/10.1016/j.atmosenv.2019.116989

Yoo, J.-I., Kim, K.-H., Jang, H.-N., Seo, Y.-C., Seok, K.-S., Hong, J.-H., & Jang, M. (2002). Emission characteristics of particulate matter and heavy metals from small incinerators and boilers. *Atmospheric Environment*, *36*(32), 5057-5066. https://doi.org/https://doi.org/10.1016/S1352-2310(02)00557-5

Yu, G. H., & Park, S. (2021). Chemical characterization and source apportionment of PM2.5 at an urban site in Gwangju, Korea. *Atmospheric Pollution Research*, *12*(6). https://doi.org/10.1016/j.apr.2021.101092

Zhao, Y., & Gao, Y. (2008). Acidic species and chloride depletion in coarse aerosol particles in the US east coast. *Sci Total Environ*, *407*(1), 541-547. https://doi.org/10.1016/j.scitotenv.2008.09.002

Zhao, Y., Xu, R., Xu, Z., Wang, L., & Wang, P. (2022). Temporal and Spatial Patterns of Biomass Burning Fire Counts and Carbon Emissions in the Beijing–Tianjin–Hebei (BTH) Region during 2003–2020 Based on GFED4. *Atmosphere*, *13*(3). https://doi.org/10.3390/atmos13030459

Zíková, N., Wang, Y., Yang, F., Li, X., Tian, M., & Hopke, P. K. (2016). On the source contribution to Beijing PM2.5 concentrations. *Atmospheric Environment*, *134*, 84-95. https://doi.org/10.1016/j.atmosenv.2016.03.047

Supplementary

Table S1. Hourly meteorological parameters in Seoul (yellow shades indicate statistically higher value at $p \leq 0.05$)

Season	Wind speed (m/s)	MLH (m)	VC (m^2/s)
All period	2.64	450.42	1708.85
Heating season	2.73	454.83	1815.20
Non-heating season	2.46	441.06	1483.43
Dining hour	2.81	352.44	1467.56
Other hour	2.57	490.79	1808.26

Table S2. Hourly meteorological parameters in Incheon (yellow shades indicate statistically higher value at $p \leq 0.05$)

Season	Wind speed (m/s)	MLH (m)	VC (m^2/s)
All period	3.69	465.11	2339.44
Heating season	3.79	471.82	2522.10
Non-heating season	3.43	449.08	1903.04
Dining hour	3.78	399.16	2185.68
Other hour	3.65	492.27	2402.75

Table S3. Hourly meteorological parameters in Gwangju (yellow shades indicate statistically higher value at $p \leq 0.05$)

Season	Wind speed (m/s)	MLH (m)	VC (m^2/s)
All period	3.27	461.07	2006.63
Heating season	3.42	469.51	2181.69
Non-heating season	2.97	443.32	1638.86
Dining hour	3.14	386.00	1676.59
Other hour	3.33	492.00	2142.61

Table S4. Hourly meteorological parameters in Gwangju (yellow shades indicate statistically higher value at $p \leq 0.05$)

Site	Seoul	Incheon	Gwangju
ILCR	3.2E-06	4.0E-06	1.9E-06
HI	1.3E-01	2.6E-01	6.5E-02

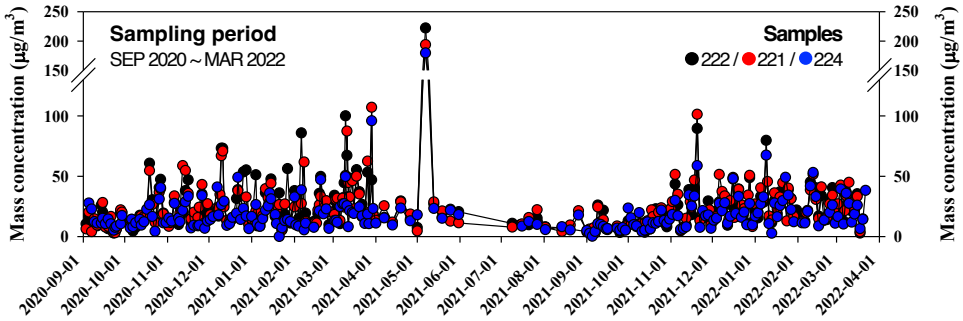

Figure S1. Time series of $PM_{2.5}$ mass concentrations in Seoul, Incheon, and Gwangju.

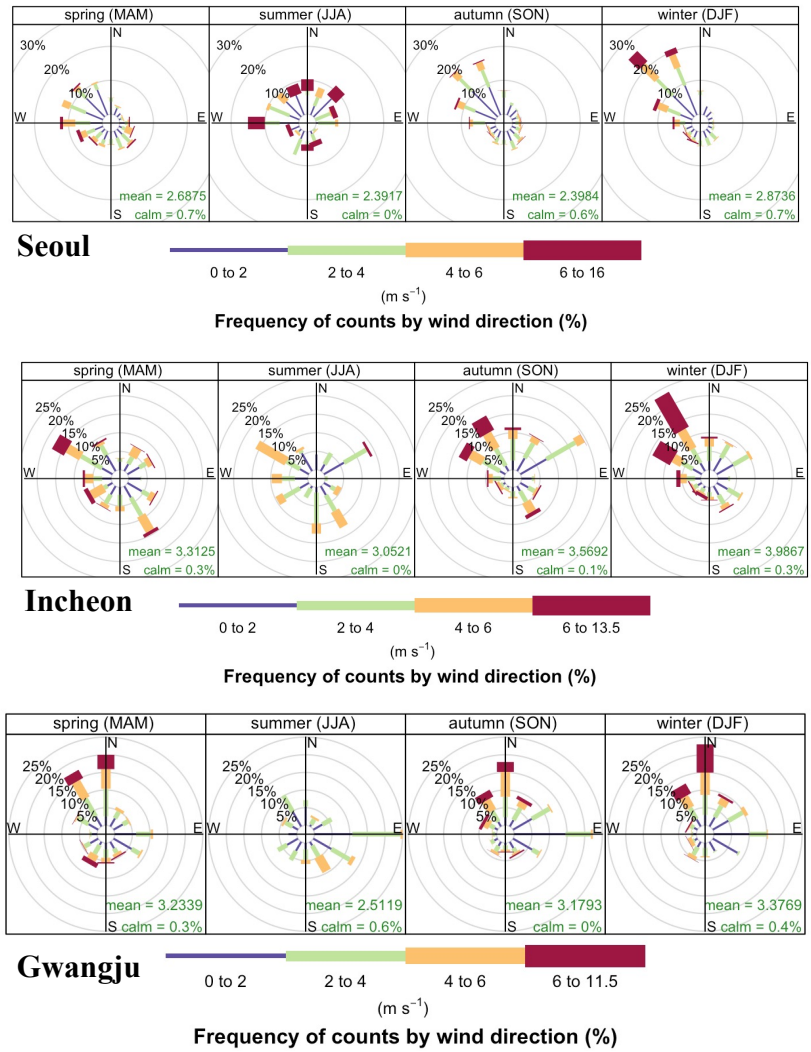

Figure S2. Windrose plots by seasons in Seoul, Incheon, and Gwangju.

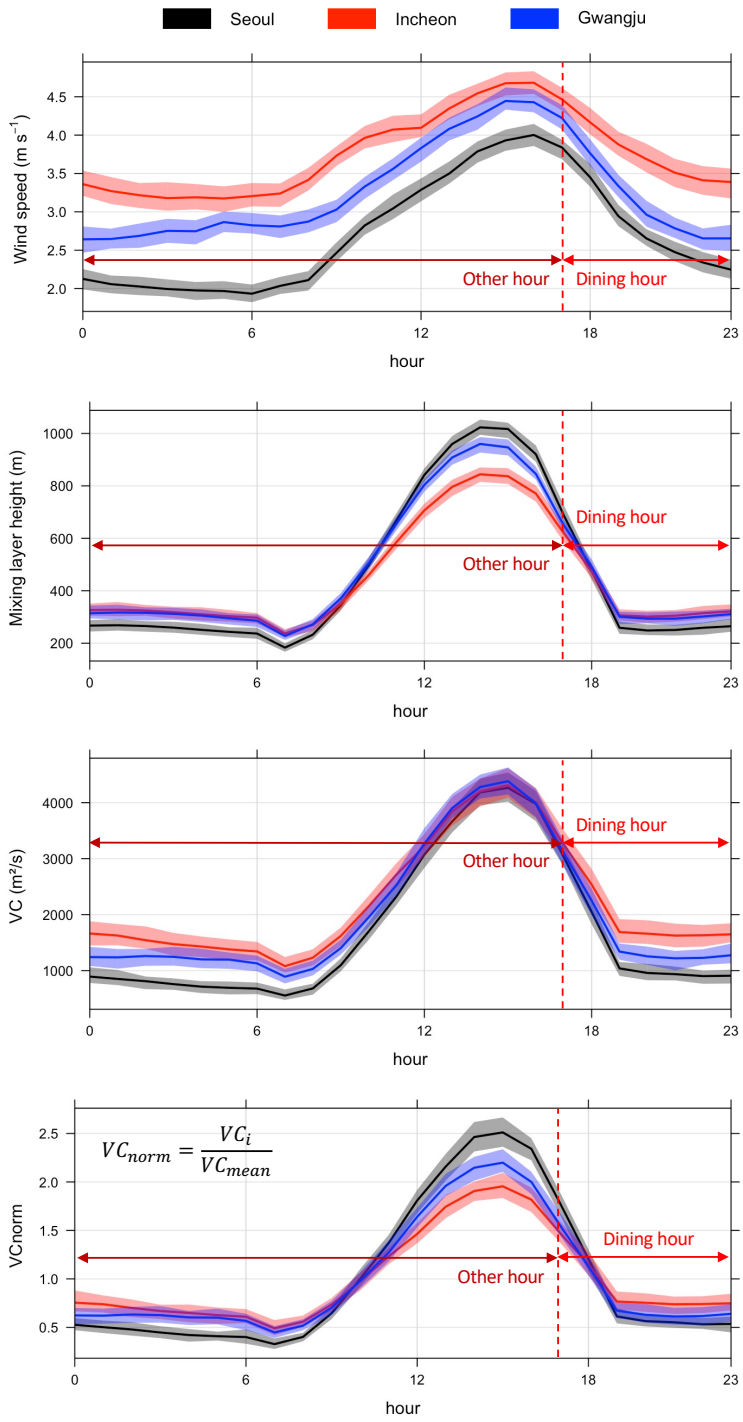

Figure S3. Temporal variation of hourly meteorological parameters (dining hours: 17:00-23:00, other hours: 00:00-16:00). The lines represent mean values, and the shaded areas are the 95% confidence intervals.

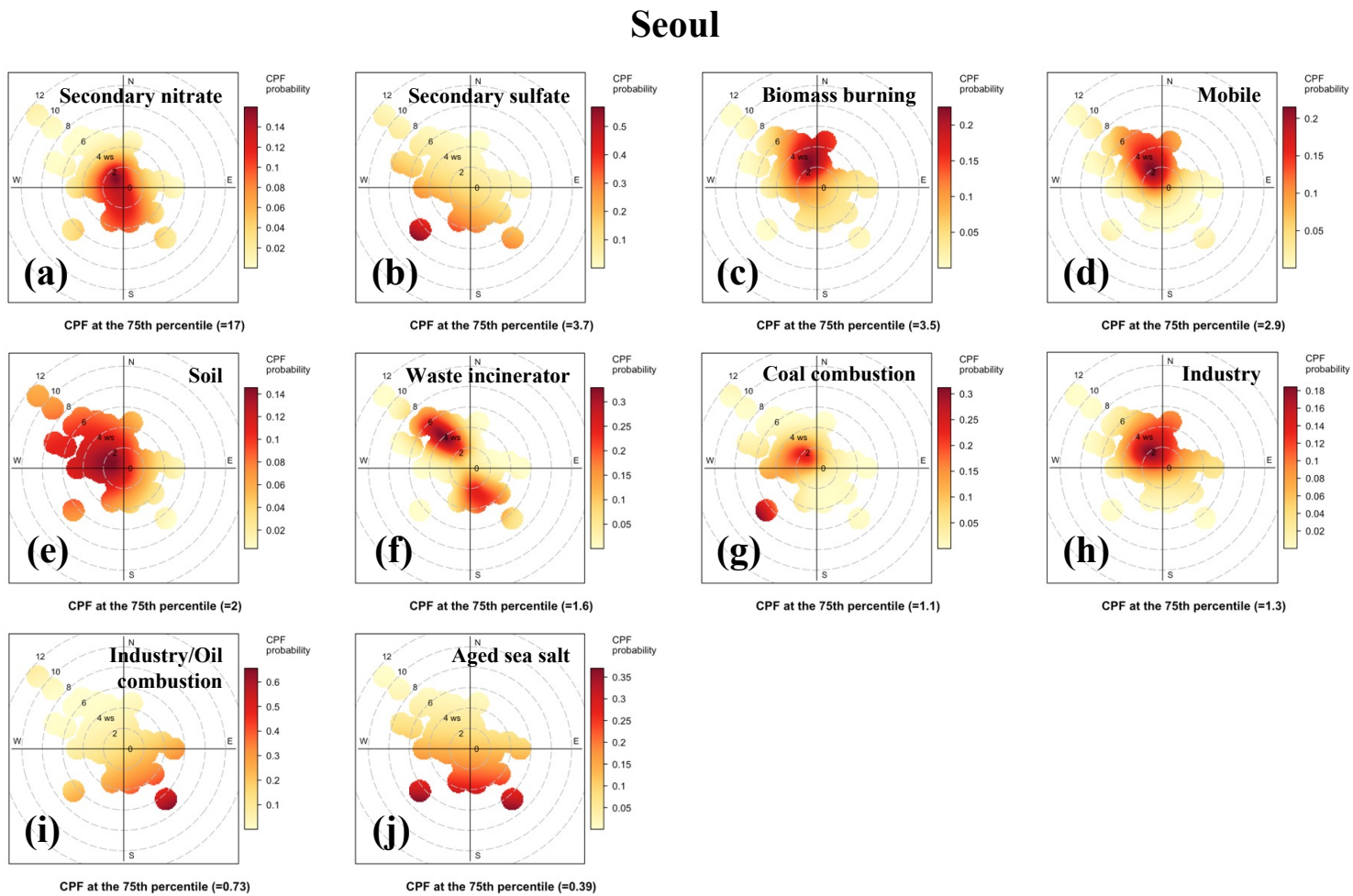

Figure S4. CBPF plots of $PM_{2.5}$ sources in Seoul.

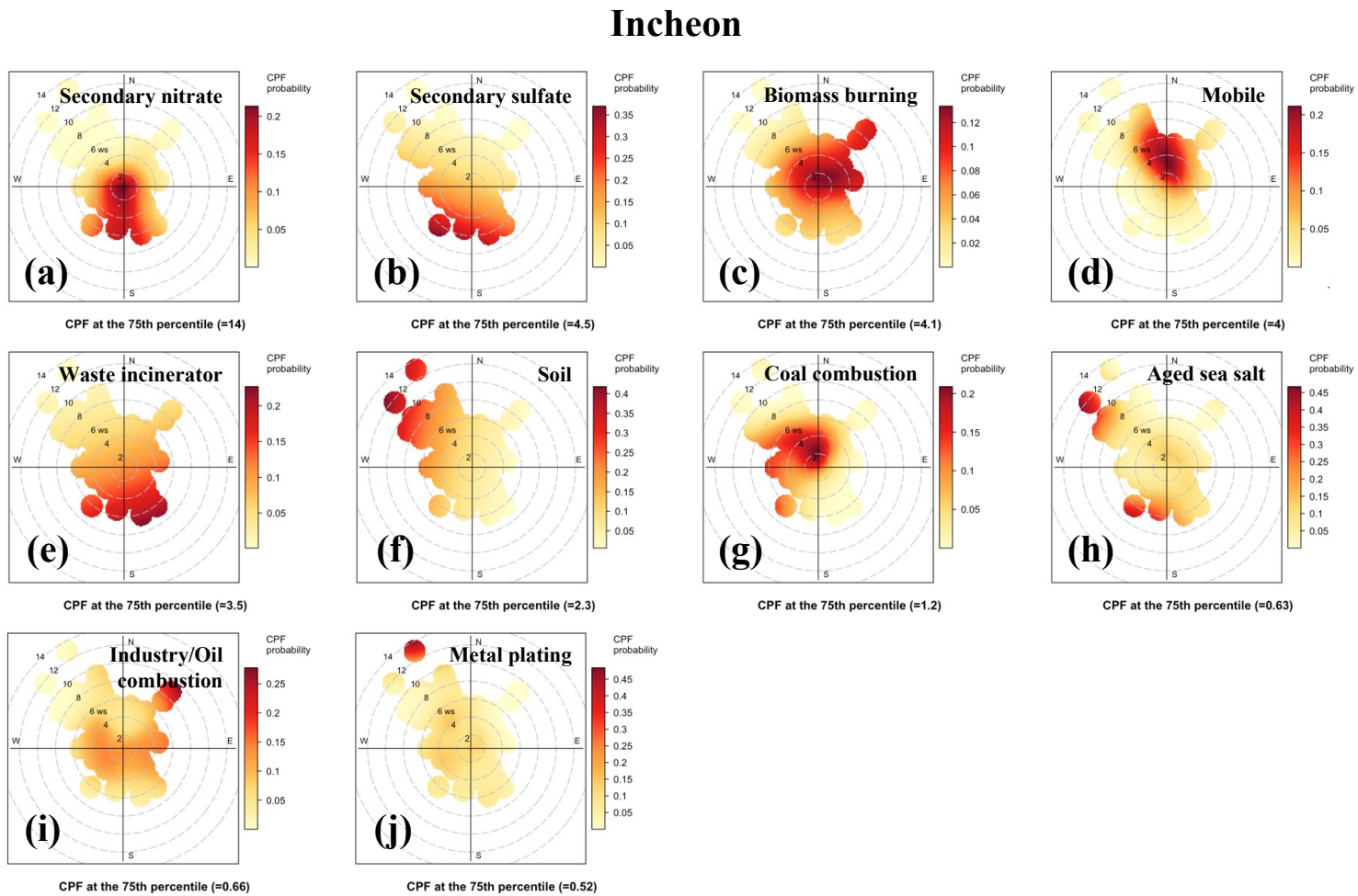

Figure S5. CBPF plots of $PM_{2.5}$ sources in Incheon.

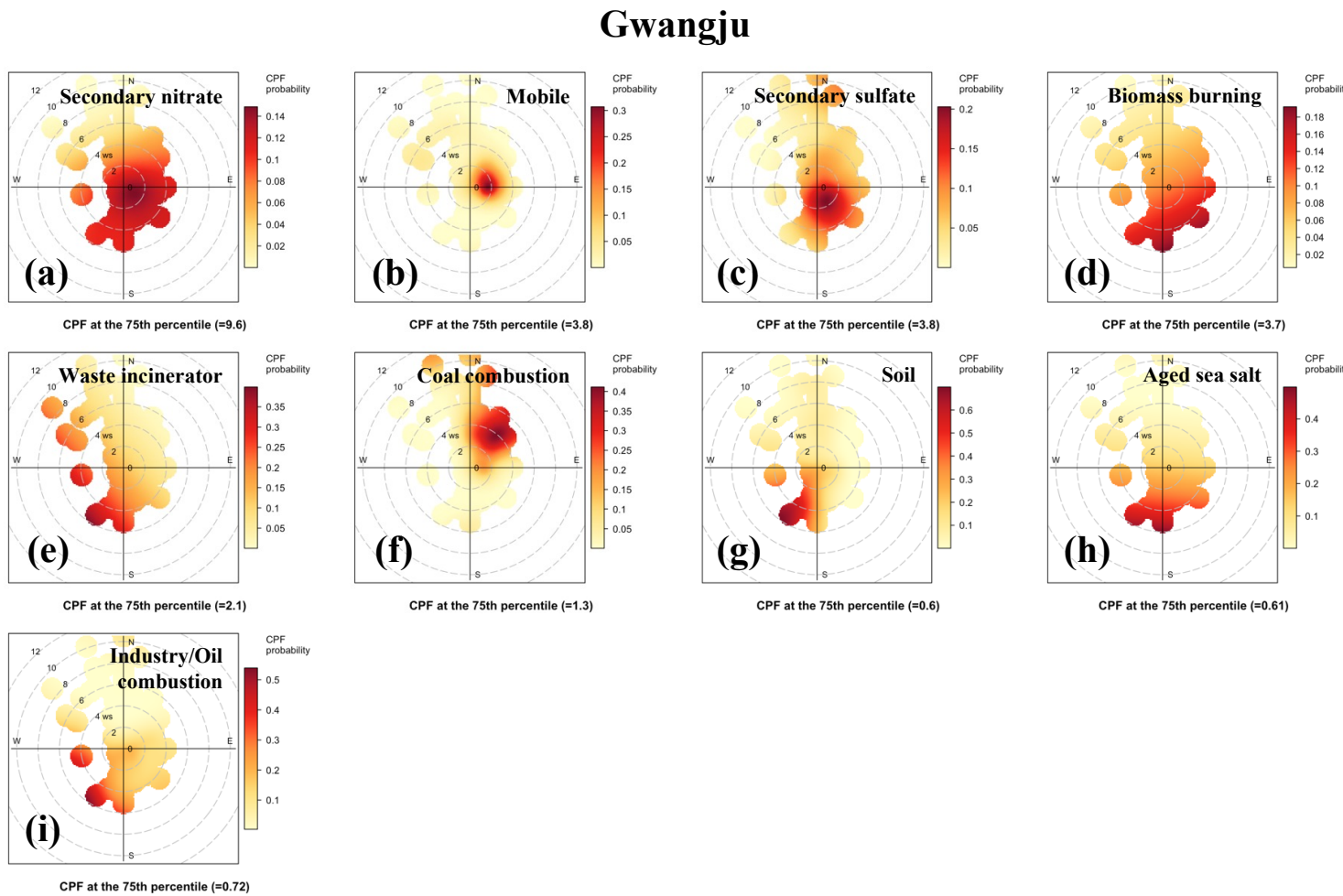

Figure S6. CBPF plots of $PM_{2.5}$ sources in Gwangju.

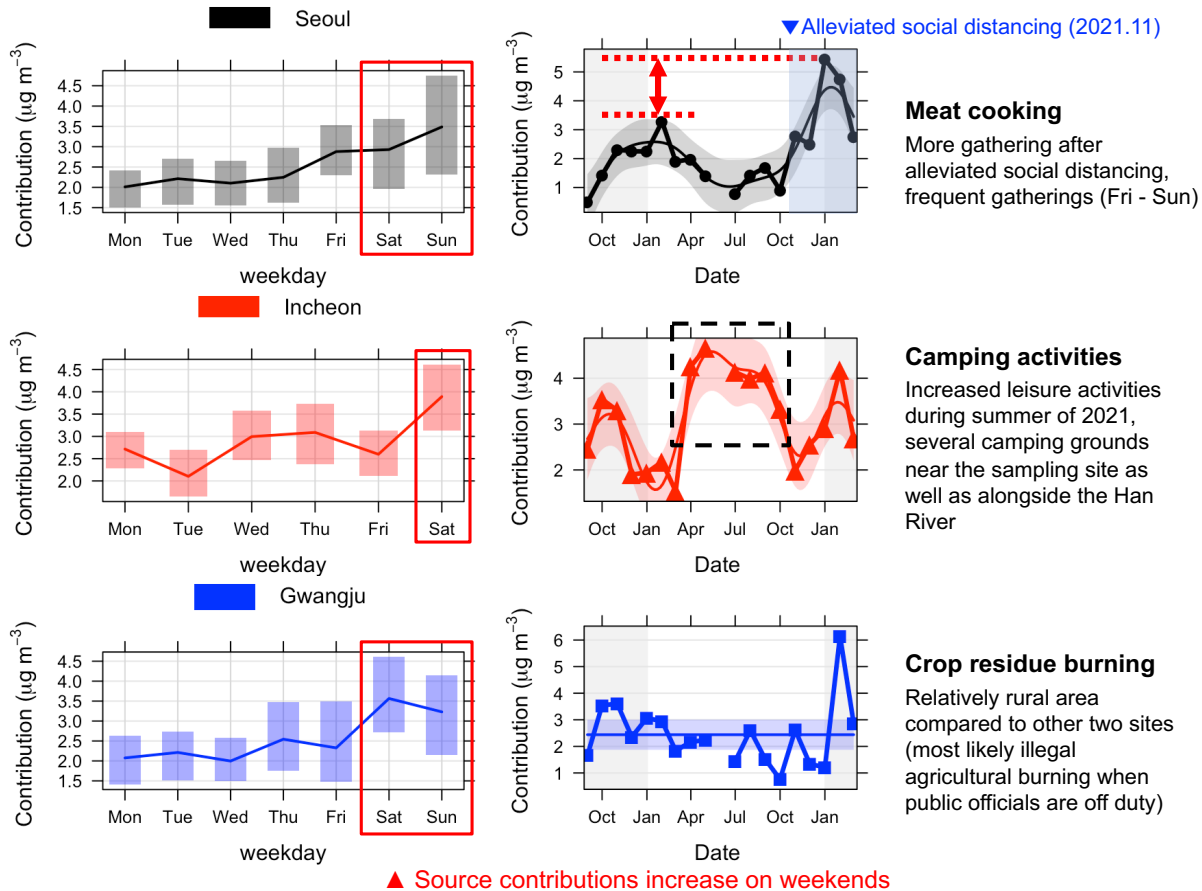

Figure S7. Weekday and monthly time series plots of biomass burning sources in Seoul, Incheon, and Gwangju.

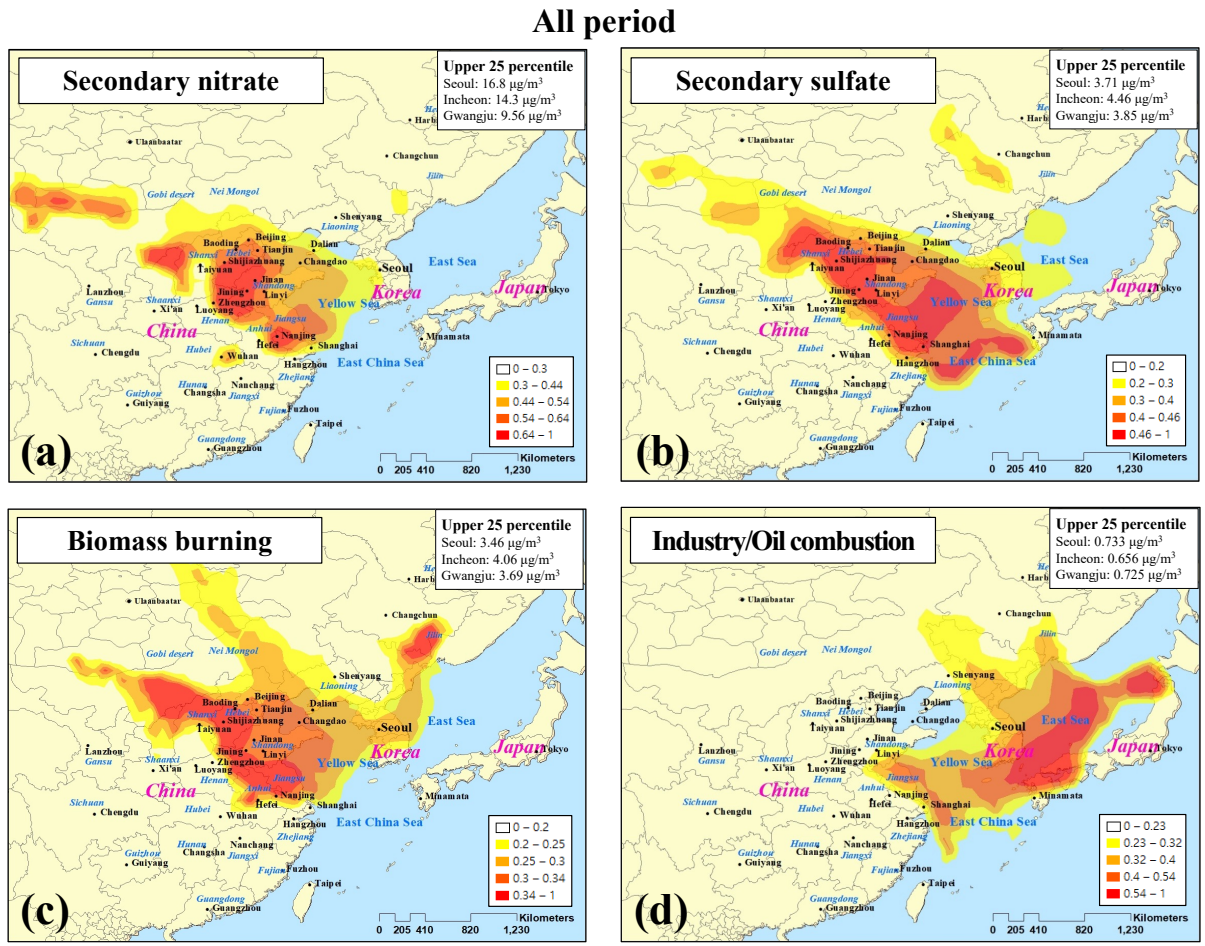

Figure S8. J-PSCF plots of (a) secondary nitrate; (b) secondary sulfate; (c) biomass burning; (d) industry/oil combustion during the study period

국문 초록

서울, 인천, 광주의 $PM_{2.5}$ 오염원 추정과 건강영향 평가

정연승

환경보건학과 환경보건학전공

서울대학교 보건대학원

$PM_{2.5}$는 발생원이 복잡다단하고 인체보건학적인 영향이 큰 대기오염물질로서 정확한 오염원 규명과 건강영향 평가에 근거한 체계적인 저감 대책이 필요하다. 서울, 인천, 광주는 우리나라에서 $PM_{2.5}$ 오염 수준이 높은 대도시들이며, 편서풍 풍하지역에 위치하여 중국으로부터의 장거리 이동 오염원에 의한 영향을 많이 받기 때문에 위 도시들에 대한 $PM_{2.5}$ 저감이 시급하다. PMF (Positive Matrix Factorization) 모델은 대표적인 수용 모델로서, $PM_{2.5}$의 오염원 추정 연구에 널리 사용되고 있다. 그러나 기존의 PMF (Conventional PMF, C-PMF)가 가지는 한계점은 배출량 변화, 대기화학 반응, 기상 효과에 의한 희석 등에 따른 대기 중 농도 변화를 고려하지 못한다는 점이다. Dispersion-normalized PMF (DN-PMF) 모델은 기상효과를 제거하여 오염원의 실제 영향력을 향상시킬 수 있다. 따라서, 본 연구에서는 DN-PMF를 사용하여 서울, 인천, 광주의 $PM_{2.5}$ 오염원을 추정하였고, C-PMF의 결과와 비교하여 기상 영향에 대한 보정을 평가하였다. 각 도시에서의 지역 오염원의 위치는 Conditional Bivariate Probability Function (CBPF) 모델을 사용하여 파악하였으며, 세 도시에 공통적으로 영향을 미치는 장거리 이동 오염원의 위치는 Joint Potential Source Contribution Function (J-PSCF)모델을 사용하여 추정하였다. 이어서,

DN-PMF 모델 결과를 사용하여 $PM_{2.5}$ 중의 미량 원소성분에 대한 건강영향 평가를 수행하여 인체 건강에 영향을 많이 미치는 오염원을 규명하였다.

2020년 9월부터 2022년 3월까지 서울, 인천, 광주에서 포집한 222, 221, 224개의 $PM_{2.5}$ 시료에 대해 DN-PMF와 C-PMF 모델을 사용하여 오염원을 도출하였다. 두 모델 공통적으로 서울과 인천에서 각각 10개의 오염원, 그리고 광주에서 9개의 오염원이 도출되었다. 9개의 공통 오염원은 이차 질산염, 이차 황산염, 생물성 연소, 자동차, 토양, 소각장, 석탄 연소, 산업/기름 연소, 노후 해염 오염원들이며, 서울과 인천에서는 각각 산업 오염원과 금속 도금 오염원이 추가적으로 도출되었다. DN-PMF는 C-PMF와 같은 개수의 오염원을 도출하였으며 오염원 프로파일도 크게 다르지 않은 반면, 오염원의 기여도에서 차이가 발생하였다. 오염원 기여도의 차이는 지역 확산의 정도에 따른 보정 효과에서 기인하는 것으로 판단된다. 이차 질산염과 생물성 연소 오염원의 경우 환기 계수가 높은 기간에 대해 과소평가 되던 해당 오염원들의 기여도가 상향 조정되었다. 또한, DN-PMF가 자동차 오염원의 계절적 특성을 두드러지게 잘 나타내는 것으로 나타났다. CBPF 모델 결과로부터 각 도시 내에 존재하는 1차 배출원 위치들이 파악되었으며 자동차, 소각장, 그리고 산업 관련 오염원들의 영향이 존재하는 것으로 확인되었다. J-PSCF 모델 결과, 북동 중국과 내몽골 일부 지역이 이차 질산염, 이차 황산염, 그리고 생물성 연소 오염원의 잠재적 오염원 위치로 추정되었다.

DN-PMF 모델 결과를 사용하여 미량 원소성분에 의한 건강영향 평가를 수행하여 각 도시에서의 발암 및 비발암 위해도를 추정하였다. 세 도시 모두 발암 위험이 존재하였으며, 특히, As와 Cr^{6+} 성분의 발암 위해도 기여도가 컸다. 위와 같은 발암성 미량 원소성분을 배출하는 석탄 연소 및 금속 도금 오염원에 대해 특별한 관리가 필요할 것으로 사료된다. 반면에 세 도시의 비발암 위험은 안전한 수준으로 나타났으며, 비발암 위해도에 크게 기여한 성분들은 Mn, As, 그리고 Pb로 나타났다.

위 성분들은 자동차, 석탄 연소, 그리고 산업 오염원과 관련된 성분들이다. 따라서 세 도시에 거주하는 사람들의 건강을 보호하기 위해서 자동차, 석탄 연소, 산업 오염원에 대한 지속적인 모니터링이 필요할 것으로 판단되었다.

주요어: $PM_{2.5}$ 오염원 추정, DN-PMF (Dispersion Normalized Positive Matrix Factorization), CBPF (Conditional Bivariate Probability Function), PSCF (Potential Source Contribution Function), 건강영향 평가

학번: 2021-22679